The Regenerative Response of Endogenous Neural Stem/Progenitor Cells to Traumatic Brain Injury

by

Genevieve M. Sullivan

Thesis submitted to the Faculty of the
MCB Graduate Program
Uniformed Services University of the Health Sciences
In partial fulfillment of the requirements for the degree of
Doctor of Philosophy 2014

UNIFORMED SERVICES UNIVERSITY, SCHOOL OF MEDICINE GRADUATE PROGRAMS
Graduate Education Office (A 1045), 4301 Jones Bridge Road, Bethesda, MD 20814

DISSERTATION APPROVAL FOR THE DOCTORAL DISSERTATION IN THE MOLECULAR AND CELL BIOLOGY GRADUATE PROGRAM

Title of Dissertation: "The Regenerative Response of Endogenous Neural Stem/Progenitor Cells to Traumatic Brain Injury"

Name of Candidate: Genevieve Sullivan
Doctor of Philosophy Degree
May 21, 2014

DISSERTATION AND ABSTRACT APPROVED:

DATE:

Joseph L McCabe 6/9/14
Dr. Joseph McCabe
DEPARTMENT OF ANATOMY, PHYSIOLOGY, AND GENETICS
Committee Chairperson

6/9/14
Dr. Regina Armstrong
DEPARTMENT OF ANATOMY, PHYSIOLOGY, AND GENETICS
Dissertation Advisor

6/9/14
Dr. Clifton Dalgard
DEPARTMENT OF ANATOMY, PHYSIOLOGY, AND GENETICS
Committee Member

Sharon L Juliano 6/9/14
Dr. Sharon Juliano
DEPARTMENT OF ANATOMY, PHYSIOLOGY, AND GENETICS
Committee Member

6/9/14
Dr. Martin Doughty
DEPARTMENT OF ANATOMY, PHYSIOLOGY, AND GENETICS
Committee Member

ACKNOWLEDGMENTS

Dr. Armstrong, thank you for mentoring me and for always setting the bar a little higher. Your help and guidance over the years has meant so much to me. I will always be grateful and honored that I had the opportunity to be a student your lab.

Committee members, thank you for your help and guidance throughout my journey.

DEDICATION

I would like to dedicate this work to mom (Kathryn L. Byers), dad (James R. Sullivan), and Douglas F. Sullivan. I love you.

COPYRIGHT STATEMENT

The author hereby certifies that the use of any copyrighted material in the dissertation manuscript entitled: The Regenerative Response of Endogenous Neural Stem/Progenitor Cells to Traumatic Brain Injury is appropriately acknowledged and, beyond brief excerpts, is with the permission of the copyright owner.

[Signature] 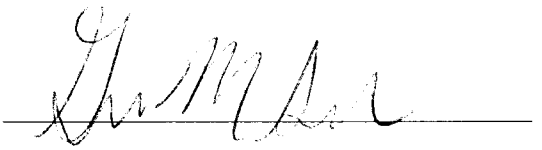

Genevieve Sullivan

August 5th, 2014 of BOR meeting

ABSTRACT

The Regenerative Response of Endogenous Neural Stem/Progenitor Cells to Traumatic Brain Injury:

Genevieve M. Sullivan, Molecular and Cell Biology, 2014

Thesis directed by: Dr. Regina C. Armstrong, PhD, APG

The complex pathological mechanisms following traumatic brain injury (TBI) limit repair of damaged tissue. Cell signaling molecules have the potential to create a supportive environment for regeneration after injury, and promote the regenerative response from endogenous cells. Sonic hedgehog (Shh) has been shown to maintain neural stem cells (NSCs) and promote oligodendrogenesis. This study examines the influence of Shh signaling on neuronal (DCX) or oligodendroglial (NG2) progenitor responses, in either gray (GM) or white matter (WM) TBI models. A WM injury model in C57BL/6J mice was characterized at the coronal level of the subventricular zone (SVZ) to compare the response of Shh-responsive-NSCs following WM and GM injury. Analysis during the first week post-injury showed a) axon damage, neuroinflammation, demyelination, and redundant myelin figures in the corpus callosum (CC), b) an increase in NG2 cell proliferation in the SVZ and CC, and c) an increase in NG2 cells in the CC. To analyze cell responses to Shh following WM and GM injury, *Gli1-CreER^{T2};R26-YFP* mice were administered tamoxifen 2 and 3 days post-TBI, with analysis of tissue at 2 and

6 weeks post-injury. GM injury was produced with a mild controlled cortical impact to the cerebral cortex. YFP cells decreased in cortical lesions. After GM injury, total YFP and YFP+DCX+ cells increased in the SVZ. After WM injury, YFP cells within the SVZ initially decreased and then normalized. Furthermore, NG2 cells were elevated in the cortex with a similar trend in the CC. NG2 progenitors were rarely labeled with YFP. To test the potential for NG2 cells in the CC to respond through Shh-signaling, smoothened agonist was microinjected into the CC. YFP cells and NG2 cells significantly increased in the SVZ. However, YFP cells were absent in CC and rarely co-localized with NG2. These observations indicate an in vivo effect of smoothened signaling without *Gli1* activation in NG2 cells, which may utilize a variant Shh-signaling pathway from neuroblasts or indirectly respond to Shh. Furthermore, characterization of a WM TBI model allowed for comparison of the endogenous cell responses to Shh following WM and GM injury that revealed injury dependent responses in Shh-responsive-NSCs.

TABLE OF CONTENTS

LIST OF FIGURES

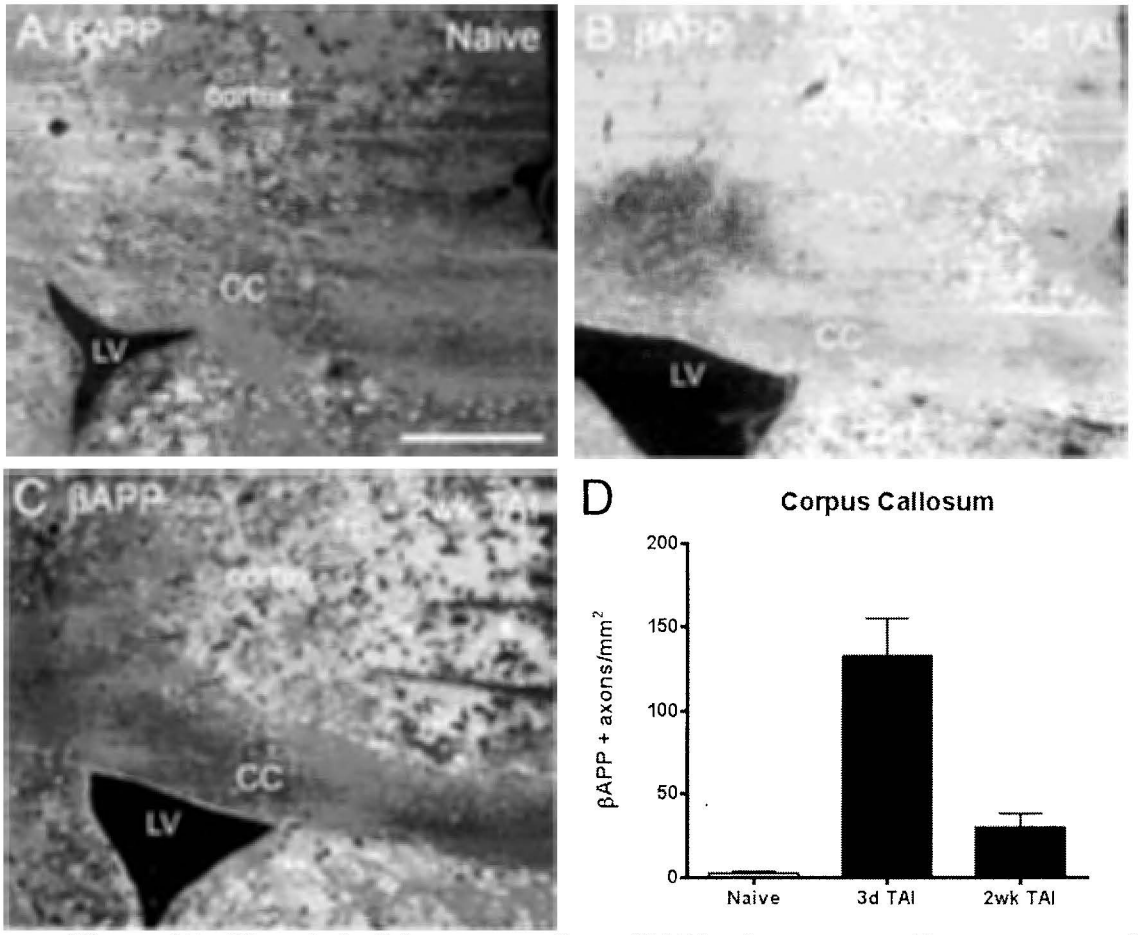

CHAPTER 1: Introduction

SIGNIFICANCE

The complex pathology of traumatic brain injury (TBI) makes it difficult to develop therapeutic strategies to treat the millions of people that sustain a TBI annually (74). The complex pathology is a result of variations in the cause, location, and severity of the injury. Even though the majority of individuals that sustain a TBI are diagnosed as mild, which is often computed tomography (CT) negative, those with mild TBI can experience limitations in functional cognitive recovery (52). These cognitive deficits are caused by underlying pathology such as neurodegeneration, demyelination, and inflammation. Even though within the adult central nervous system (CNS) there are neural stem cell and progenitor cell populations that could potentially repair damaged areas, either by replacing cells or secreting factors that create a more permissive microenvironment, the regenerative response from these cells is limited (59). Additionally there are no effective treatments for TBI (83). Therefore it is necessary to investigate the complex pathological and molecular mechanisms that occur after heterogeneous forms of TBI, in order to elucidate repair strategies targeted for either white matter or gray matter damage.

Therapeutic strategies are difficult to develop partly because it is challenging to replicate the complex pathology that occurs following TBI in humans with animal models. For example, acceleration deceleration of the brain causes diffuse axonal injury (DAI) (1), which is characterized by distribution of axonal pathology throughout white matter regions of the human gyrencephalic brain after TBI (83). This common injury that

occurs in sports or car accidents cannot be produced in lissencephalic animals such as the mouse. However, the mouse has a variety of transgenic options that allow for a more comprehensive analysis of cellular mechanisms that is not an option in other species with gyrencephalic brains. Therefore, even though a mouse model cannot fully replicate clinical DAI, mouse models are useful for mechanistic studies of specific pathological aspects of DAI, such as traumatic axonal injury (TAI), which is often used to define more localized axonal pathology rather than the diffuse patterns seen in human DAI (83). Development of potential TAI models will elucidate pathological mechanisms that prevent and promote regeneration, as well as allow for the development of more complex models to investigate the mechanisms behind the complex pathology that occurs in chronic neurodegenerative diseases.

Replicating Pathological Characteristics of Human TBI in Mouse Models

Many animal models used to replicate pathological aspects of human TBI have focused on the damage to cortical gray matter and the neuroregenerative response. The controlled cortical impact (CCI) model uses a piston to deliver an impact to the intact dura following a craniotomy (38). Many have characterized this model and the benefits include reproducibility and graded severity of injury in cortical gray matter. However this model is not ideal for studying white matter damage.

White matter injury models are important for understanding the pathological mechanisms involved in axon damage, demyelination, and neuroinflammation, which have been shown to persist in the corpus callosum years after a single TBI (42). The corpus callosum consists of numerous axons, many of which are

myelinated by oliogodendrocytes. Both myelinated and unmyelinated axonal tracts within the corpus callosum are susceptible to injury. In the weight drop injury model the skull is exposed and a free falling guided weight is dropped from a predetermined height. Variations in this model such as a skull cap or location of impact allow for investigation of TAI or hemorrhaging in white matter (105). Although this model is more useful in studying white matter pathology than the CCI model, there is limited reproducibility because the accuracy of impact is dependent on an estimation of where the weight will drop and the mechanical setup makes it difficult to prevent a rebound of the weight, which produces an additional impact onto the skull. A recently developed closed skull model of TBI utilized the stereotaxic impactor to deliver an impact to the exposed skull, which allows for greater reproducibility of impact. In this model, an impact was delivered caudal to bregma, in order to observe the regenerative response from the subgranular zone after damage was produced in the corpus callosum (24).

Repetitive mild closed skull injury models are particularly relevant for studying the effect multiple concussions have on the adult brain and the potential pathological mechanism that are involved in chronic traumatic encephalopathy (CTE). CTE is a neurodegenerative disease with pathology that includes tau accumulation at the depths of the sulci in superficial layers of the cortex, astrocytic tangles and spindle-shaped and threadlike neuritis that is dispersed throughout the brain (51). Gross anatomical analysis often shows atrophy of the cerebral hemispheres, thalamus, mammillary bodies, medial temporal lobe and brainstem, with dilatation of the ventricles and a fenestrated cavum septum pellucidum (51). In repetitive mild closed skull injury models repetitive hits are

delivered to the skull or in some cases the scalp using the stereotaxic impactor. Time between hits, size and construction of the impactor tip, depth of impact and location of impact allow for variation in these models. Even with the variation in experimental design, separate models of repetitive mild TBI produce common pathology that includes axon damage and microglial activation in the corpus callosum. (60; 80).

REGENERATION OF THE CNS IS LIMITED FOLLOWING INJURY

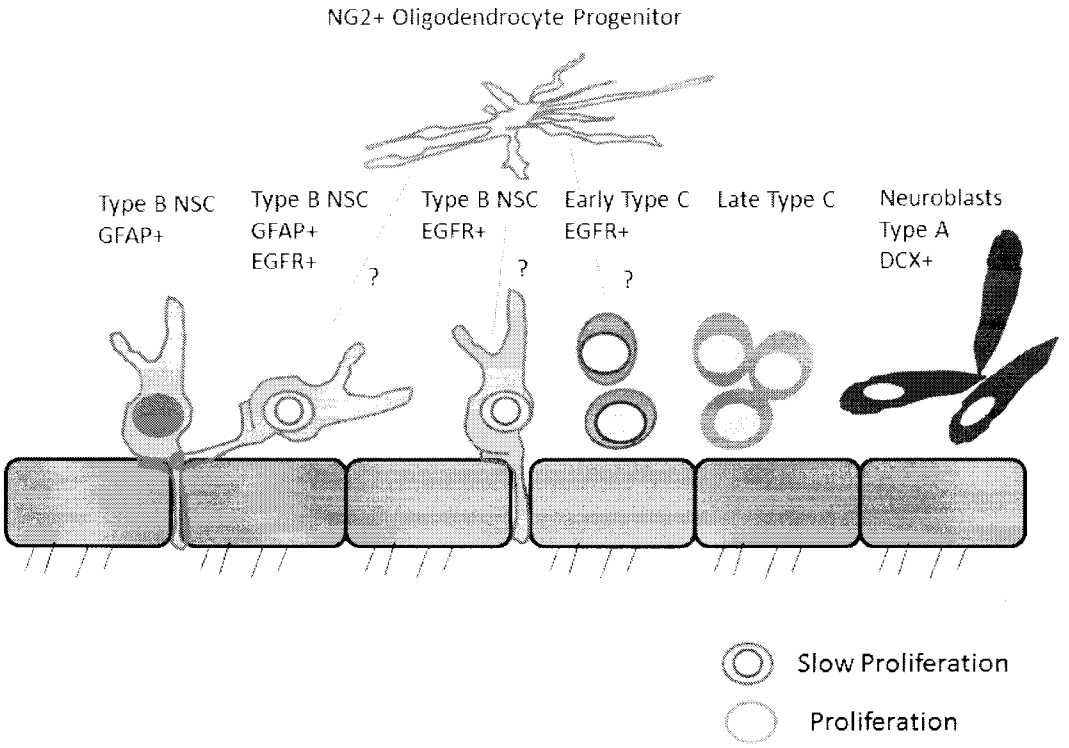

Figure1. The neural stem and progenitor cells of the subventricular zone.
In the subventricular zone (SVZ), type B cells give rise to neuronal and glial lineages. Although type B cells have been shown to give rise to oligodendrocyte lineage cells, the progression from type B cells to the oligodendrocyte lineage is not well defined.

The neural stem cells (NSCs) within the subventricular zone (SVZ), located adjacent to corpus callosum, are an ideal population of cells to study because they are capable of producing a regenerative response following TBI. Others have shown that TBI induces cells from the SVZ to increase proliferation and DCX+ cells have been shown to migrate from the SVZ to the lesion site following CCI (70). However, little is known about the factors that regulate the regenerative responses from cell populations within the SVZ after injury or which cell types are being signaled to respond. Fate mapping of the stem/progenitor cells in the SVZ niche would shed light on which cells are responding to injury and allow for the analysis of the mechanisms that enhance or impede their response.

The NSCs of the SVZ, referred to as type B cells, have self-renewal capability and have the ability to differentiate into glia and neuronal cell types(28; 53). Additionally, it has been implicated that the NSCs of the SVZ are a heterogeneous population of cells with each population expressing their own set of markers(37). Traditionally type B cells within the SVZ are identified as GFAP+ and give rise to the transit amplifying cells, type C cells, which are EGFR+. The transit amplifying population gives rise to DCX+ neuroblasts, type A cells. In naïve conditions neuroblasts and NG2+ oligodendrocyte progenitors that also reside in the SVZ, migrate through the rostral migratory stream to the olfactory bulb. It has been shown that some type B cells and a small population of type C cells that colabel with the oligodendrocyte lineage transcription factor Olig2, are capable of producing NG2+ nonmyelinating and mature myelinating oligodendrocytes (53).

Progenitor cells and cells with reactive potential in the cortex and corpus callosum are also targets for modulating regeneration after injury. Oligodendrocyte progenitors, which have the potential to become mature oligodendrocytes and contribute to remyelination after injury, proliferate in naïve mice as well as become activated and proliferate more frequently following injury(40; 46). Cortical astrocytes, not only become reactive following injury but also acquire stem cell properties following blood brain barrier breakdown (19; 82). The astrocyte population is also capable of enhancing or impeding regeneration with scar formation. Although initial scar formation may be beneficial in preventing further damage, by creating a barrier between the hostile microenvironment of the lesion and the spared tissue, it can also be detrimental for migration of new cells into the lesion to regenerate the damaged tissue (85).

Microglia are significant contributors to the pathological mechanisms that occur following injury and have the potential to be modified to enhance regeneration. Although microglia are better known for the role they have as inflammatory cells and are often characterized as having an either an M1 pro-inflammatory or an M2 anit-inflammatory phenotype, recently it was discovered that microglia promote neurogenesis and oligodendrogenesis in the postnatal SVZ (79), and secret factors that are beneficial for axon regrowth and promote oligodendrocyte differentiation after injury (57) . Additionally, the ability of microglia populations to transition between a M1 and M2 is of particular interest because modulating this transition could possibly create a supportive environment for regeneration(58).

Sonic Hedgehog Signaling in the Mammalian Brain

Cell signaling molecules have the potential to create a supportive environment for regeneration after injury. NSCs and progenitor cells require cell signaling molecules to direct self-renewal, differentiation, and migration. Sonic hedgehog (Shh) has been shown to be involved in regenerative cell processes that include chemotaxis (9), proliferation, and lineage specification. Understanding the endogenous NSC and progenitor cell response to cell signaling molecules like Shh after injury could lead to the design of therapeutic strategies that target specific cell types required for regeneration of the damaged tissue.

The Shh signaling pathway is tightly regulated, complex, and occurs at the cell's primary cilium (73). Shh is synthesized in endothelial cells, ventral forebrain neurons, astrocytes and the choroid plexus of the mammalian brain as an inactive precursor protein that is cleaved and modified by a cholesterol moiety (6; 29; 41). Once released by dispatched, Shh can bind to either patched (Ptch) or hedgehog interacting protein (Hip). Hip acts as a negative regulator of the pathway and can bind Shh on the cell surface or as an untethered receptor. In the absence of Shh, Ptch inhibits signaling by preventing smoothened (Smo) from traveling into the primary cilium. In the canonical Shh signaling pathway, Smo is required for the glioma-associated oncogene (GLI) transcriptional response to occur. Therefore once Shh binds to Ptch, Ptch releases inhibition of Smo that allows Smo to block repression of the GLI transcription factors. GLI transcription factors are then cleaved, become active, and travel to the nucleus where they activate transcription of target genes. GLI3 is the primary transcriptional repressor, while GLI2 is the

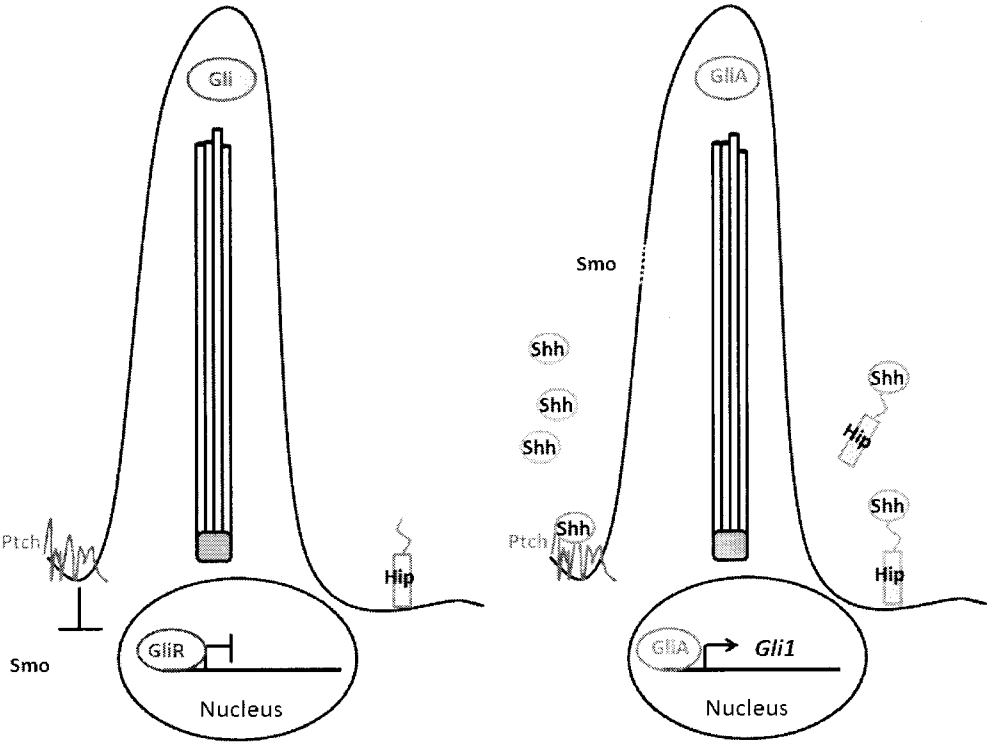

Figure2. A simplified schematic of the sonic hedgehog (Shh) signaling pathway. In the absence of Shh ligand patched (Ptch) inhibits smoothened (Smo) from traveling into the primary cilium. In the presence of Shh ligand Ptch relieves inhibition of Smo allowing Smo to travel up the primary cilium where it can relieve inhibition of the glioma-associated oncogene (GLI) transcription factors. Once activated the GLI transcription factor can travel to the nucleus where it can regulate the transcription of target genes. This figure was modified from Ruat et al., 2012.

principal Shh-regulated transcriptional activator. Nuclear localization of GLI2 indicates active Shh signaling and target genes of GLI2 include *Gli1*, *Wnt*, and *Pdgfrα* (77). GLI1, a transcriptional activator, is often used as a primary readout for active canonical Shh signaling. Target genes of GLI1 include *Ptch*, *Hip*, *Gli1*, *CXCR4* and *cyclinD* (110).

Induction of the Shh pathway can be achieved by the activation of Smo, which can be accomplished by administering smoothened agonist (SAG) (76). Smo activation is not only required in order for GLI transcription factors to become activated but plays a significant role in proliferation and neurogenesis. Interestingly activation of Smo can also lead to noncanonical signaling where Smo function is independent of the primary cilium and activation of the GLI transcription factors (17).

Shh plays a significant role in the specification of lineages in development and involved in regenerative processes following injury. Shh is a morphogen and signaling is dependent on the gradient of Shh in the tissue (32). The concentration of Shh and the duration of signal are important factors that determine neuronal cell fate (102). Shh also induces the expression of *Olig1* and *Olig2*, which are important for production of oliogodendrocyte lineage cells (32). Macrophage mediated pro-inflammatory processes and cytokine production was required for induction of

reactive astrocytes and consequently the expression of Shh, which was maximally active three days after cortical stab wound injury (7). The increase is Shh after injury was also shown to be important in the proliferative response and the number of Olig2+ cells in the injured cortex (7). In a demyelination model, Shh increased oligodendrocyte progenitors and mature oligodendrocytes while decreasing astrogliosiss and the macrophage response (30). Shh has also been implicated as the key factor that elicits a stem cell response from astrocytes in vitro and in vivo (Sirko et al., 2013). It is interesting that this pro-regenerative response from astrocytes may have been dependent on blood brain barrier breakdown because Shh secreted by astrocytes has been shown to promote blood brain barrier integrity through Shh responsive endothelial cells and have an anti-inflammatory effect (6).

Shh is also important for maintaining neurogenesis and proliferation in the adult SVZ (64; 66). *Gli1-CreER*^{T2} driver line of mice, showed ventral NSCs of the SVZ were responsive to Shh signaling (4). Slow cycling NSCs of the SVZ also express *Gli2* and *Gli3* (Petrova et al., 2013). GLI2 and GLI3 are responsible for maintaining adult neurogenesis and proliferation and *Gli* gene expression decreases when NSC become proliferating progenitors. NSCs of the ventral SVZ have been shown to be dependent on Shh signaling in order to give rise to olfactory interneurons, granule interneurons and periglomerular neurons (41; 64).

Summary

Regeneration within the CNS must be optimized following TBI, which may differ with the site and form of damage. Because Shh maintains NSCs and promotes oligodendrogenesis, it is important to investigate whether Shh signaling contributes

to progenitor responses in TBI models. This body of work focuses on the pathological mechanisms and the regenerative response that follow TBI in two heterogeneous models of TBI. The first chapter of this work investigates the pathology and the cellular responses that occur in the first week following TAI in the corpus callosum. The second chapter examines the SVZ repair potential and the contribution of the Shh signaling pathway, based on fate labeling in *Gli1-CreER^{T2}* driver mice, to the regenerative response, following either white or gray matter injury. The regenerative response from *Gli1* heritably labeled neural stem cells was analyzed 2 and 6 weeks post-injury in order to investigate the potential impact this population has on long term regeneration and recovery.

CHAPTER 2:

Oligodendrocyte lineage and subventricular zone response to traumatic axonal injury in the corpus callosum

Genevieve M. Sullivan, B.S.[1,2,3], Amanda J. Mierzwa, Ph.D.[2,3], Naruchorn Kijpaisalratana, M.D.[3,6], Haiying Tang, Ph.D.[3,4,*], Yong Wang, Ph.D.[5], Sheng-Kwei Song, Ph.D.[5], Reed Selwyn, Ph.D.[3,4], and Regina C. Armstrong, Ph.D.[1,2,3]§

Affiliations:

[1]Program in Molecular and Cell Biology

[2]Department of Anatomy, Physiology and Genetics

[3]Center for Neuroscience and Regenerative Medicine

[4]Department of Radiology

Uniformed Services University of the Health Sciences, Bethesda, Maryland USA

[5]Department of Radiology

Washington University, St. Louis, Missouri USA

[6]Department of Internal Medicine, Faculty of Medicine,

Chulalongkorn University, Bangkok, Thailand

doi: 10.1097/NEN.0000000000000009.

ABSTRACT

Traumatic brain injury frequently causes traumatic axonal injury (TAI) in white matter tracts. Experimental TAI in the corpus callosum of adult mice was used to examine the effects on oligodendrocyte lineage cells and myelin in conjunction with neuroimaging. The injury targeted the corpus callosum over the subventricular zone, a source of neural stem/progenitor cells. TAI was produced in the rostral body of the corpus callosum by impact onto the skull at bregma. During the first week post-injury, magnetic resonance diffusion tensor imaging (DTI) showed axial diffusivity decreased in the corpus callosum and corresponding corpus callosum regions exhibited significant axon damage accompanied by hypertrophic microglia and reactive astrocytes. Oligodendrocyte progenitor proliferation increased in the subventricular zone and corpus callosum. Oligodendrocytes in the corpus callosum shifted toward upregulation of myelin gene transcription. *Plp/CreER^T:R26IAP* reporter mice showed normal reporter labeling of myelin sheaths 0-2 days post-injury yet increased labeling between 2-7 days. Electron microscopy revealed axon degeneration, demyelination and redundant myelin figures. Our findings expand the cell types and responses examined to inform DTI evaluation of white matter injuries. Taken together, these results identify pivotal white matter changes following TAI that can potentially impact axonal vulnerability versus recovery following brain injury.

INTRODUCTION

Traumatic brain injury (TBI) is experienced by millions of people worldwide (74) White matter tracts, particularly the corpus callosum (CC), are a common site of damage in TBI that causes traumatic axonal injury (TAI) from high strain forces, including those experienced in contact sports (1; 16; 43; 50; 83). TBI with TAI is associated with neuroimaging indicators of white matter abnormalities which can be detected by computed tomography (CT) in severe TBI patients with diffuse axonal injury but are more difficult to detect in mild-moderate injuries (16; 43; 54). Consequently, additional approaches are being developed with magnetic resonance imaging, such as diffusion tensor imaging (DTI)(15; 39; 43; 54; 63). While mild-moderate TBI patients often recover substantially during a subacute period, one or more symptoms may be experienced chronically, even as a result of a single TBI exposure or without positive findings on a head CT (52; 74). Therefore, improved assessment tools are needed to detect the pathological features that are predictive of a worse outcome. It is particularly important to understand the cellular and molecular changes that can facilitate endogenous repair processes and guide the development of interventions to improve recovery among those identified as at risk of poor recovery. Currently, there are no effective treatments for TAI (83).

TAI is accompanied by complex reactions among glial populations in white matter tracts. Damage to myelin can be a major component of white matter injury. Oligodendrocyte cell loss has been demonstrated within the first week after a moderate fluid percussion injury in rats (48) and in acute and chronic human TBI (78). It is unclear to what extent different forms of TBI result in demyelination along viable axons versus myelin sheath degeneration subsequent to axonal transection. Remyelination of denuded

axons, which can promote functional recovery and prevent further axonal damage, has been clearly demonstrated to occur within the first month after trauma from experimental spinal cord injury (68). Further studies are needed to examine the capacity for remyelination after white matter damage from TBI. In multiple sclerosis and models of experimental demyelination of the CC, oligodendrocyte progenitor (OP) cells persisting in adult white matter, or generated from the subventricular zone (SVZ), proliferate and differentiate into myelin-forming oligodendrocytes to accomplish remyelination (2; 61; 62; 71). Multiple factors in pathological tissues can impair this spontaneous remyelination capacity (33). For example, activated microglia must clear myelin debris for remyelination to proceed effectively (23). However, neuroinflammation from reactive microglia has been observed in the CC of human TBI cases and may contribute to chronic degenerative changes even a year or more after a single TBI (42). Experimental models have shown that in response to diverse forms of CNS trauma reactive astrocytes can produce growth factors that support axon integrity and OP proliferation but can also form glial scars that impair regeneration of transected axons (100). The complement of cellular responses to TAI is important to characterize in order to understand the progression of damage versus repair in the white matter following TBI.

The current study is the first to examine oligodendrocyte lineage changes, from the endogenous neural stem/progenitor cell response through myelination, relative to TAI in white matter in conjunction with neuroimaging. Rodent studies of axonal damage in the CC have focused on the caudal CC overlying the hippocampus to examine memory impairment and regenerative responses from the subgranular zone. The current study examines TAI focused more rostrally to facilitate analysis of the potential for white

matter repair from OP cells within the CC and neural stem cells in the adjacent SVZ, the largest germinal zone in the mammalian CNS. Ex vivo and in vivo DTI were combined with post-imaging histological and immunohistochemical analyses. The extent of TAI was quantified along with changes in myelination. Reactive stages of microglia and astrocytes were characterized as potentially contributing to the interpretation of DTI changes and to regulatory signaling in the lesion environment. The proliferative response of the OP cells in the SVZ and CC was monitored using bromodeoxyuridine (BrdU) pulse-chase labeling. In situ hybridization for proteolipid protein (PLP) enabled identification of oligodendrocytes and comparison of transcriptional activation of this major myelin gene. The PLP promoter was also exploited in *Plp/CreER^T* mice crossed to the *R26IAP* reporter line for conditional inducible expression of alkaline phosphatase (AP) in oligodendrocytes. After tamoxifen administration, only oligodendrocytes with intact processes can label myelin sheaths with AP, which enables screening for potential disruption of the oligodendrocyte-myelin unit after injury. CC regions of interest were further examined by electron microscopy to provide ultrastructural correlation of the pathological findings with the corresponding DTI values and cellular responses. This combination of approaches strengthens the interpretation of DTI findings and indicates potential regenerative changes ongoing in the white matter following TAI.

MATERIALS AND METHODS

All procedures were performed with 8-10 wk old male C57BL/6 mice (Jackson Laboratories, Bar Harbor, Maine) or *Plp/CreER^T:R26IAP* mice (detailed below). Mice were housed singly or in pairs on-site in the animal facility according to the guidelines of

the National Institutes of Health and the Institutional Animal Care and Use Committee of the Uniformed Services University of the Health Sciences.

Traumatic Axonal Injury (TAI)

The method to induce TAI in mice was modified from Creed et al. (24) to involve the rostral body of the CC adjacent to the SVZ and increase head stabilization. An Impact One™ Stereotaxic Impactor device was used to produce a controlled impact to the skull. Mice were placed in the stereotaxic frame and secured with ear bars that were inverted and covered with rubber stoppers. Isoflurane was administered continuously at 2% via a nose cone until immediately after impact. A 3 mm diameter flat impact tip was centered over bregma and set to an impact depth of either 1.0 mm (n = 14), 1.5 mm (n = 29), or 2.0 mm (n = 10) from the skull surface, an impact velocity of 5 m/s, and a dwell time of 100 ms. With these settings for the 1.5 mm depth, video analysis of the impact velocity and depth verified an average impact velocity of 4.7 m/s and depth of 1.7 mm. Sham mice (n = 12) received anesthesia as well as an incision to the scalp. Naïve mice (n = 11) did not receive anesthesia or surgery.

Ex Vivo Cross-Sectional DTI

For ex vivo DTI, CBI (n = 5) and sham (n = 5) mice were perfused with 4% paraformaldehyde at 3 days post-surgery and brains were post-fixed overnight in fixative. Brains were kept in PBS at 4°C for approximately 2 weeks prior to scanning. Images were acquired using a 4.7T Agilent DirectDrive™ small-animal MRI system (Agilent Technologies, Santa Clara, CA) equipped with Magnex/Agilent HD imaging gradient coil (Magnex/Agilent, Oxford, UK) with pulse gradient strength up to 58 G/cm and a gradient rise time $\leq$ 295 μs). Coronal images were acquired throughout the rostral-caudal extent of

the CC and were registered according to the anatomical position at which the anterior commissure crossed the midline. A multiple-echo spin-echo imaging sequence was used to acquire diffusion-weighted images with the acquisition parameters: TR = 800 ms; TE = 33.2 ms; Data matrix: 256 x 256; Field of view = 22 x 22 mm^2; number of slices = 8; slice thickness = 0.5 mm; 3 repetitions; total scanning time = 17 hours. The diffusion encoding scheme employed 99 diffusion-weighting directions selected as prescribed in diffusion spectrum imaging (DSI) where the position vectors are the entire grid points (qx, qy, qz) over the 3-D q-space under the relationship that (qx^2+qy^2 +qz^2) $\leq$ r^2 (sum of square <= square of r), where r = 3 for the current measurements (45; 95; 99): time between diffusion gradients (Δ) = 16 ms; diffusion gradient duration (δ) = 5 ms; Max b_value = 3200 s/mm^2. As previously reported (91), fractional anisotropy (FA), axial ($\lambda_{\parallel}$), and radial diffusivity ($\lambda_{\perp}$), were derived using software written in Matlab (MathWorks, Natick, MA) on a pixel-by-pixel basis. The CC from the midline laterally to the point of ventral curvature in the external capsule was manually defined as Region of Interest (ROI) on the color-coded relative anisotropy maps using NIH ImageJ, as in our previous study (104).

In Vivo DTI Longitudinal Study

An in vivo longitudinal study was carried out on an additional cohort of 5 mice with DTI conducted at -1 (baseline), 1, 3 and 7 days post-surgery. Images were acquired at each time point using a 7T/20 cm BioSpec® system (Bruker NMR Inc., Billerica, MA). Accelerated T2-weighted images were acquired using a 2D RARE (Rapid Acquisition and Relaxation Enhancement) protocol with TR = 12000; TE = 7.5 ms; effective echo times = 15, 45, 75, 105 ms; NA = 4; RARE factor = 4; matrix = 128 x 128

x 50; Field of view = 12.8 mm x 12.8 mm; number of slices = 50; slice thickness = 0.25 mm; slice gap = 0.05 mm/interlaced. T2 images were processed using VivoQuant™ (inviCRO, Boston, MA). Spin echo multi-shot echo-planar-imaging (EPI) sequence was used to acquire diffusion-weighted images with the following acquisition parameters: EPI segments = 8; TR = 3000 ms; TE = 20 ms; Δ = 9 ms; δ = 3.6 ms; Max b_value = 1000 s/mm^2; diffusion directions = 30; Data matrix: 128 x 128; Field of view = 12.8 x 12.8 mm^2; number of slices = 12; slice thickness = 0.5 mm; total scan time 40 minutes. DTI in vivo data was analyzed using TORTOISE software (67).

Histopathology and Immunohistochemistry

Mice were perfused with paraformaldehyde using 3% for frozen section preparations and 4% for paraffin embedding. Brains were further post-fixed by immersion overnight. Paraffin embedded 7 μm sections were stained with hematoxylin and eosin for general analysis of cellular organization and Luxol fast blue with Periodic acid-Schiff (LFB/PAS) to detect myelin and activation of macrophages/microglia, respectively. Frozen 14 μm coronal cryosections were used for Prussian blue stain for hemosiderin combined with pararosaniline nuclear stain (Sigma, St. Louis, MO).

Cryosections (14 μm) were immunostained with the following primary antibodies: rabbit polyclonal βAPP (1:100; Life Technologies, Grand Island, NY), rabbit polyclonal NG2 (1:500; a gift from Dr. William Stallcup), rabbit polyclonal GFAP (1:500, DAKO, Carpinteria, CA), mouse monoclonal myelin oligodendrocyte glycoprotein (MOG; (11)), and rat monoclonal CD11b (1:100; AbCam, Cambridge, MA). Secondary antibodies included donkey anti-rabbit IgG F(ab')$_2$ conjugated with Cy3 (Jackson Immunoresearch, West Grove, PA) to detect βAPP or NG2, goat anti-rat IgG

conjugated with Alexa Fluor 555 (1:200; Life Technologies) to detect CD11b, donkey anti-mouse IgG conjugated with Cy3 (Jackson Immunoresearch) to detect MOG, and goat anti rabbit IgG conjugated with Alexa Fluor 488 (1:200; Life Technologies) to detect GFAP. Sections were counterstained with DAPI (Sigma Aldrich, St. Louis, MO) before mounting with Vectashield (Vector Laboratories, Burlingame, CA). NG2/BrdU and Ki67/GFAP combined immunostained tissues were quantified by manually counting cells immunolabeled in each fluorescent channel and using Spot Advanced (Sterling Heights, MI) to measure the area counted within the corpus callosum and SVZ based on DAPI nuclear staining. Myelination (MOG) was estimated based on pixel intensity values to determine the immunolabeled pixels above background levels within the corpus callosum using Metamorph (Molecular Devices; Downington, PA) as previously detailed (10). Astrogliosis (GFAP) and microglia activation (CD11b) were also quantified by similar thresholding so that pixels above background level correspond to the immunostained area to take into account changes in morphology and/or expression that can accompany reactive gliosis. Axons were identified as damaged based on the presence of dense βAPP immunoreactivity either appearing as large single end bulbs or as multiple swellings along a longitudinal axonal profile (42; 107). Quantification of immunohistochemistry post-TBI was compared to sham or naïve depending on the cross-sectional or longitudinal neuroimaging study design. In the cross-sectional study, the ex vivo DTI data is compared between sham and TBI with both tissues analyzed post-imaging. In the longitudinal study, the in vivo DTI data post-TBI is compared to baseline so that additional naïve mice are the appropriate comparison.

In Situ Hybridization

In situ hybridization was performed using a riboprobe to hybridize to PLP mRNA as previously described (10; 11). After hybridization, labeling was detected with alkaline phosphatase (AP) conjugated sheep anti-digoxigenin and reaction with substrate solution (nitroblue tetrazolium chloride/5-bromo-4-chloro-3-indolyl-phosphate; NBT/BCIP, Dako Carpinteria, CA). The majority of oligodendrocytes of the normal adult CC can be identified by the presence of PLP mRNA transcripts in the perinuclear cytoplasm. A minority of oligodendrocytes in the normal adult CC exhibit a higher level of PLP expression creating a darker substrate reaction that fills the cell body and often extends into the processes. In conditions of remyelination, high PLP expressing cells increase in frequency and in substrate intensity (10; 11).

Analysis of Cell Proliferation

Cells actively dividing at the time of perfusion were identified by immunostaining for Ki67 (rat monoclonal, 1:50; DAKO), which was detected with goat anti-rat IgG conjugated with Alexa Fluor 555 (1:200; Life Technologies). In addition, a pulse-chase labeling protocol was used to monitor the proliferative response of endogenous neural stem and progenitor cells throughout the first week post-surgery. Mice received an intraperitoneal injection with 200 mg/kg of 5-bromo-2'-deoxyuridine (BrdU; Sigma Aldrich) at 24 and 22 hours prior to CBI or sham surgery and tissue was collected at 1, 3, or 7 days post-injury. Tissue sections were processed for immunohistochemistry as above with the addition of digestion with proteinase K (Sigma Aldrich) followed by treatment with 2N HCL prior to the addition of blocking solution. Sections were incubated overnight with anti-BrdU antibody conjugated to fluorescein (Roche Diagnostics, Indianapolis, IN).

Plp/CreER^T:R26IAP mice:

Transgenic *Plp/CreER^T:R26IAP* mice were generated from crosses of the *Plp/CreER^T* driver line to the *R26IAP* reporter line. Mice of both genders were divided into each cohort. In *Plp/CreER^T* mice, the *Plp* promoter drives conditional expression in oligodendrocyte lineage cells of Cre recombinase fused to a mutated estrogen receptor (27). The *R26IAP* mice constitutively express a floxed inverted second exon of the gene for the membrane-associated form of human AP (12). In *Plp/CreER^T:R26IAP* mice, tamoxifen induces heritable AP synthesis in oligodendrocytes, with corresponding AP accumulation in myelin membranes (109). Tamoxifen was administered by oral gavage on two consecutive days (10 mg/day). The primary injury stage of 0-2 days post-injury was examined with tamoxifen administered on day 0 (2 hours prior to sham surgery or 1.5 mm impact) and on day 1 (24 hours post-surgery) followed by perfusion on day 2 after surgery. For analysis of a secondary injury stage between 2-7 days post-injury, tamoxifen was administered on days 2 and 3 after surgery (sham or 1.5 mm impact) followed by perfusion on day 7 after surgery. Coronal tissue sections (14 μm) were incubated in PBS for heat inactivation of endogenous AP activity (69°C for 90 min) and reacted with NBT/BCIP substrate (see above) followed by methyl green nuclear counterstain (Vector Laboratories, Burlingame, CA). The intensity of the AP substrate reaction within the CC was quantified using Metamorph to measure the area of pixels within the range of low, medium, or high intensity levels. Pixel intensities for each level were distinguished and thresholded based on pseudocolor boundaries using the LUT histogram. Levels were set relative the overall AP reaction in the tissue which can be compared between sham and injured mice but not between the two different time periods

due to different lengths of time after tamoxifen administration. The AP intensity index was calculated as the sum of the pixel number in each area multiplied by a weighting factor based on intensity, i.e. index = (low x 1) + (medium x 2) + (high x 3). AP reaction was not detected in tissue sections from mice administered vehicle instead of tamoxifen or in mice with the *R26IAP* allele without *Plp/CreER^T* allele (data not shown).

Electron Microscopy

Mice were perfused with 4% paraformaldehyde. Brains were extracted and post-fixed in 4% paraformaldehyde at 4°C overnight. Sagittal and coronal vibratome sections (40 μm) were cut and placed into 2.5% glutaraldehyde in 0.1M phosphate buffer at 4°C overnight and then processed for osmication and plastic embedding. Ultrathin sections were collected on formvar-coated copper slot grids and post-stained with 2% uranyl acetate followed by Reynold's lead citrate. Digital images were acquired on a JEM-1011transmission electron microscope (JEOL, Peabody, MA) and a XR50 camera (Advanced Microscopy Techniques, Woburn, MA). Demyelinated axons were identified as having undetectable compact myelin when photographed at 5,000x magnification. Quantification of demyelinated axons excluded axons smaller than 0.3 μm in diameter due to overlap with the overall mean diameter of unmyelinated axons being 0.25 ± 0.01 μm in the mouse corpus callosum (89). Demyelinated axons, degenerated axons, and redundant myelin figures were manually counted in sagittal images of six areas (875 μm^2/area; 3 areas per grid) of the CC per mouse with at least 3 mice per condition.

Behavioral Assessment

A beam walk test was used to evaluate individual limb function (108). Mice were trained to walk on a 6-mm wide beam one day prior to injury. Each animal was given one

trial/test period that consisted of walking the length of the beam three times prior to data collection for the initial time point. The number of foot faults accrued over 50 steps was counted for each hind limb.

Controlled Cortical Impact (CCI), which involves craniotomy and impact onto the dura over the cerebral cortex, is known to produce behavioral deficits on a beam walk task even with a mild severity of injury (108). Therefore CCI was used as a positive control for behavioral assessment of impaired function of sensorimotor cortex when performed at the same coronal level of bregma for comparison with the TAI model of skull impact at bregma that is used throughout the current study. CCI was used to produce mild-moderate damage to the right sensorimotor cortex at the same coronal level of bregma. Mice (n = 21) were secured in the stereotaxic frame with ear bars and anesthetized as above. A 3 mm in diameter craniotomy was performed and a 2 mm diameter impact tip was set at the following coordinates: 0 AP, 1.5 ML, -1.0 DV. Cortical impact was set at a velocity of 1.5 m/s and a dwell time of 100 ms.

Statistical Analysis

Immunohistochemistry quantification included at least three sections per mouse and at least three mice per condition. Imaging studies used cohorts of five mice per condition. Behavioral assessments involved between 6-27 mice per condition as noted in results. Results of quantitative analyses were analyzed with Prism 5.0 (GraphPad Software). One-way ANOVA with post-hoc Tukey's test was performed to determine significant differences across multiple time points. The longitudinal in vivo DTI study was analyzed by one-way ANOVA with repeated measures. Significant differences between two groups for a given time point were determined using the Student's t-test,

with the exception of the AP intensity index which was analyzed using the Mann-Whitney test for nonparametric data. Chi-square analysis was performed to verify significance between percentages. Statistical significance was determined as $p < 0.05$.

RESULTS

Surgical and Histopathological Data

Three impact depths (1.0, 1.5, and 2.0 mm) were compared to determine the appropriate parameters for analysis of TAI and CC integrity (Figure 1). Increasing impact depth resulted in a longer duration of apnea and prolonged the time for the righting reflex (Figure 1A, B). Skull fracture and bleeding severity increased, particularly with the depressed skull fractures observed at the 2.0 mm depth (Figure 1C, D). These surgical and post-surgical indicators of injury severity corresponded well with histopathological features (Figure 1F-N). The 2.0 mm injury produced damage in the CC underlying the impact site (Figure 1F) that extended caudally (Figure 1I) and rostrally (Figure 1L) with hemosiderin deposits indicating areas of prior hemorrhage (Figure 1L).

Figure 3. Postsurgical response and histopathology vary with impact depth. (A-E) Increasing the depth of impact increased the duration of apnea (A), delayed the righting response (B), produced more severe bleeding (C), increased the severity of skull fractures (D) (1.0 mm, n = 14; 1.5 mm, n = 29; 2.0 mm, n = 9; sham, n = 7). (E) Behavioral testing indicated that the 1.5-mm depth did not produce a marked cortical injury based on comparison to a positive control for test validity, which was a mild controlled cortical impact (CCI). CCI involved a craniotomy and cortical contusion over the right sensorimotor cortex at the same coronal level. The number of foot faults was increased in the beam walk test only after CCI (*, $p < 0.05$; **, $p < 0.01$; ***, $p < 0.001$; naive, n = 11; CCI, n = 21; 1.5-mm skull impact, n = 11). (FYN) Histopathologic differences based on impact depth are evident in coronal sections with hematoxylin and eosin staining of cytoarchitecture (FYH), Luxol fast blue staining of myelin (IYK), and Prussian blue detection of hemosiderin (LYN). Depths of impact setting are indicated for mice examined at 3 days (FYM) or 1 week (N) after injury. The extensive tissue destruction associated with the 2-mm-impact depth at the level of impact (F) extended caudally (I) as well as rostrally (L) and included extravasation of blood cells (brown), and hemosiderin laden macrophages (L, blue cells; arrows; inset shows enlargement of area near upper arrow) within the cerebral cortex, corpus callosum (CC), and subventricular zone (SVZ) adjacent to the lateral ventricle (LV). The 1.5-mm depth (G, J, M) resulted in less overt tissue destruction with reduced myelin staining in the CC over the LV (J, with higher magnification shown in K). The 1.5-mm depth produced areas with hemosiderin in the superficial cortex (MYN, blue cells; arrows). The 1.0-mm impact did not produce changes detected by hematoxylin and eosin (H) or the other histologic techniques examined (data not shown). Scale bars = (FYJ, shown in H) 1 mm; (K) 100 Km; (LYM) 0.5 mm; (L insert) 100 Km; (N) 2 mm. n.d. = not detected.

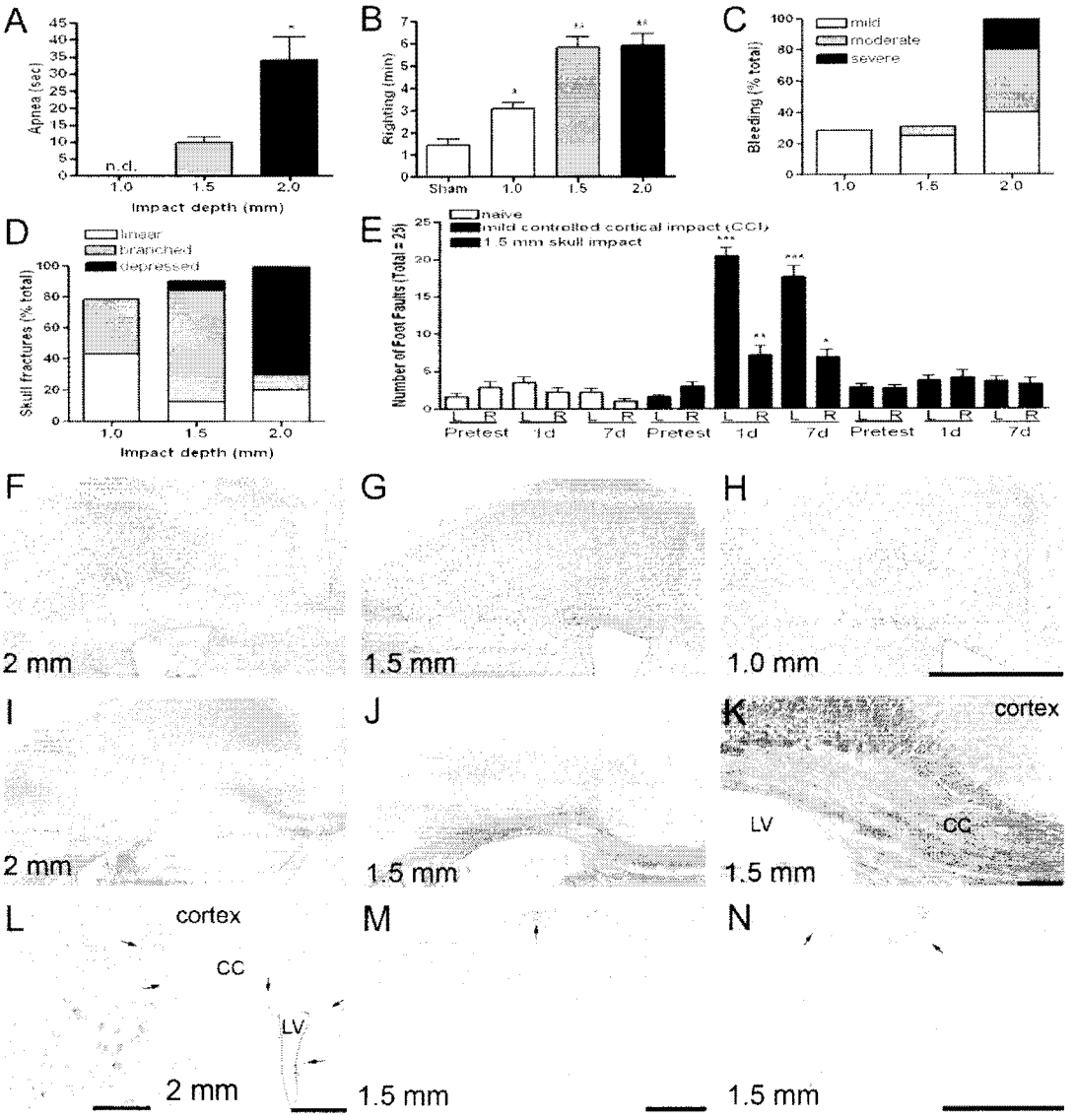
A
Apnea (sec)
n.d.
1.0
1.5
2.0
Impact depth (mm)
B
Righting (min)
Sham
1.0
1.5
2.0
C
mild
moderate
severe
Bleeding (% total)
1.0
1.5
2.0
D
linear
branched
depressed
Skull fractures (% total)
1.0
1.5
2.0
Impact depth (mm)
E
naive
mild controlled cortical impact (CCI)
1.5 mm skull impact
Number of Foot Faults (Total = 25)
L R
Pretest
1d
7d
F
2 mm
G
1.5 mm
H
1.0 mm
I
2 mm
J
1.5 mm
K
cortex
LV
CC
1.5 mm
L
cortex
CC
LV
2 mm
M
1.5 mm
N
1.5 mm

At the 1.5 mm depth, skull fractures were less severe than at 2.0 mm and were typically linear or branched rather than depressed fractures (Figure 1D). Mice with the 1.5 mm impact did not show impairment on the beam walk test in contrast to a positive behavioral control of mice subjected to a mild CCI injury, which involves a craniotomy and contusion damage of sensorimotor cortex (Figure 1E). Following the1.5 mm injury, cortical cavitation was absent (Figure 1G and 1J) or minor and associated with hemosiderin aggregates indicating areas of prior bleeding (Figure 1M-N). The CC exhibited potential areas of demyelination (Figure 1J-K) without marked changes in cellularity (Figure 1G). The 1.0 mm depth produced the least severe post-injury characteristics (Figure 1A-D) but failed to produce consistent evidence of cortical or CC pathology (Figure 1H and data not shown for Luxol fast blue and Prussian blue staining). Based on this characterization of injury severity, the 1.5 mm depth is most relevant for further analysis of the CC to examine TAI without extensive concomitant pathology from cortical cavitation or focal white matter loss.

Ex Vivo DTI with Post-imaging Immunohistochemistry Localizes CC Damage Over Ventricles

Ex vivo DTI was used to localize areas of tissue damage within the CC following 1.5 mm impact. Post-imaging immunohistochemistry was performed to distinguish specific pathological features in the CC at coronal levels with significant DTI findings at 3 days after 1.5 mm impact or sham surgery. Color encoded FA maps illustrate the region-of-interest used for analysis of the CC (Figure 2A-B). The midline crossing of the anterior commissure is also visible and corresponds with the coronal level of the impact centered at bregma.

Figure 4. ***Cross-sectional ex vivo DTI with post-imaging tissue analysis.***
A-B: Color encoded fractional anisotropy (FA) maps from ex vivo DTI of brains at 3 days post-sham (A) or 1.5 mm impact (B). Coronal slices show the level of the anterior commissure (ac) midline crossing, which corresponds with the coronal level of impact to the skull at bregma. The color reflects the fiber orientation within the white matter tracts (red = medial-lateral; green = superior-inferior; blue = anterior-posterior). The corpus callosum region-of-interest is outlined in white. Scale bar = 1 mm. **C-E:** Comparison across 0.5 mm coronal slices for values of fractional anisotropy (C) and the underlying components of axial (D) and radial (E) diffusivity. Data shows slices throughout the body of the corpus callosum (2 = caudal; 6 = ac; 7 = rostral) at 3 days after sham surgery or CBI. A significant decrease in axial diffusivity was observed in slices 5 and 6 of TBI mice as compared to sham. $*p < 0.05$ and $**p < 0.01$ for injury (n = 5) vs sham (n = 5) for each slice based on two-way ANOVA. **F-J:** Quantification of axon damage (F; βAPP, β-amyloid precursor protein immunolabeling), microglia/macrophage activation (G; CD11b immunolabeling), astrogliosis (H; GFAP, glial fibrillary acidic protein immunolabeling), myelination (I; MOG, myelin oligodendrocyte glycoprotein immunolabeling), and cellularity (J; DAPI nuclear stain) in the corpus callosum at coronal levels within slices 5 and 6 after ex vivo MR imaging. Significant increases in axon damage (F), microglia/macrophage activation (G), and astrogliosis (H) are evident without changes in myelination (I) or cellular density (J). $***p < 0.0001$, $*p < 0.05$ in TBI (n = 5) vs sham (n = 5). Values shown as mean ± s.d.

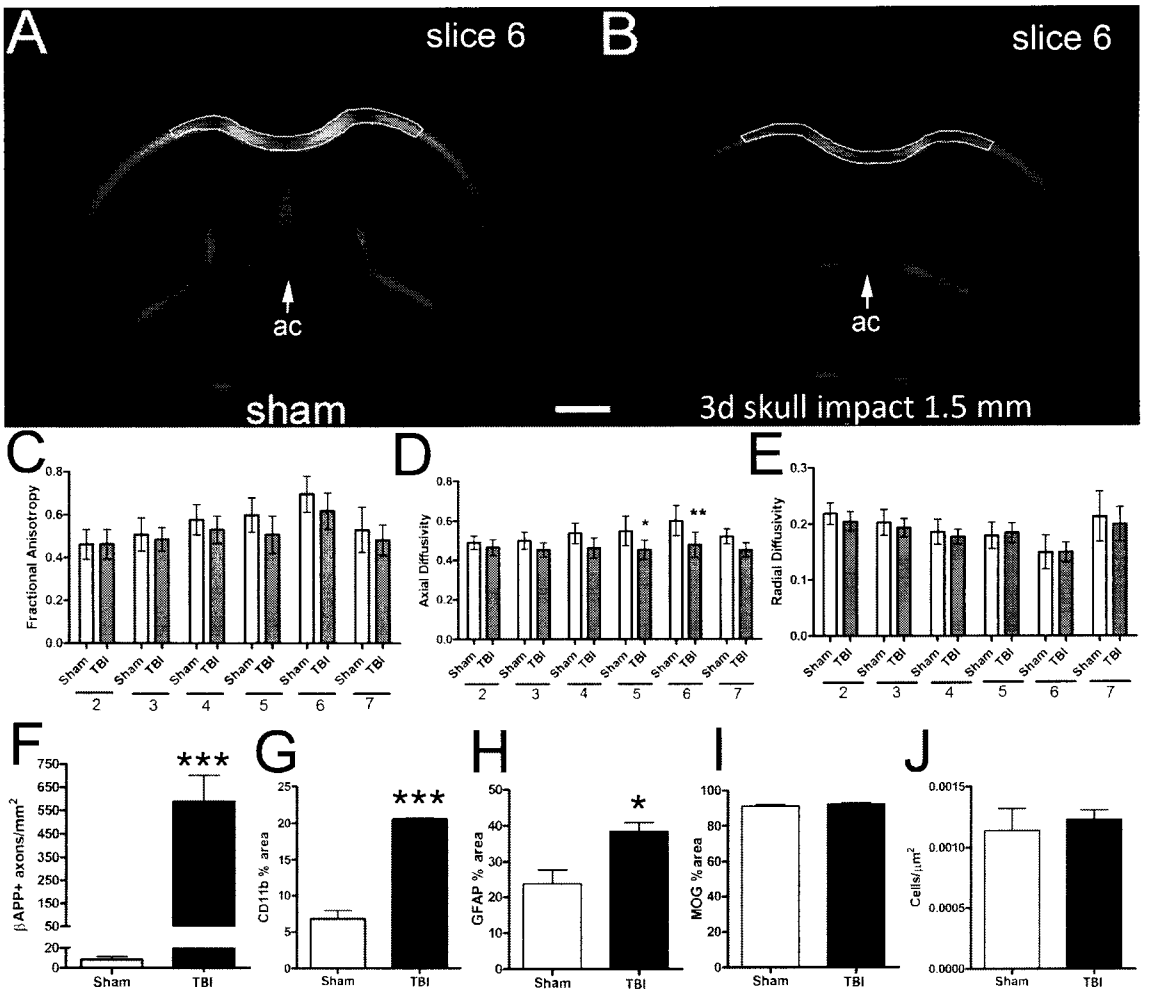
A
slice 6
ac
sham
B
slice 6
ac
3d skull impact 1.5 mm
C
Fractional Anisotropy
D
Axial Diffusivity
E
Radial Diffusivity
Sham
TBI
2
3
4
5
6
7
F
βAPP+ axons/mm²
***
Sham
TBI
G
CD11b % area
***
H
GFAP % area
*
I
MOG % area
J
Cells/μm²

Coronal slices (0.5 mm thick) throughout the rostro-caudal extent of the CC were analyzed to quantify FA and the diffusion tensor derived components of axial ($\lambda_{\parallel}$; parallel to fiber tract) and radial ($\lambda_{\perp}$; perpendicular to fiber tract) diffusivity (Figure 2 C-E). A progressive variation of FA values is observed across coronal levels that may be associated with neuroanatomical changes in the CC thickness and fiber composition (72; 104). The FA values for injured mice were reduced but not significantly different from sham mice. Analysis of axial and radial diffusivity showed that a significant difference between injured and sham occurs only in axial diffusivity and was specifically found in coronal slices near the plane of bregma, the point of impact.

In CC regions with reduced axial diffusivity, immunohistochemistry for βAPP showed a significant increase in the number of labeled axon profiles, indicating axonal damage (Figure 2F). Microglial activation was also significantly increased based on CD11b immunoreactivity (Figure 2G). Immunolabeling for GFAP was increased as well indicating reactive gliosis (Figure 2H). Widespread demyelination was not apparent based on the similarity of myelin immunoreactivity between the CBI and sham mice (Figure 2I). The cell density was not altered between injured and sham mice (Figure 2J).

In Vivo Longitudinal DTI Demonstrates Reduced CC Integrity Through the First Week Post-Injury

We next performed an in vivo longitudinal series of MR scans to evaluate the progression of changes in the CC from pre-injury baselines values across the first week post-injury from the 1.5 mm impact (Figure 3). The CC did not show overt structural changes with T2-weighted imaging. However, signal hyperintensity in T2-

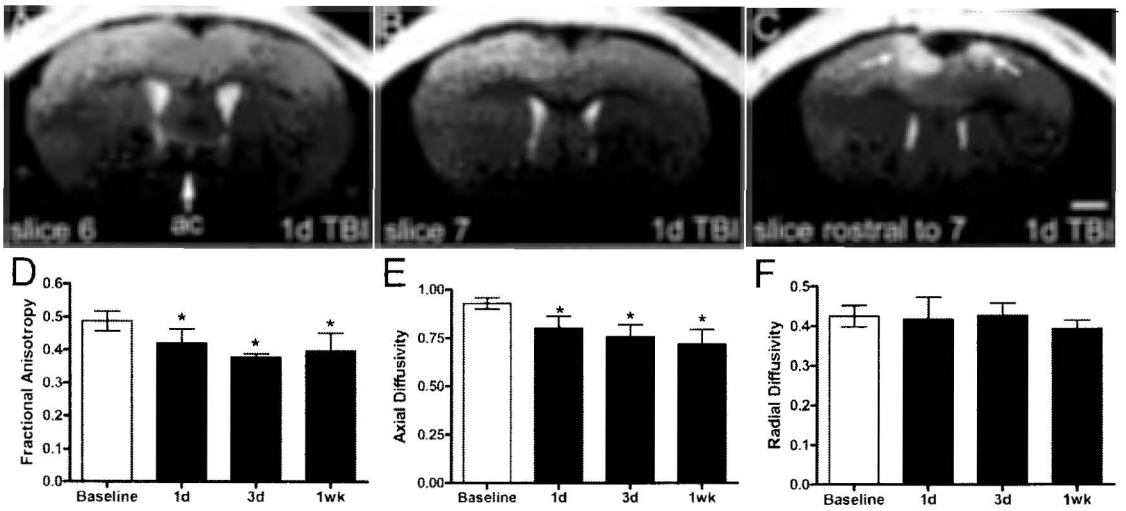

Figure 5. Longitudinal in vivo MRI of the cerebral cortex and corpus callosum after 1.5 mm skull impact.

A longitudinal cohort (n = 5 mice) was scanned for baseline measurements on the day prior to TBI with repeat scans post-injury after 1 day (1d), 3 days (3d) and 1 week (1wk). A-C: T2-weighted imaging at the coronal level corresponding to the impact site (A; ac = midline crossing of the anterior commissure; slice 6) and at more rostral levels within the body of the corpus callosum (B; slice 7) and further rostral (C; rostral to scanned region). Areas of T2 signal hyperintensity are present in the superficial cortex in C (arrows). Scale bar for A-C shown in C = 1 mm. D-F: Quantitative analysis of fractional anisotropy (D) and the underlying components of axial (E) and radial (F) diffusivity across pre- and post-injury time points. Data represents values from the corpus callosum in coronal slices (0.5 mm x 2) corresponding to slices 5 and 6 of the ex vivo analysis (see Figure 2 for region-of-interest and coronal levels). FA and axial diffusivity values are significantly reduced after injury. *$p < 0.05$ using one way ANOVA with post-hoc comparisons to baseline. Values shown as mean ± s.d.

weighted imaging was often observed in the superficial region of the cortex, particularly at coronal levels rostral to the impact (Figure 3C; slice level is rostral to slices quantified for DTI and shows the same mouse with cortical hemosiderin deposits in Figure 1N). In vivo DTI quantitative analysis of the CC focused on coronal levels corresponding to significant DTI differences identified in the ex vivo analysis (Figure 2D; slices 5 and 6). Consistent with reduced white matter integrity, FA values in the CC were significantly reduced at 1, 3, and 7 days post-TBI compared to baseline. Axial diffusivity values were also significantly decreased at each post-injury time point while radial diffusivity was unchanged from baseline. Mice were perfused after the last in vivo MRI scans at 7 days post-TBI and examined for immunohistochemistry along with additional cohorts of mice to compare naïve mice with the progression of changes at 1, 3, and 7 days post-TBI.

Acute TAI is Present in the CC Through First Week Post-Injury

βAPP accumulations in axons of the CC were significantly increased at all time points following 1.5 mm impact (Figure 4A-F). Therefore, the reduced FA and axial diffusivity values correspond with axon damage in the CC in the same mice analyzed after ex vivo (Figure 2F; 3 days post-TBI) and in vivo imaging (Figure 4E; 7 days post-TBI). An additional cohort of mice demonstrates βAPP accumulations in axons at each of the time points (1, 3, and 7 days post-TBI) corresponding to the longitudinal DTI study (Figure 4F). βAPP accumulations were also observed in the cingulum and external capsule, but not in the internal capsule (data not shown).

Microglia in CC Exhibit Hypertrophic Activation

The microglial response is an important element for interpreting the pathological environment relative to the influence on DTI and the tissue milieu following

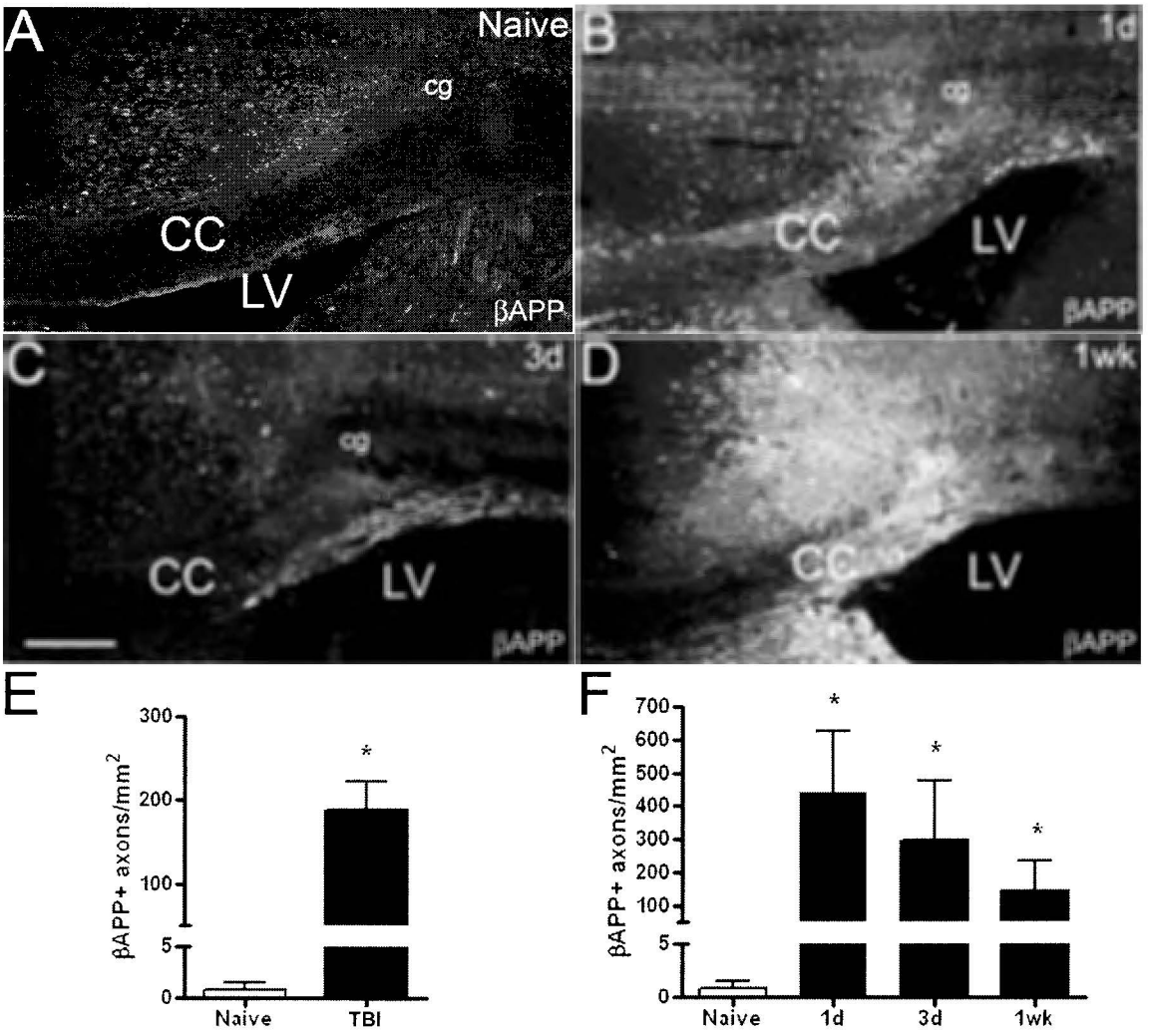

Figure 6. βAPP demonstration of impaired axonal transport in the corpus callosum. A-D: Immunohistochemistry on coronal brain sections for β-amyloid precursor protein (βAPP) as an indicator of axon damage that is associated with impaired rapid axonal transport. A: In naïve mice, βAPP is present in the cytoplasm of cortical neurons but immunoreactivity in the corpus callosum (CC) reflects only background staining. B-D: Mice with 1.5 mm injury show βAPP immunoreactivity in axonal swellings in the CC that are most prominent over the lateral ventricles (LV). E-F: Quantification of the βAPP immunolabeled axons in the CC. E: Comparison of naïve and CBI mice at 1 week post-injury (*$p < 0.05$; $n = 5$) from the cohort of mice used for the longitudinal DTI (Figure 3). F: Analysis of βAPP within cohorts sampled at each of the time-points used for MRI (naïve/baseline, 1 day, 3 days, and 1 week post-CBI; $n = 3$ mice per time point). A significant increase of βAPP indicates axon damage at each time point (*$p < 0.05$ compared to naïve). Scale bar for A-D is shown in C = 200 μm. Cg = cingulum.

Figure 7. Microglia/macrophage activation within the corpus callosum. Immunohistochemistry for CD11b to detect microglia/macrophage cells in coronal sections from non-injured naïve mice (A-B) and mice at 1 week after 1.5 mm skull impact (C-D). The corpus callosum is indicated by hashed lines in A and C. E-G: Higher power images illustrate the range of reactive morphological changes of CD11b immunolabeled cells in the corpus callosum. CD11b cells in naïve mice have fine elaborate processes (E). CD11b immunolabeled cells have more condensed processes after 1.5 mm skull impact which is present from 1 day (F) through 1 week (D) post-injury. After a 2.0 mm impact, more severe reactive changes are associated with a rounded morphology and lack of processes among CD11b immunolabeled cells (G). H: Quantification of CD11b immunoreactivity in the corpus callosum shows a significant increase in microglia/macrophage activation at 1 week post-TBI (1.5 mm impact) compared to naïve control mice (*$p = 0.0122$; $n = 5$). Quantification shows post-imaging tissue analysis from the cohort of mice used for the longitudinal DTI (Figure 3). Scale bar for A, C shown in A = 200 μm. Scale bar for B, D shown in B = 75 μm. Scale bars in E-G = 40 μm. LV = lateral ventricle.

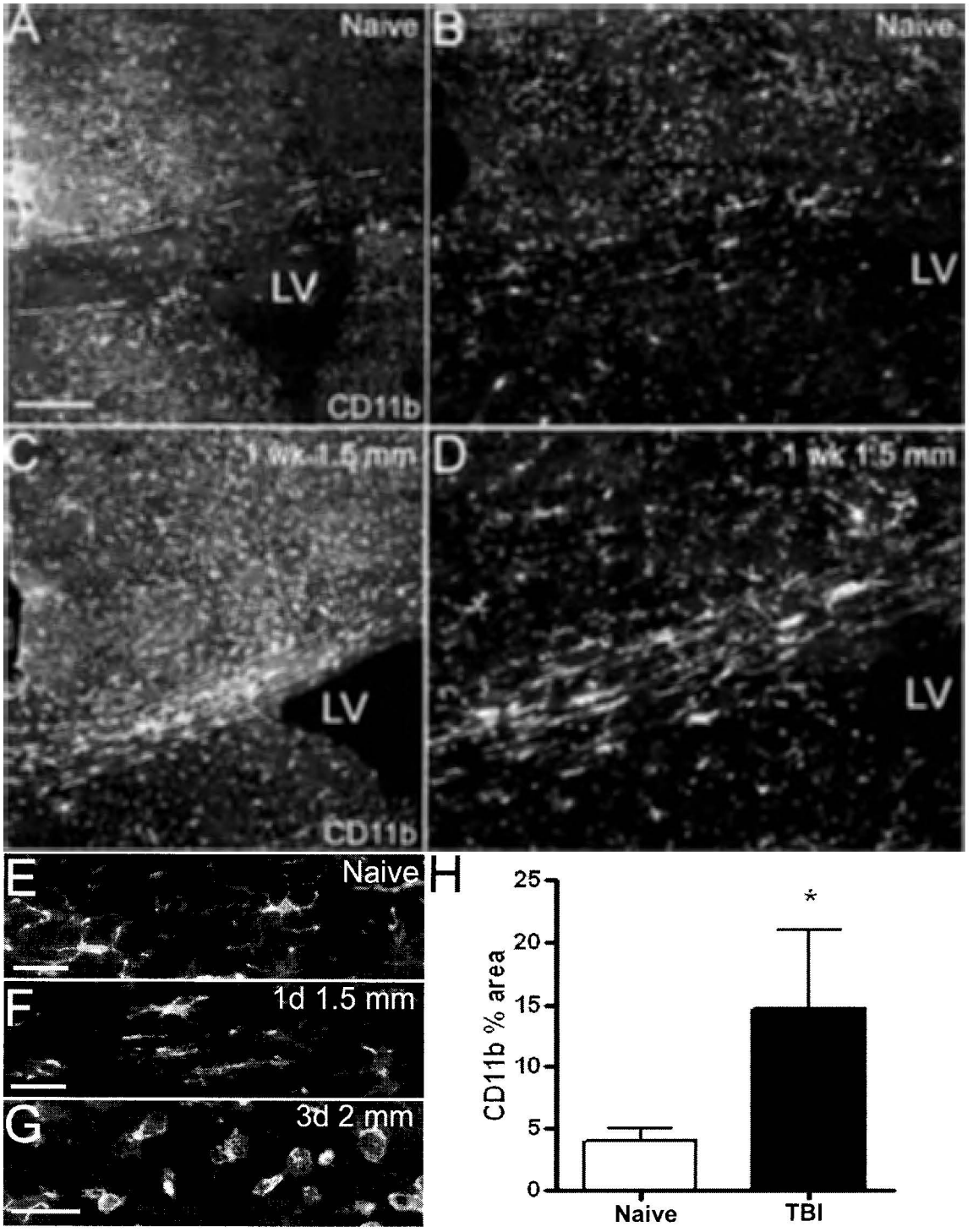
A
Naive
LV
CD11b
B
Naive
LV
C
1 wk 1.5 mm
LV
CD11b
D
1 wk 1.5 mm
LV
E
Naive
F
1d 1.5 mm
G
3d 2 mm
H
CD11b % area
25
20
15
10
5
0
*
Naive
TBI

TAI. CD11b immunohistochemistry was used to characterize microglia and macrophage activation following 1.5 mm impact (Figure 5). CD11b immunoreactivity was significantly increased in the CC in injured mice at 7 days post-injury as compared to naïve mice (Figure 5). Interestingly, the morphology of the CD11b immunolabeled cells in mice with the 1.5 mm impact indicated an intermediate hypertrophic stage of activation with thickened processes (Figure 5D, F). This activation appeared within the first day and continued throughout the time points examined. With a 2.0 mm depth impact, microglial activation progressed to a full ameboid stage (Figure 5G). Therefore, microglial activation in the CC white matter corresponded more directly with injury severity than time post-injury within this first week.

Proliferative Response in CC is Distinct From Astrogliosis

Astrogliosis was characterized by expression of GFAP, cell morphology, and proliferation (Figure 6). GFAP expression was increased in the CC at 1, 3, and 7 days post-injury (1.5 mm; Figure 6A-D). Periventricular astrogliosis was present in injured mice but was not a consistent finding. GFAP immunoreactivity showed marked staining of dense astrocyte processes in the CC in TBI mice as compared to naïve mice. Proliferation is an indicator of progression to more severe stages of astrogliosis (85). Actively proliferating cells were identified by Ki67 immunolabeling (Figure 6A-D). Cell proliferation was increased significantly in the CC at 1 and 3 days post-TBI (Figure 6F). However, astrocyte proliferation (Ki67+ GFAP+ cells) was not significantly increased in injured mice at 1, 3, or 7 days versus naïve mice (peak = 12.59 ± 3.91 s.d. cells/mm^2 at 1 day post-TBI).

Figure 8. Astrogliosis and cell proliferation within the corpus callosum.

A-D: Immunohistochemistry in coronal brain sections to detect actively dividing cells with Ki67 and evaluate astrogliosis based on expression of glial fibrillary acidic protein (GFAP). Ki67 shows proliferating cells within the subventricular zone at all time points (A-D) and in the corpus callosum mainly at 1 and 3 days post-TBI (B, C). GFAP expression is increased through 1 week post-TBI (B-D) as compared to naïve conditions (A). Proliferating cells include reactive astrocytes (C, inset) but relatively few cells are double labeled (GFAP+ Ki67+). E: Quantification of GFAP immunolabeling indicates that reactive gliosis is significantly increased in the corpus callosum 1 week after injury (*$p < 0.0001$; $n = 5$). This quantification shows values obtained post-imaging for the cohort of mice used in the longitudinal DTI study (Figure 4). F: Quantification of Ki67 immunolabeled cells within the corpus callosum shows proliferation is significantly increased at 1 and 3 days after injury and returns to baseline values at 1 week (*$p < 0.05$ compared to naïve; $n = 3$ per time point). Scale bar for A-D shown in D = 200 μm. LV = lateral ventricle.

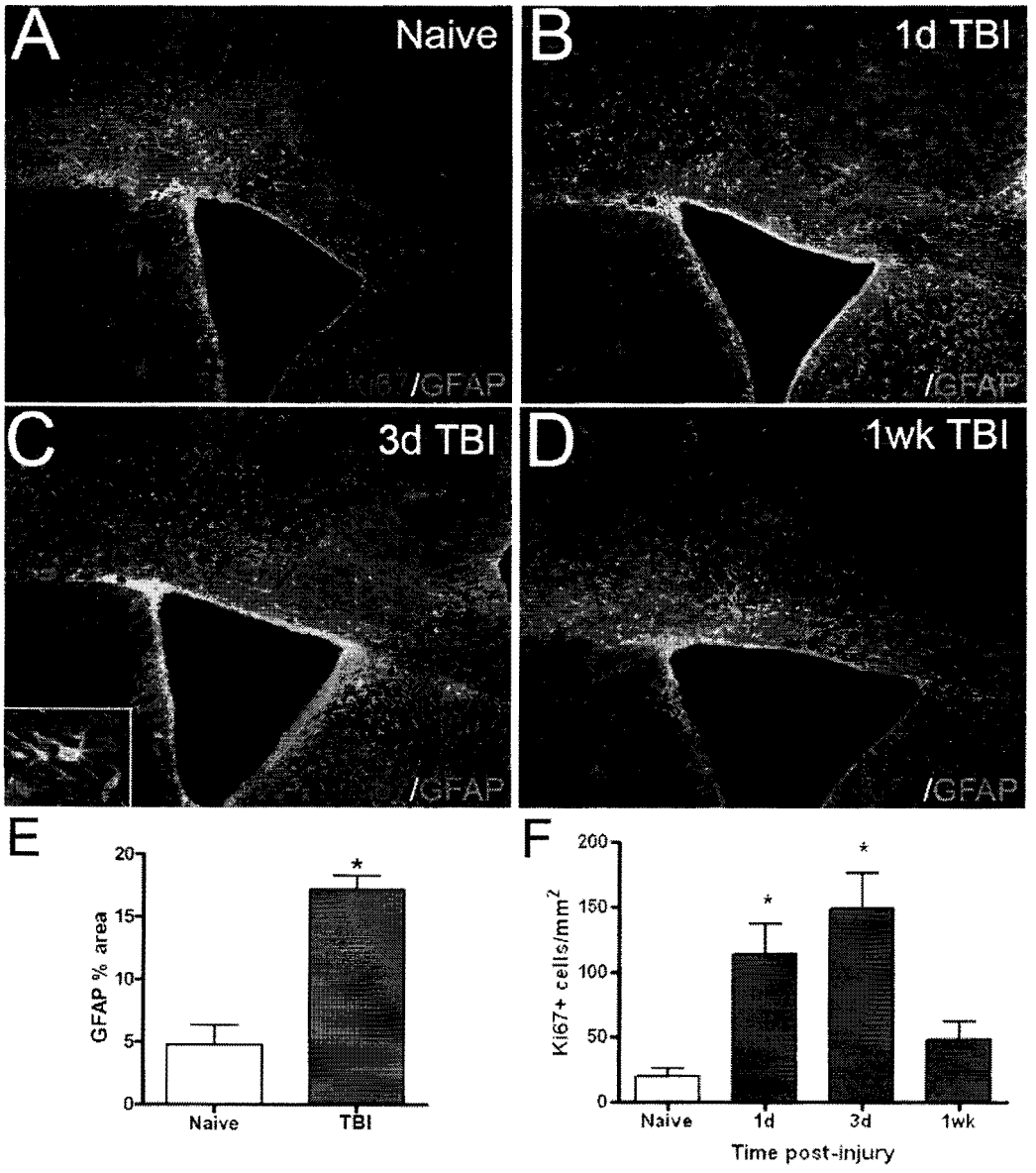
A
Naive
/GFAP
B
1d TBI
/GFAP
C
3d TBI
/GFAP
D
1wk TBI
/GFAP
E
GFAP % area
20
15
10
5
0
*
Naive
TBI
F
Ki67+ cells/mm2
200
150
100
50
0
*
*
Naive
1d
3d
1wk
Time post-injury

Figure 9. Proliferation within the subventricular zone.

Overall proliferation within the subventricular zone (SVZ) was quantified using Ki67 to immunolabel actively dividing cells (A, and images in Figure 6) and a BrdU pulse-chase protocol to label endogenous cycling cells prior to injury and monitor the post-injury response (B-D). **A:** The density of Ki67 immunolabeled cells in the SVZ is similar across post-TBI (1.5 mm impact) time points, indicating that there is not a significant difference of cells actively dividing within the SVZ at the time of tissue analysis ($p = 0.702$; $n = 3$ mice per time point). **B-D:** BrdU was administered 1 day before TBI and cells were analyzed in the SVZ at 1, 3 and 7 days post-TBI. Age matched naïve mice were injected with BrdU and perfused in parallel with the TBI mice. Quantification of BrdU immunohistochemistry shows similar values in the SVZ for each time point (B; for each time point, $n = 3$ naïve, $n = 5$ injured). Coronal sections illustrating BrdU immunolabeled cells in the SVZ for a BrdU pulse-chase shown at 1 day post-TBI (D) and for a matched naïve mouse (C). **E-H:** NG2 immunohistochemistry to determine the oligodendrocyte progenitor response in the SVZ relative to axonal injury in the overlying corpus callosum (CC). Coronal sections illustrate BrdU pulse-chase shown at 3 days post-TBI (F) and at matched time point for a naïve mouse (E). Arrows denote examples of NG2 cells in SVZ. Arrowheads indicate examples of BrdU labeled nuclei (E, F). The total NG2 cell density remained constant throughout the first week after injury (G). The proportion of NG2 cells labeled with BrdU indicates that the proliferative response changes significantly in the injured mice relative to the matched naïve time points (H, $^{**}p = 0.0047$ for 1d; $p = 0.0058$ for 3d; $n = 3$ naïve and $n = 5$ TBI for each time point). Scale bar for C-D = 100 μm as shown in D and for E-F = 100 μm as shown in F. LV = lateral ventricle.

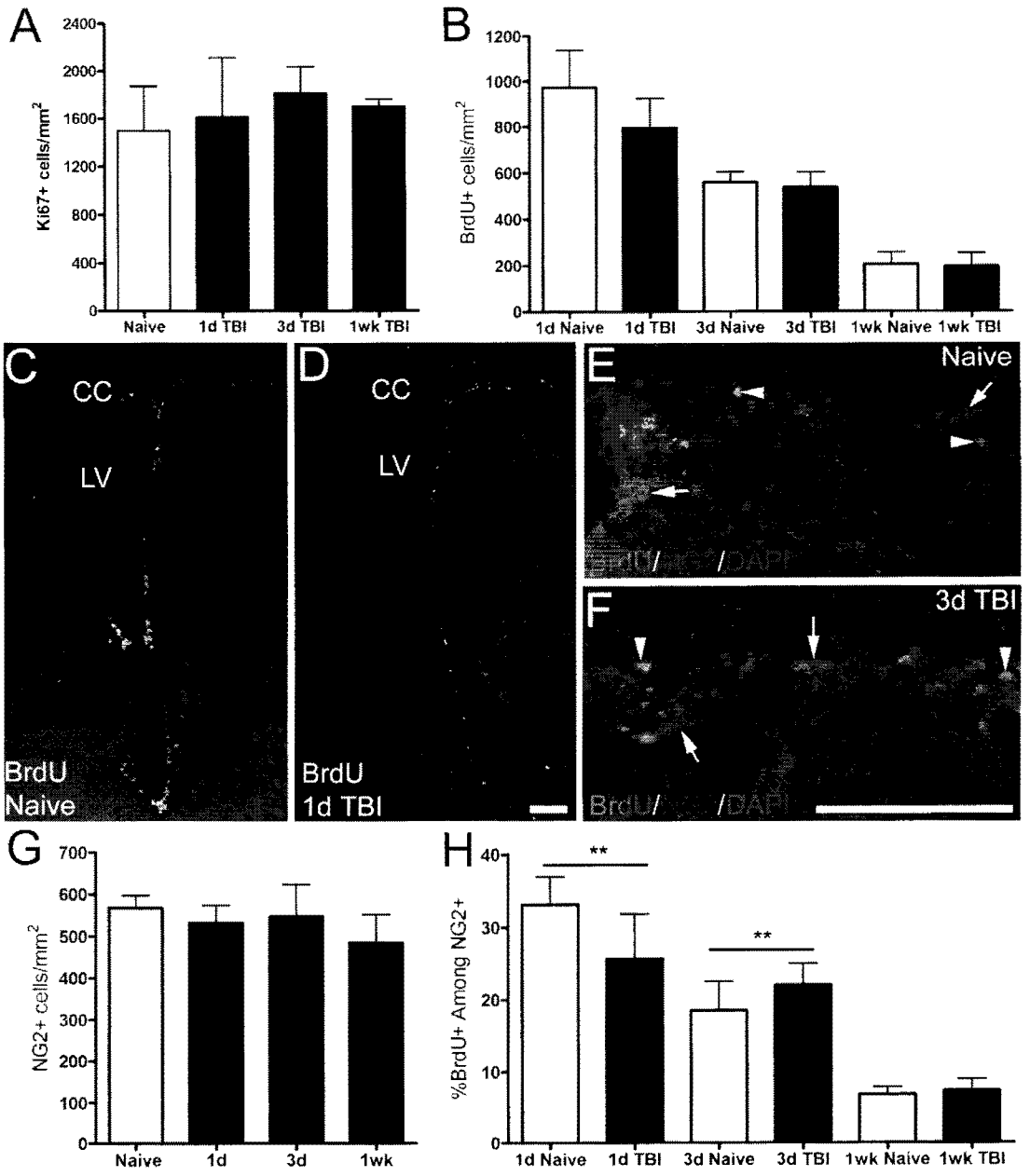
A
Ki67+ cells/mm2
2400
2000
1600
1200
800
400
0
Naive
1d TBI
3d TBI
1wk TBI
B
BrdU+ cells/mm2
1200
1000
800
600
400
200
0
1d Naive
1d TBI
3d Naive
3d TBI
1wk Naive
1wk TBI
C
CC
LV
BrdU
Naive
D
CC
LV
BrdU
1d TBI
E
Naive
/DAPI
F
3d TBI
BrdU/
/DAPI
G
NG2+ cells/mm2
700
600
500
400
300
200
100
0
Naive
1d
3d
1wk
H
%BrdU+ Among NG2+
40
30
20
10
0
**
**
1d Naive
1d TBI
3d Naive
3d TBI
1wk Naive
1wk TBI

NG2 Progenitor Proliferation Increases in the SVZ and CC Post-TBI

The SVZ is a source of neural stem cells that can replace cells in the adjacent CC following damage. Ki67 immunohistochemistry showed similar levels of cells actively dividing in the SVZ throughout the first week post injury (Figure 7A). To specifically examine the SVZ neural stem cell response between pre- and post-injury stages, BrdU was administered 1day prior to injury and then mice were perfused at 1, 3, or 7 days post-injury. BrdU labeling in the SVZ was similar at each time point between paired injured and naïve cohorts (Figure 7B-D). Therefore, the severity of this TBI is not sufficient to stimulate an overall proliferative response in the SVZ.

Among the neural cell types generated from the SVZs the OP population is specifically relevant to CC white matter damage. Therefore, BrdU incorporation was examined among OP cells identified by NG2 immunolabeling (Figures 7E-H and 8). In the SVZ region, OP proliferation was initially reduced but increased significantly by 3 days post-TBI (Figure 7H), indicating potential induction of oligodendrocyte lineage cell generation from neural stem cells of the SVZ. Within the CC, proliferation of OP cells was increased 3 and 7days after injury (Figure 8F, G). Furthermore, by 1 week after injury, the OP population was significantly increased in the CC in comparison with the matched naïve cohort (Figure 8H).

Oligodendrocytes Shift Transcriptional Activation Post-TBI

In situ hybridization for PLP mRNA was used to examine the oligodendrocyte response to 1.5 mm impact (Figure 9). During myelination and remyelination, oligodendrocytes up-regulate transcription of myelin genes, with PLP being the most abundant myelin gene. Therefore the presence of PLP mRNA signal was used to identify oligodendrocytes while the signal intensity and distribution provided additional

Figure 10. Oligodendrocyte progenitor population increases within the corpus callosum. A-D: Immunohistochemistry for oligodendrocyte progenitors, identified by NG2 (red), and BrdU (green) to detect proliferation in coronal brain sections. BrdU was administered on the day before TBI (1.5 mm impact). Mice were perfused on days 1 (B), 3 (C) and 7 (D) post-injury. Age matched naïve mice (A) were injected with BrdU and perfused in parallel with the TBI mice. Green arrows show examples of cells immunolabeled only for BrdU. White arrows show examples of cells double labeled for BrdU and NG2. **E:** BrdU immunolabeling in the corpus callosum appears higher after injury but does not reach significance ($p = 0.0709$). **F:** The proportion of NG2 cells that have detectable BrdU increases at 3 and 7 days post-TBI ($*p < 0.05$, $**p< 0.01$, respectively). **G:** Illustration of double labeling for BrdU (green) in the nucleus and NG2 (red) on the cell body and processes along with DAPI nuclear staining (blue). Example shown is cell at arrow in D. **H:** The total NG2 population is significantly increased at 7 days post-TBI compared to naïve values ($*p < 0.05$). For each value shown (E, F, and H), n = 3 naïve mice and n = 5 TBI mice at each time point. Scale bar for A-D shown in A = 200 μm. Scale bar for G = 15 μm. CC = corpus callosum, cg = cingulum, LV = lateral ventricles.

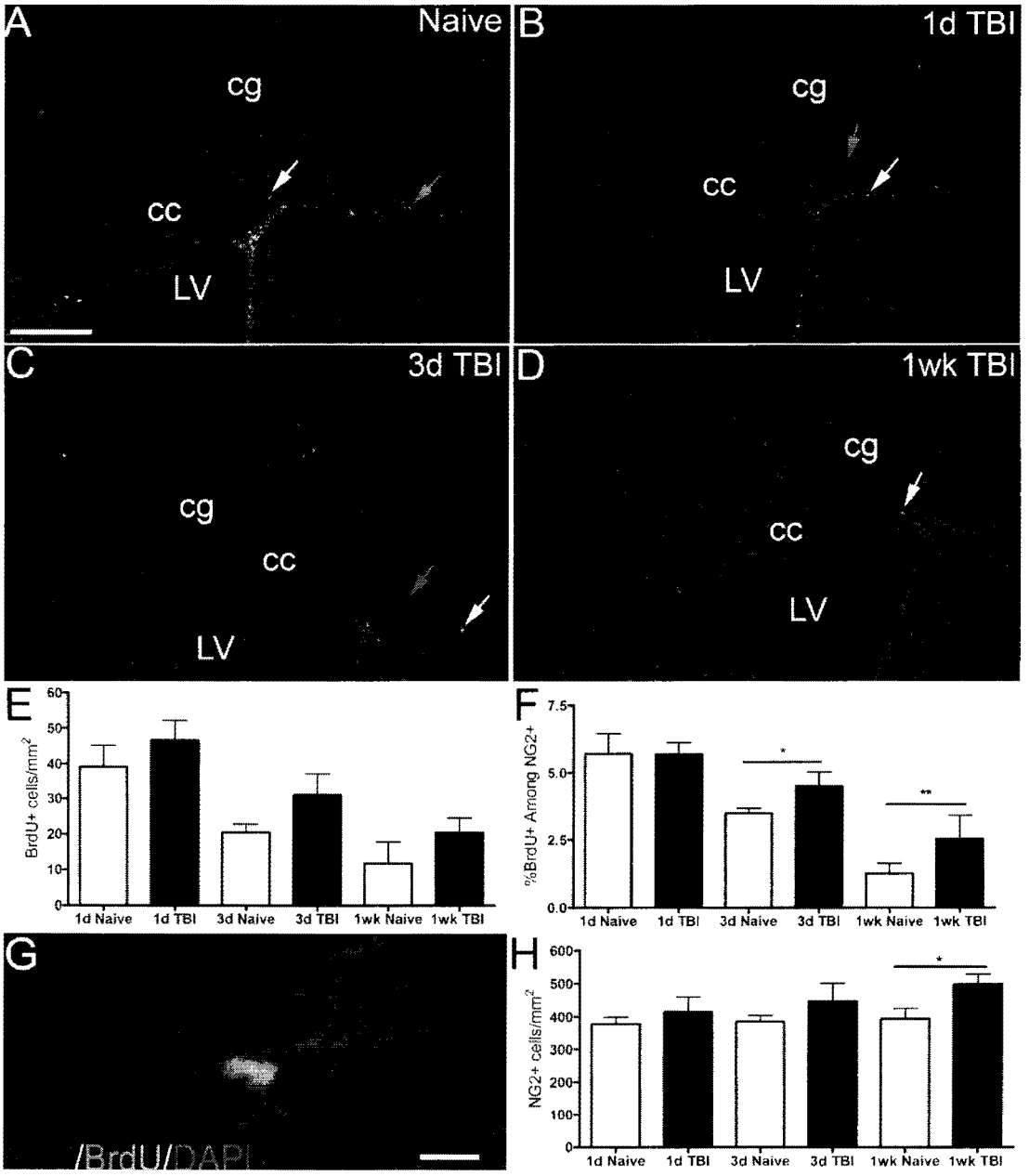
A
Naive
cg
cc
LV
B
1d TBI
cg
cc
LV
C
3d TBI
cg
cc
LV
D
1wk TBI
cg
cc
LV
E
BrdU+ cells/mm2
60
50
40
30
20
10
0
1d Naive
1d TBI
3d Naive
3d TBI
1wk Naive
1wk TBI
F
%BrdU+ Among NG2+
7.5
5.0
2.5
0.0
*
**
1d Naive
1d TBI
3d Naive
3d TBI
1wk Naive
1wk TBI
G
/BrdU/DAPI
H
NG2+ cells/mm2
600
500
400
300
200
100
0
*
1d Naive
1d TBI
3d Naive
3d TBI
1wk Naive
1wk TBI

Figure 11. PLP transcription is altered in oligodendrocytes of the corpus callosum. In situ hybridization for PLP mRNA in coronal sections from mice perfused at 1day, 3 days, and 1week post-TBI (1.5 mm impact) compared to naïve mice. A-B: Coronal sections illustrating PLP transcripts in naïve (A) and 1 week post-TBI mice (B). Insets show examples of oligodendrocytes with low (A inset) and high (B inset) levels of PLP mRNA signal. C-E: Quantification in the corpus callosum for the total number of PLP expressing oligodendrocytes (C). Oligodendrocytes with a low level of PLP transcripts are more abundant in normal adult mice (D) than oligodendrocytes with high PLP expression (E). Sample size of cohorts was n = 3 (naïve and 1 day post-TBI), n = 4 (3 days post-TBI), and n = 5 (1 week post-TBI). The density of total oligodendrocytes does not differ significantly across time points (C, $p = 0.0949$). The number of oligodendrocytes with low levels of PLP transcript decreased 1 and 3 days after injury (D, $*p < 0.05$). Oligodendrocytes that expressed high levels of PLP mRNA were increased at 1 week after TBI but not significantly different (E; $p = 0.1769$). F: Analysis of the proportion of PLP low and high expressing cells shows a significant shift that takes into account the simultaneous changes in both populations at a given time point (F, $**p < 0.001$, $***p < 0.0001$). Scale bar for A and B shown in B = 200 μm. Scale bar for inserts in A and B shown in insert B = 10 μm. CC = corpus callosum, cg = cingulum, LV = lateral ventricle.

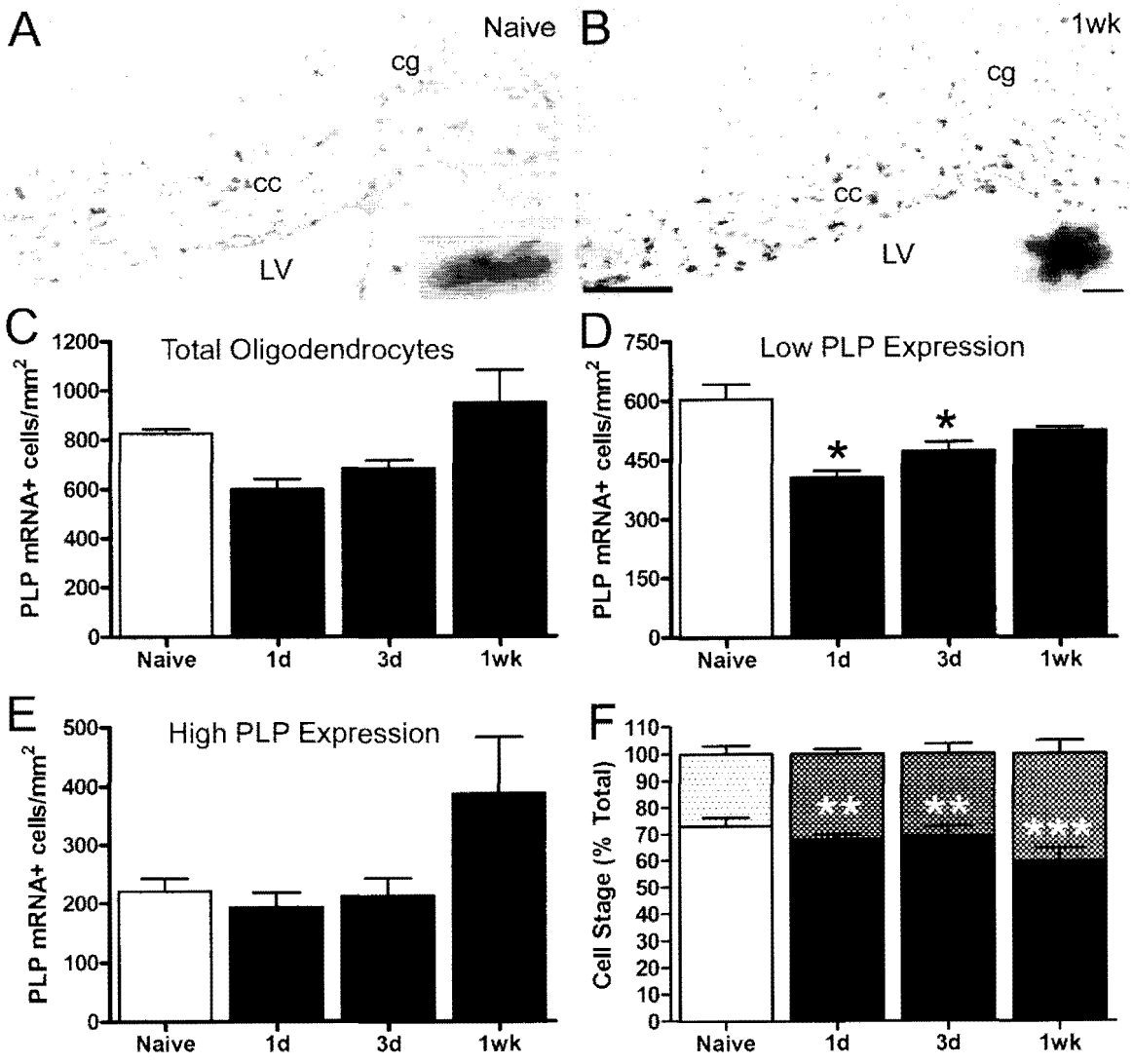
A
Naive
cg
cc
LV
B
1wk
cg
cc
LV
C
Total Oligodendrocytes
PLP mRNA+ cells/mm2
1200
1000
800
600
400
200
0
Naive
1d
3d
1wk
D
Low PLP Expression
PLP mRNA+ cells/mm2
750
600
450
300
150
0
*
*
Naive
1d
3d
1wk
E
High PLP Expression
PLP mRNA+ cells/mm2
500
400
300
200
100
0
Naive
1d
3d
1wk
F
Cell Stage (% Total)
110
100
90
80
70
60
50
40
30
20
10
0
**
**
***
Naive
1d
3d
1wk

indications of transcriptional activity. Oligodendrocytes were classified according to PLP transcript expression being low (Figure 9A inset) or high (Figure 9B inset). The total oligodendrocyte population decreased by approximate 30% within a day of injury (Figure 9C). Low PLP cells represent the majority (73.14 ± 5.4%) of the oligodendrocyte population in the normal CC of naive mice and were significantly decreased at 1 and 3 days in injured mice (Figure 9D). At 7 days post-TBI, high PLP expressing cells were visually notable (Figure 9B). A shift toward an increase in high versus low PLP expression in injured versus naïve mice was significant at all post-injury time points and most prominent at 1 week.

Integrity of Myelin-oligodendrocyte Unit Following Impact Injury

Immunohistochemistry for MOG myelin protein correlates well with electron microscopy and Luxol fast blue myelin stain for quantification of focal demyelination within the mouse CC (10; 47). However, after the 1.5 mm impact injury, MOG immunoreactivity did not detect differences in the extent of myelination within the CC (Figure 10A-B). Reduced intensity of MOG immunoreactivity was often noted but focal regions of frank myelin loss were not evident. During this first week post-injury, MOG immunoreactivity could reflect intact myelin but degenerating myelin could also stain along axons prior to phagocytosis and clearance (49).

To more specifically evaluate the integrity of the myelin-oligodendrocyte unit after injury, we developed a novel approach utilizing Plp/CreERT driver mice crossed to R26IAP reporter mice. The Plp/CreERT:R26IAP mice conditionally express the AP membrane protein after tamoxifen administration (Figure 10C). After 1.5 mm impact

Figure 12. The oligodendrocyte-myelin unit is altered during the secondary injury stage. A-B: A coronal section immunolabeled for myelin oligodendrocyte glycoprotein (MOG) to detect myelin and for glial fibrillary acidic protein (GFAP) to examine astrogliosis. MOG immunoreactivity appeared less intense in regions of astrogliosis (A) but the myelinated area in the corpus callosum was not significantly different between sham and TBI mice throughout the first week of injury (B). C-L: Plp/CreERT:R26IAP reporter mice were used to test the ability of oligodendrocytes to synthesize alkaline phosphatase (AP; a membrane-associated reporter molecule), transport AP along processes, and incorporation AP into myelin sheaths (C). Plp/CreERT:R26IAP mice were administered tamoxifen to induce recombination and expression of AP via inversion of the floxed AP second exon. Tamoxifen (Tam) induction was used to visualize AP labeling of myelin during either a primary injury stage (0-2 days) or during a secondary injury stage (2-7 days) (D). AP incorporation into myelin was apparent as a blue substrate reaction in coronal brain sections, particularly in the corpus callosum (E-H). I-L: Quantification of the area of AP labeling took into account variation in the intensity of signal among regions of the corpus callosum. During the primary injury stage, the sham and TBI (1.5 mm impact) mice had similar proportions of labeling within the corpus callosum for all AP intensities (I). During the secondary injury stage, the overall proportion of the corpus callosum labeled was not different but there was a shift among the areas based on AP intensity (K). A weighted AP intensity index (J, L) was used to semi-quantitatively compare the AP labeled areas while taking into account the relative area exhibiting low, medium, and high AP levels. The AP intensity index is significantly increased in TBI mice compared to sham only during the secondary injury phase (L; *$p = 0.0260$). Sample size of cohorts was $n = 12$ for was primary injury stage (6 sham, 6 TBI) and $n = 11$ for secondary injury stage (5 sham, 6 TBI). Scale bar for A = 200 μm. Scale bar for E-H shown in E = 200 μm.

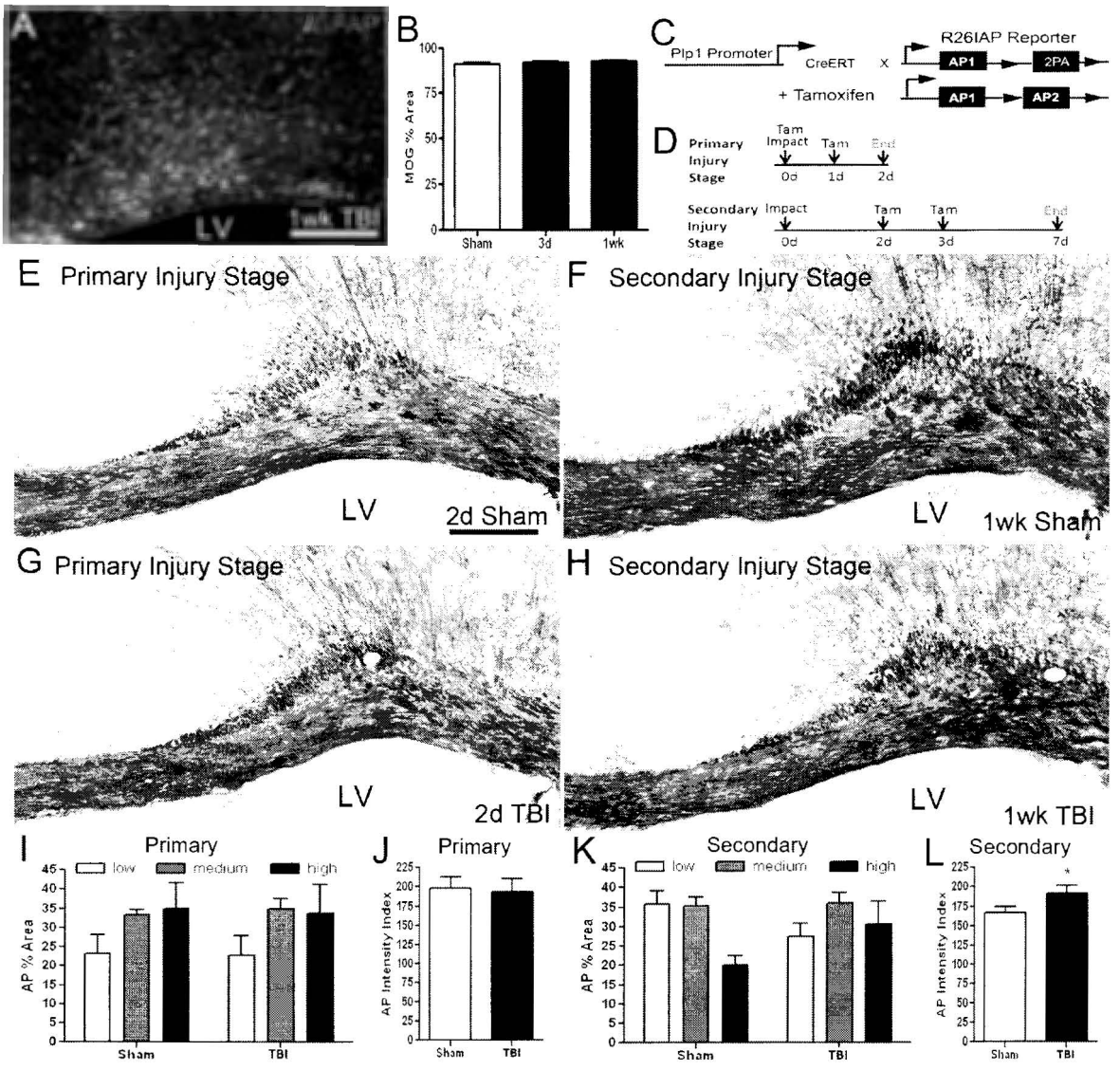
A
LV
1wk TBI
B
MOG % Area
Sham
3d
1wk
C
Plp1 Promoter
CreERT
X
R26IAP Reporter
AP1
2PA
+ Tamoxifen
AP1
AP2
D
Primary Injury Stage
Tam Impact
Tam
End
0d
1d
2d
Secondary Injury Stage
Impact
Tam
Tam
End
0d
2d
3d
7d
E Primary Injury Stage
LV
2d Sham
F Secondary Injury Stage
LV
1wk Sham
G Primary Injury Stage
LV
2d TBI
H Secondary Injury Stage
LV
1wk TBI
I
Primary
low
medium
high
AP % Area
Sham
TBI
J
Primary
AP Intensity Index
Sham
TBI
K
Secondary
low
medium
high
AP % Area
Sham
TBI
L
Secondary
AP Intensity Index
Sham
TBI

injury, Plp/CreERT:R26IAP mice were examined with tamoxifen treatment protocols designed to evaluate oligodendrocyte synthesis and translocation of AP into myelin during either a primary injury stage (0-2 days) or a secondary injury stage (2-7 days) (Figure 10D). This approach demonstrated AP labeling of myelin in the CC during the primary injury stage was similar between injured and control mice (Figure 10E, G, I, J). Therefore, oligodendrocyte processes to myelin sheaths are not significantly disrupted by the initial impact-injury. During the secondary injury phase, AP labeled regions had proportionally higher signal intensity values in the injured mice which resulted in a significant increase of the AP intensity index compared to sham mice (Figure 10F, H, K, L).

Ultrastructural Evidence of Myelin Abnormalities and Axon Damage After Injury

Electron microscopy of the CC was used to further investigate changes related to myelination and the correlation with TAI after 1.5 mm impact injury (Figure 11). Sagittal sections from sham mice illustrate the small diameter and thin myelin of axons in the CC over the lateral ventricles (Figure 11A). CC regions from mice 1 week post-TBI exhibited degenerating axons with dark axoplasm and accumulation of vesicles, indicative of disrupted axonal transport (Figure 11B-C). The majority of degenerating axons still had visible myelin, which often was split or ballooned off the remaining axon segment (Figure 11D). Myelin sheaths were often collapsed around a dystrophic axon or back onto themselves if the axon was no longer present. Extensive myelin figures that resembled redundant myelin sheaths were significantly increased in the injured tissue (sham = 0.63 ± 0.1269/mm2x103; TBI = 25.37 ± 4.055/mm2 x103; p = 0.0037. These redundant myelin figures were distinctive for the large extent of myelin, usually folded

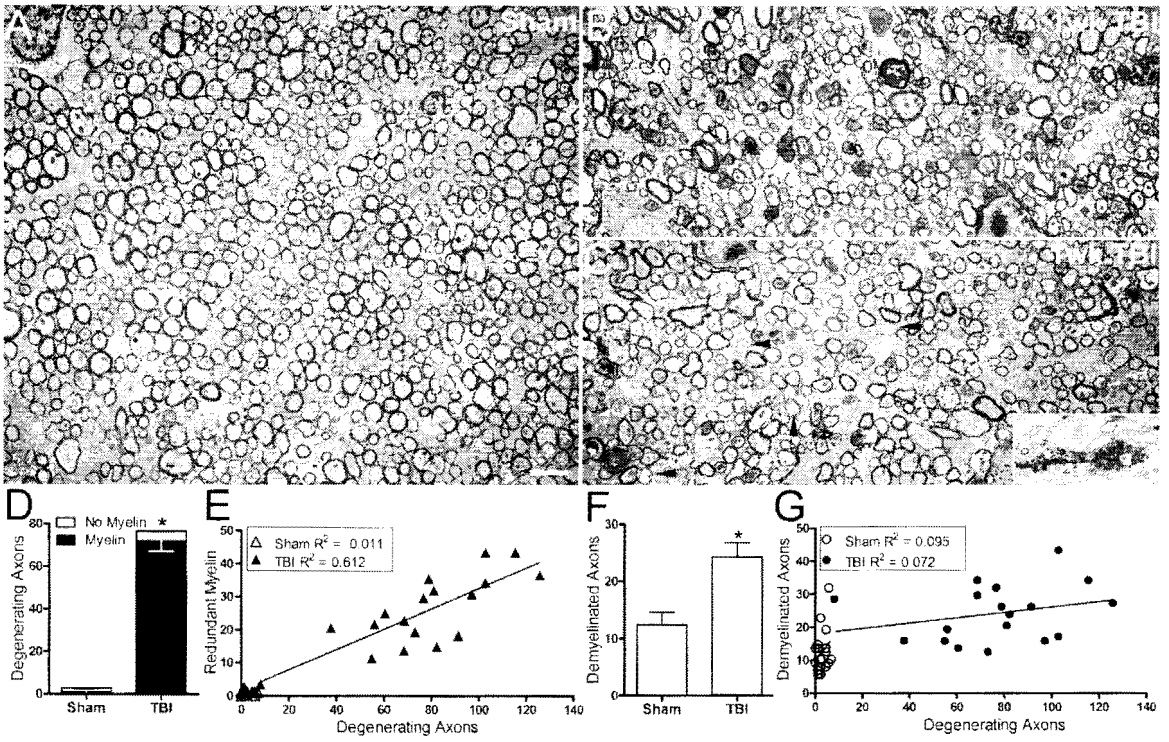

Figure 13. Electron microscopy of the corpus callosum illustrates axon and myelin changes following injury. A-C: Sagittal sections of the corpus callosum from sham (A) and 1 week post-TBI (B, C; 1.5 mm impact). A normal distribution of myelinated fibers is shown in the sham mouse (A). After TBI, axon degeneration (white arrows; B, C) is prominent. Degenerating axons exhibit swellings with accumulation of vesicles (inset C). Examples of demyelinated fibers are also apparent in images from the TBI mice (black arrowheads; B, C). The TBI tissues also had notably elongated, redundant myelin figures (white arrowheads) associated with degenerating axons (B, arrowhead furthest to right) or void of an axon (B, arrowhead along bottom). D-G: Quantification of axon and myelin pathology. Axon degeneration was significantly increased at 1 week post-injury (1.5 mm) versus sham ($p < 0.0001$ for total fibers) which was mainly associated with myelinated fibers ($p < 0.0001$ fibers with myelin, black; $p < 0.0058$ fibers without myelin, gray)(D). Redundant myelin figures were highly correlated with degenerating axons in TBI mice (E). Demyelinated axons were significantly increased in TBI mice (F) but did not correlate with the frequency of degenerating axons (G). Sample size of cohorts was n = 3 for each condition, sham and TBI at 1 week post-surgery. Scale bar for A-C in C = 2μm. Scale bar for inset in C = 2 μm. Values shown are mm2x103.

back onto itself, well beyond simple sheath collapse (Figure 11B, C). Redundant myelin figures were highly correlated with degenerating axons (Figure 11E). Demyelinated axons were also more prevalent in the injured tissues (Figure 11F) (sham = 12.43 ± 2.16/mm^2 x10^3; TBI = 24.29 ± 2.47/mm^2 x10^3; p = 0.0226. However, demyelination did not correlate specifically with the frequency of degenerating axons (Figure 11G).

DISCUSSION

The current study interrogates white matter integrity using DTI and multiple methods of tissue analysis to characterize the complement of dynamic cellular responses to TAI in the CC. These findings are the first to demonstrate oligodendrocyte lineage changes, from neural stem cell through myelination, in the context of white matter TAI without extensive concomitant pathology from cortical cavitation or focal white matter loss.

Surgical and neuroimaging data (Figures 1-3) establish important benchmarks for reproducibly generating CC TAI pathology and for comparison with other studies of experimental TBI. The electrically controlled impact device provides a relatively consistent system but variation in using impactor devices cannot be avoided even with the same manufacturer and model device. High speed video recording of the impact was used to improve calibration across cohorts in the current study (data not shown). Variation could be reduced by excluding mice based on specific parameters, such as depressed skull fractures which correspond with more severe bleeding. However, linear skull fractures may be considered an interesting component of the impact injury given that skull fractures are found in over 30% of mild-moderate human TBI cases (103).

MR imaging provided important cross-sectional and longitudinal data throughout the first week post-TBI (Figures 2-3). T2-weighted imaging indicated normal CC structure but showed initial signal hyperintensity in the rostral cerebral cortex that largely resolved between 3-7 days after 1.5 mm impact (Figure 3C-F). This finding indicates potential edema in the superficial cortex immediately below the impact site. In a similar injury model involving the posterior CC, measurement of tissue water content demonstrated cortical edema that did not extend to involve the hippocampus or thalamus (24). Our studies also show that cell density in the CC is not changed at 3 days post-injury (Figure 2J). These findings support a lack of detectable CC edema in this TAI model. The CC also did not exhibit marked hemorrhages, which could be detected in the superficial cortex by varying extents of hemosiderin in macrophages (Figure 1M-N). Our DTI studies show that axial diffusivity was reduced throughout the first week post-TBI while radial diffusivity was unchanged. These DTI measures may be less predictive of

axon and myelin changes in conditions of edema, hemorrhage, and/or increased cell density from inflammation (97). However, these conditions in the CC do not appear to be significant with this injury at the time points examined. Our DTI data and tissue analysis of cellular responses to TAI should be useful for analyzing the progression of TBI pathology over time and for comparing the advantages of other neuroimaging techniques in detecting more complex pathologies. Our findings of reduced axial diffusivity (Figures 2-3) are consistent with findings in the CC following repetitive mild closed head trauma producing mild axonal damage with microglial activation (14). Radial diffusivity is often increased in demyelinating conditions (86; 104) and the lack of change in the current study (Figures 2-3) is important for correlation with the dispersed pattern of limited demyelination observed (Figures 10-11).

The axon damage in the CC at this early injury stage shows impaired fast axonal transport occurring in a diffuse pattern. Immunoreactivity for βAPP which accumulated in axons after injury (Figure 4) detects βAPP in vesicles carried by fast axonal transport (88). Accumulation of βAPP in axons within a day post-TBI (Figure 4F) is consistent with the timing of βAPP accumulation in the CC in a rat model of impact acceleration TBI (107). Electron microscopy also provided ultrastructural evidence of vesicle accumulation in degenerating axons at one week post-injury (Figure 12B, C). This ultrastructural analysis demonstrated a pattern of degenerating axons interspersed among populations of apparently intact axons, as is typical of TAI associated with diffuse axonal injury in human white matter after TBI (1; 83). Additional approaches would be required to detect the full extent of axon degeneration in the CC (25; 26; 94). In clearly demonstrating impaired axonal transport by βAPP and electron microscopy, the current

findings can be interpreted as reproducibly producing limited TAI in the CC to examine the subsequent cellular and neuroimaging changes of white matter. However, the current studies do not attempt to examine very early time points or events initiating TAI since mechanical forces that initiate TAI in gyrencephalic human brain may not be appropriately replicated in lissencephalic mice (83; 93).

Astrogliosis and microglial activation were observed during the first week after TAI. Astrocyte reactivity included hypertrophy and disruption of distinct territories without a significant increase in proliferation (Figure 6). Microglia became hypertrophic but did not progress to an ameboid morphology (Figure 5). In a subset of mice subjected to a deeper 2 mm impact injury, ameboid microglia were prevalent in regions of hemorrhage indicated by hemosiderin aggregates (Figures 1L and 5G). Similar to our results, human TBI specimens also do not typically exhibit ameboid microglia in the CC during the acute stage (42). Microglial activation may increase when TBI is experienced at an older age (44) or after a second concussive injury (80). In addition, microglia may become activated early after a single injury and subsequently transition to an ameboid state with persistent activation during subacute through chronic stages in cases of diffuse TAI (42; 84). The majority of cell death observed in chronic TBI white matter is comprised of activated microglia, which may also have a "by-stander" effect in causing continued oligodendrocyte cell death (101). Myelin debris also stimulates microglial neuroinflammation (23). These complex cellular interactions of microglia, oligodendrocytes, and myelin may initiate during the acute stage and contribute to a cycle of perpetuating white matter pathology.

Limited demyelination was present in this early stage CC injury, consistent with a lack of ameboid microglial morphology that would correspond with significant phagocytosis of myelin debris. Demyelinated fibers were identified by electron microscopy as distributed among adjacent intact myelinated fibers (Figure 11C). CC areas under the cingulum often showed reduced myelin staining with Luxol fast blue (Figure 1K). Focal regions of frank demyelination were not observed with the 1.5 mm impact depth (Figures 1J and 10) but were produced with a more severe injury from the 2.0 mm depth (Figure 1F and 1). Our findings indicate that focal myelin loss is mainly associated with more severe TAI and white matter hemorrhage or neuron cell body damage (1; 31). However, even with moderate forms of TAI, oligodendrocyte loss has been demonstrated and may be due to caspase 3 mediated cell death mechanisms (48).

Our data demonstrate that TAI in the CC resulted in an early loss of oligodendrocytes (Figure 9D) followed by OP proliferation (Figures 7H and 8F) and a phenotypic shift of oligodendrocytes toward increased transcription of myelin genes (Figure 9F). These changes indicate a potential regenerative response following white matter injury. Studies in multiple sclerosis models of experimental demyelination of the CC have shown that OP cells are generated from neural stem cells of the SVZ and/or from proliferation of resident cycling cells within the CC. Importantly, these OP cells are capable of differentiating into oligodendrocytes during remyelination (2; 35; 61). Overall cell proliferation in the SVZ was not stimulated by TAI based on Ki67 immunolabeling up to 1 week post-injury (Figure 7A). This finding is consistent with rat fluid percussion data for Ki67 in the SVZ that showed no difference at 2 weeks followed by an increase at 6 months (21). Within the overall SVZ response, we identified changes relevant to white

matter injury using NG2 to identify early OP cells and administering BrdU prior to injury for incorporation into endogenous cycling cells to avoid reactive proliferation of astrocytes and microglia. This approach detected increased proliferation of OP cells in the SVZ at 3 days post-TBI followed by an increase in the CC at 3 and 7 days. An increase in total NG2 cells occurred in the CC by 7 days. CCI injury also resulted in a significant increase of NG2 cells in the CC but with an opposite time course that was significantly increased at 1 day post-injury and resolved by 7 days (21). This difference may reflect a rapid reactive OP response after damage to cortical neuron cell bodies with CCI as compared to our data of TAI injury within the white matter that stimulated a proliferative response to generate an increase in the number of OP cells by 7 days. A study using tcf4 to identify OP cells using a moderate-severe fluid percussion model of TBI also reported increases in the CC (31). However, these tcf4 cells are difficult to interpret as OP cells since co-labeling was not found with Olig2, which labels cells at all stages of the oligodendrocyte lineage. Prior studies of oligodendrocyte and OP responses in the CC have not been combined with the approaches used here to interpret potential regenerative changes of proliferation, myelin gene upregulation, or SVZ changes.

A shift toward a higher level of PLP transcription and AP labeling in *Plp/CreER^T:R26IAP* mice suggests activation of oligodendrocyte synthesis after TAI. Oligodendrocyte processes appear intact after the impact injury since AP labeling of myelin was not reduced during the 0-2 day period (Figure 10J). This novel approach definitively distinguishes active oligodendrocyte protein synthesis and transport to myelin which could not be otherwise detected as occurring specifically during this 0-2 day period. During the subsequent 2-7 day post-TBI period, AP labeling shifted from low

to high levels (Figure 10L). Importantly, our findings of oligodendrocytes with high levels of PLP mRNA transcripts are similar to observations of remyelination in experimental models of multiple sclerosis (10; 11). An increased density of oligodendrocytes with high PLP mRNA levels (Figure 9F) indicates increased PLP promoter activity to drive Cre recombinase expression, which remains active after tamoxifen administration, and therefore increases the probability of AP expression between 2-7 days post-injury. Differences in the AP labeling of myelin sheaths could also indicate differences in the proportion of non-compact versus compact myelin after TBI. Non-compact myelin can have components move by lateral diffusion in the membrane as well as vesicular transport in the cytoplasm while compact myelin is a barrier to vesicular transport (81). Therefore, higher AP levels may be observed when new oligodendrocyte processes are being elaborated while low AP levels may correspond with areas of compact mature myelin.

Ultrastructural demonstration of remyelination by electron microscopy would require a longer post-injury period for remyelination to progress and would also be extremely challenging to quantify given the distributed pattern of axon damage and demyelination in this model along with the very thin myelin and small axon diameters of the mouse CC (68). Interestingly, we observed extensive myelin associated with degenerating axons or absent of an intact axon (Figure 11B). These structures resemble redundant myelin sheaths that have been attributed to excess myelin outgrowth during myelin formation or in conjunction with changes in axon diameter (65; 75). Analyses of demyelination and remyelination should take into consideration the volume of excess

myelin membrane in these abnormal myelin sheaths, which could skew quantitative measures such as western blot analyses.

The first week post-TBI examined in the current study sets the stage for the progression to recovery versus chronic disease. The diverse glial cell responses to TAI indicate different potential contributions to pathological outcome. The astrogliosis and microglial activation are relatively mild during this first week, which could present an opportunity to prevent transition to a more aggressive neuroinflammatory environment. OP proliferation and oligodendrocyte upregulation of myelin synthesis is required for remyelination that can protect viable axons and restore function. However, myelin synthesis may also be a maladaptive response if myelin forms in excess in association with degenerating axons. Extensive abnormal myelin figures were observed in the current pathology so that subsequent degradation and production of myelin debris is a concern for exacerbating the microglial response. Productive remyelination requires post-injury periods of two or more weeks to evaluate effectively and may require specialized approaches, such as remyelination reporter mouse lines to distinguish newly formed myelin as demonstrated after spinal cord injury (68). Further studies of these cellular responses to TAI in later stages after TBI will be important to determine factors that exacerbate or attenuate progression to chronic neurodegenerative processes and to further develop neuroimaging for differentiating the complexity of ongoing neuropathology in TBI.

Chapter 3
Heterogeneous Traumatic Brain Injury Models Reveal Differential Effects in the Subventricular Zone and Divergent Sonic Hedgehog Signaling Pathways in Neuroblasts and Oligodendroglial Progenitors

Amanda J. Mierzwa[a,c,+], Genevieve M. Sullivan[a,b,c,+], Laurel A. Beer[a,c], Sohyun Ahn[d], and Regina C. Armstrong[a,b,c]*

[a] Department of Anatomy, Physiology and Genetics, Uniformed Services University of the Health Sciences, 4301 Jones Bridge Road, Bethesda, MD 20814, USA

[b] Program in Molecular and Cell Biology, Uniformed Services University of the Health Sciences, 4301 Jones Bridge Road, Bethesda, MD 20814, USA

[c] Center for Neuroscience and Regenerative Medicine, Uniformed Services University of the Health Sciences, 4301 Jones Bridge Road, Bethesda, MD 20814, USA

[d] Eunice Kennedy Shriver National Institute of Child Health and Human Development, National Institutes of Health, Bethesda MD, 20814, USA

[+] Authors contributed equally to this work

ABSTRACT

The regenerative capacity of the CNS must be optimized to promote repair following traumatic brain injury (TBI) and may differ with the site and form of damage. Sonic hedgehog (Shh) maintains neural stem cells and promotes oligodendrogenesis. We examined whether Shh signaling contributes to neuronal (DCX) or oligodendroglial (NG2) progenitor responses to two distinct TBI models. Shh-responsive cells were heritably labeled in vivo using Gli1-CreERT2;R26-YFP bitransgenic mice with tamoxifen administration on days 2 and 3 post-TBI. Injury to the cerebral cortex was produced with mild controlled cortical impact. YFP cells decreased in cortical lesions. Total YFP and YFP cells double-labeled with DCX increased in the subventricular zone (SVZ), indicating Shh pathway activation in neural stem cells and neuroblasts. The alternate TBI model produced traumatic axonal injury in the corpus callosum. YFP cells within the SVZ decreased at 2 weeks and then normalized by 6 weeks. In the corpus callosum, YFP cells were extremely rare, even after injury. NG2 progenitors increased in the cortex, with a similar trend in the corpus callosum. NG2 progenitors rarely labeled with YFP. Smoothened agonist (SAG) was microinjected into the corpus callosum to activate Shh signaling. YFP cells and NG2 progenitors increased in the SVZ but were not double-labeled, indicating an in vivo effect of Smoothened signaling without Gli1 activation in NG2 progenitors. Therefore, in all conditions, neuroblasts exhibited differential Shh pathway utilization compared to oligodendroglial progenitors. Accordingly, cortical versus white matter damage from TBI produced opposite responses of Shh-activated neural stem/progenitor cells within the SVZ.

INTRODUCTION

Traumatic brain injury (TBI) is a heterogeneous injury most commonly resulting from direct impact to the head and/or forces from rapid acceleration-deceleration of the head. While many patients do recover substantially within a subacute period, it is clear that even without positive findings on a head CT many patients go on to experience chronic symptoms (52; 74). Even a single mild TBI will leave up to 33% of patients functionally impaired at 3 months post-injury and many continue to have symptoms at 1 year (52). The regenerative capacity of CNS neural stem and progenitor cells must be optimized to promote repair and recovery following TBI, which can involve damage to multiple brain regions and cell types.

Endogenous neural stem cells of the subventricular zone (SVZ), a major germinal zone in the adult brain, have potential repair capacity that is not well understood relative to the heterogeneous forms of TBI. Promoting endogenous repair is particularly attractive in mild-moderate forms of TBI, for which stem cell therapy may not be required or appropriate. Sonic hedgehog (Shh) is a critical signaling pathway that maintains the neural stem cells in the adult SVZ (13; 66). Shh signaling is a complex pathway with many levels of modulation (18). In the canonical pathway, high levels of Shh binding to the Patched receptor lead to release of Smoothened (Smo) inhibition. Smo then travels to the primary cilium where processing of GLI2 and GLI3 shifts to reduce repressor forms, mainly Gli3R, and accumulate activator forms, mainly GLI2A. GLI2/3 transcriptionally regulate *Gli1*, which serves as an effective readout of high levels of Shh pathway activation.

We used in vivo fate labeling to monitor the Shh-responsive cell population relative to neuroblasts and oligodendroglial progenitors following experimental TBI.

Shh-responsive cells were heritably labeled in *Gli1-CreER^{T2}* mice crossed to *R26-IAP* and *R26-YFP* reporter lines. Reporter expression is induced after tamoxifen administration, which enabled temporal control to fate label cells during the post-TBI period. The mosaic nature of the Cre recombination detects a relative ratio of expressing cells in a given population, rather than absolute numbers. In the normal adult mouse CNS, *Gli1-CreER^{T2}* mice have provided important insights into the role of Shh in self-renewal and multipotentiality of neural stem cells and in regulating astrocytic phenotypes (4; 34; 41). *Gli1-CreER^{T2}* fate mapping of Shh pathway activation has not previously been studied in the context of CNS pathology.

We examined the SVZ repair potential after TBI and the contribution of the Shh signaling pathway based on fate labeling in *Gli1-CreER^{T2}* mice. Two different TBI models were used that produced either primarily gray matter or primarily white matter damage to determine whether the response to injury was specific to the site and/or cell type damaged. Controlled cortical impact (CCI) produced damage to the cerebral cortex. A mild severity of CCI was chosen to avoid cavitation and extension of the lesion into the corpus callosum. Traumatic axonal injury (TAI) produced a white matter injury with dispersed axonal injury throughout the corpus callosum (90). In both TBI models, the impact was centered at the coronal level of bregma to target regions near the SVZ. The data support a role for Shh signaling in both neuronal and oligodendroglial progenitor responses, with different downstream effectors of the pathway. Of particular note, the distinct injuries resulted in opposite responses of Shh-activated cells within the SVZ.

METHODS

Heritable Labeling of Shh-Responsive Cells In Vivo

Mice were cared for according to the guidelines of the National Institutes of Health and the Institutional Animal Care and Use Committee of the Uniformed Services University of the Health Sciences. *Gli1-CreER^{T2}* transgenic mice contain a construct with tamoxifen-inducible Cre recombinase fused to the mutated estrogen receptor (CreER^{T2}) that is expressed from the *Gli1* genomic locus in response to activation of the Shh pathway (3). *Gli1-CreER^{T2}* driver mice were crossed to either *R26-YFP* or *R26-IAP* mice. The *R26-YFP* reporter mice contain the YFP reporter gene downstream of a floxed stop codon (87). The *R26-IAP* reporter mice constitutively express a floxed inverted second exon of the gene for the membrane-associated form of human alkaline phosphatase (AP), which accumulates in cell membranes after Cre mediated recombination (12). To induce Cre mediated expression of YFP or AP in Shh-responsive cells, 10 mg of tamoxifen (Sigma, St. Louis, MO) in corn oil was administered by oral gavage on days 2 and 3 post-TBI (90).

Controlled Cortical Impact (CCI)

Male (8-10 weeks old) *Gli1-CreER^{T2}:R26-YFP* or *Gli1-CreER^{T2}:R26-IAP* mice were anesthetized with isofluorane and body temperature was maintained at 37°C. A craniotomy was performed to just exceed the size of the flat impact tip. The dura was impacted using an Impact One^{TM} Stereotaxic Impactor device at 1.5 mm lateral (right hemisphere) to bregma using a tip diameter of 2 mm, a depth of 1 mm, a velocity of 1.5 m/s, and a dwell time of 100 ms. Sham animals underwent craniotomy without impact and naïve animals did not receive anesthesia or surgery.

Traumatic Axonal Injury

TAI was produced in male (8-10 weeks old) *Gli1-CreER^{T2}:R26-YFP* or *Gli1-CreER^{T2}:R26-IAP* mice, as previously characterized in C57BL/6J mice (Sullivan et al., 2013). Briefly, impact to the skull was centered at bregma using an Impact One™ Stereotaxic Impactor device with a 3-mm diameter flat tip set to a depth of 1.5 mm, a velocity of 5 m/s, and a dwell time of 100 ms. Sham mice received anesthesia as well as a scalp incision. Naive mice did not receive anesthesia or an incision.

Smo agonist (SAG) microinjection

GliCreER^{T2}:R26-YFP mice were anesthetized with isofluorane and placed in a stereotaxic frame to drill a small hole in the skull for microinjection. A 10 μL Hamilton syringe (Cat# 7653-01, Hamilton Company; Reno, NV) with RN compression fitting adapters (Cat# 55750-01, Hamilton Company; Reno, NV) to mount a pulled glass pipette (outer diameter 50μm) was used to microinject 1 μL of SAG (Smo agonist; 10 μM; Cat# 566661, EMD chemicals; San Diego, CA) or HBSS vehicle (GIBCO; Grant Island, NY) into the corpus callosum (1.25 mm to the right of bregma and 1.3 mm deep) over 5 min followed by 1 min of rest prior to removal of the pipette. The skin was closed using Tissumend II SC (Veterinary Products Laboratories; Phoenix, AZ).

Reporter Detection and Cell Type Identification

Mice were perfused with 3% paraformaldehyde at 3 days, 2 weeks, or 6 weeks after surgery, and brains were post-fixed by immersion overnight. Coronal cryosections (14 μm) were processed either to detect AP activity or for immunohistochemistry. To detect AP activity, tissue sections from *Gli1-CreER^{T2};R26-IAP* mice were incubated in phosphate-buffered saline for heat inactivation of endogenous AP activity (69°C for 90 min) and reacted with NBT/ BCIP substrate (DAKO, Carpinteria, CA) followed by

methyl green nuclear counterstain (Vector Laboratories). Tissue sections from *Gli1-CreER^{T2};R26-YFP* were immunostained with the following primary antibodies: rabbit polyclonal β-amyloid precursor protein (βAPP, 1:100; Life Technologies, Grand Island, NY), rabbit polyclonal DCX (1:200; Cell Signaling, Danvers, MA), rabbit polyclonal NG2 (1:500; gift from Dr. William Stallcup), rabbit polyclonal Olig2 (1:200; Millipore Billerica, MA), mouse monoclonal S100β (1:1000; clone SH-B1, Sigma), and rat monoclonal green fluorescent protein (GFP, 1:100; Nacalai, Japan), to detect YFP reporter expression. Secondary antibodies included donkey anti-rabbit IgG F(ab')2 conjugated with Cy3 (Jackson ImmunoResearch, West Grove, PA) to detect βAPP, goat anti-rabbit IgG conjugated with Alexa Fluor 488 (Life Technologies, Grand Island, NY) to detect DCX, NG2 and Olig2, donkey anti-mouse IgG F(ab')2 conjugated with Cy3 (Jackson ImmunoResearch), and goat anti-rat IgG conjugated with Alexa Fluor 555 (Life Technologies) to detect YFP. Sections were counterstained with DAPI (Sigma) before mounting with Vectashield (Vector Laboratories, Burlingame, CA).

Quantification and Statistical Analysis

Stereological quantification included 3 serial sections per mouse with 4 mice in each cohort. Each SVZ was outlined in the coronal sections (at the level of the anterior commissure) and images were collected using the exhaustive grid setting in Stereo Investigator (MBF Bioscience, Williston, VT). The traced SVZ region was identified by DAPI nuclear staining to include cells along the edge of the lateral ventricle and extending from the dorsal SVZ less than 400 μm from the ventricle edge. Images were collected with the Z-stack interval of 1μm. All YFP and/or DAPI labeled cells were counted using a 50 μm x 50 μm grid, with a counting frame of 45 μm x 45 μm, placed

over the outlined contours. All coefficient of error values (using Gunderson m = 1) were < 0.08.

AP labeled cells and immunolabeled cells or axons were manually counted in regions of interest in at least 3 sections per mouse and at least 3 mice per condition. In coronal brain sections from *Gli1-CreER^{T2};R26-YFP* mice, Spot Advanced (Sterling Heights, MI) was used to measure the area of the cerebral cortex (superior to the corpus callosum), corpus callosum, and SVZ or the length of the SVZ extension. Images of coronal sections taken from *Gli1-CreER^{T2};R26-IAP* mice were collected using a NanoZoomer 2.0-RS (Hamamatsu, Hamamatsu, Japan), and the area of the cortex was measured using Metamorph (Molecular Devices, Downington, PA).

Prism 6.0 (GraphPad Software) was used for graphing and statistical analysis. βAPP in the corpus callosum was analyzed using one-way analysis of variance followed by a Dunnett's post-hoc analysis for multiple comparisons. Two-way analysis of variance was performed to determine significant differences between injured and sham or naïve cohorts across multiple conditions, such as time point and side (for injury or injection), followed by Tukey's post-hoc analysis for significant interactions. Statistical significance was determined as $p < 0.05$. Unless otherwise stated, interactions and effect sizes with a $p > 0.05$ are not specified.

RESULTS

Heritable labeling of Shh-responsive cells after mild CCI

We performed a mild CCI injury at the coronal level of bregma to facilitate simultaneous evaluation of the cortical lesion area along with the SVZ (Fig. 1).

Shh-responsive cells were fate labeled using *Gli1-CreER*^{T2} driver line of mice crossed to two different reporter lines. A prior study of cortical cryoinjury demonstrated that Shh signaling was increased at 3 days post-injury (7). Thus, we administered tamoxifen on days 2 and 3 post-injury to induce reporter expression during the acute Shh response and then evaluated those heritably labeled cells at 2 and 6 weeks post-injury. *R26-IAP* reporter mice were used to generate strong labeling that could be evaluated in the overall tissue sections based on cell location and morphology. At 2 weeks after CCI (Fig. 1A-D) or sham surgery (data not shown), *Gli1-CreER*^{T2}*;R26-IAP* mice exhibited AP reaction indicative of Shh pathway activation through *Gli1* transcription in cells of the SVZ and cortical astrocytes with rare labeling of oligodendrocytes.

Cortical astrocyte response to mild CCI

We then crossed the *Gli1-CreER*^{T2} driver mice to *R26-YFP* reporter mice to enable immunohistochemical double labeling of Shh-responsive cells with specific cell type markers. The astrocytic response to injury was examined with GFAP (data not shown) and S100β (Fig. 1E, F). YFP cells with the finely-branched morphology of cortical astrocytes were more consistently double labeled with S100β (Fig. 1E, inset), confirming the findings of Garcia et al. (34) that S100β is a more useful marker of the *Gli1* labeled astrocyte population than GFAP. S100β also identified reactive astrocytes in the lesion and penumbra that do not express YFP (Fig. 1F). In fact, in both reporter lines, the density of AP or YFP labeled cells was dramatically reduced in cortical lesions (Fig. 1A, E, F). In the *Gli1-CreER*^{T2}*;R26-YFP* mice, YFP labeled cells were significantly reduced in the cerebral cortex ipsilateral to impact at both 2 and 6 weeks

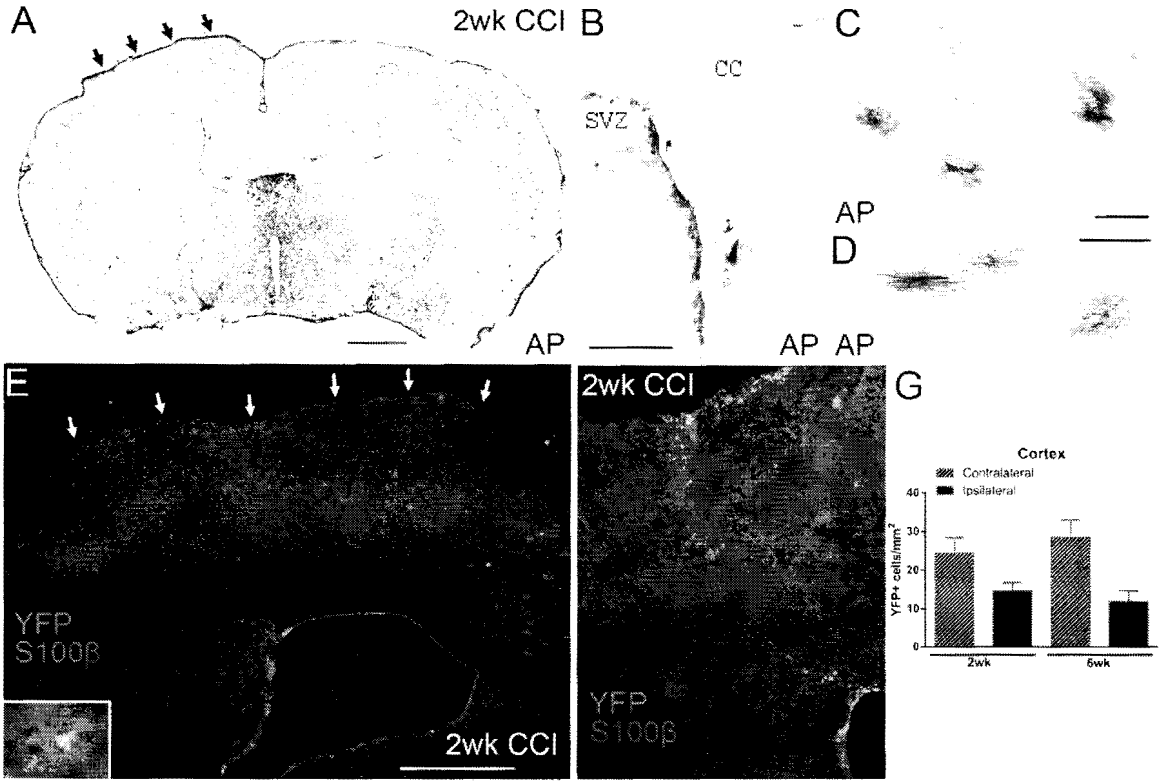

Figure 14. Shh-responsive cells heritably labeled after mild CCI. A-D: Gli1-CreERT2;R26-IAP mice show strong AP labeling of multiple cell types. Mice were administered tamoxifen on days 2 and 3 post-CCI followed by survival until 2 weeks post-CCI (A, arrows indicate site of impact on dura). This heritable labeling identifies cells that were responding to high levels of Shh to drive Gli1 transcription during tamoxifen induced nuclear translocation of the Cre-ER fusion protein. AP labeled cells are abundant in the SVZ (B). AP labeled cells with the morphology of astrocytes are common in the cerebral cortex (C) while rare oligodendrocytes are distinctive in white matter (D, from box in A, rotated). E-F: Gli1-CreERT2;R26-YFP mice show that the pattern of heritable labeling is similar with AP and YFP reporters at 2 weeks post-CCI (S100 β in red, YFP in green, DAPI in blue). Cortical astrocytes double labeled with YFP and S100β have thin, highly branched processes (E, inset). Not all S100β cells are labeled with YFP, particularly in the lesion and penumbra (E, arrows indicate site of impact on dura). YFP cells that remain in the lesion and penumbra maintain a morphology with fine, complex processes which is distinct from the reactive astrocytes labeled for S100□ but not YFP (F). Nuclear DAPI co-localization was used to differentiate intact YFP cells from debris or autofluorescence in lesions (F). G: At both 2 and 6 weeks post-CCI, YFP labeled cells are reduced in the cortex under the site of impact (injury effect, $p = 0.0023$, $n = 4$ mice per condition). SVZ = subventricular zone, CC = corpus callosum. Scale bars A = 1 mm, B = 200 μm, C = 50 μm, D = 150 μm, E and F = 250 μm.

post-injury (Fig. 1G). Furthermore, *Gli1* fate labeled cells that were present in the lesion and penumbra maintained a finely-branched morphology and did not transition to a reactive morphology. This finding illustrates that the YFP labeled population of cortical astrocytes, although often labeled by S100β, exhibits a distinctly different response to injury compared to the S100β expressing population of reactive astrocytes that fill the lesion area.

Shh-responsive cells in the SVZ after mild CCI

Gli1 is actively transcribed in slow cycling neural stem cells in the adult SVZ (66). Fate labeling of Shh-responsive cells in the SVZ was examined at 2 and 6 weeks post-CCI and in matched sham *Gli1-CreER^{T2};R26-YFP* mice (Fig. 2). Cells located mainly in the ventral SVZ labeled for both YFP and GFAP, a marker of quiescent (type B) neural stem cells, at the 2 week time point (Fig. 2A-C). Double labeling for YFP and EGFR indicated *Gli1* fate labeling of transit amplifying (type C) cells (Fig 2D). This pattern appeared to be consistent in both CCI and sham mice. Therefore, tamoxifen administration on days 2 and 3 post-CCI resulted in *Gli1* fate labeling of neural stem cells that gave rise to transit amplifying cells through at least 6 weeks post-CCI. The density of YFP cells in the SVZ was significantly increased after CCI (Fig. 2E). Additional analysis using stereology to quantify the YFP cells relative to the overall SVZ population (DAPI+ cells) also showed that YFP cells were significantly increased after CCI (Fig. 2F).

Neuroblast response to mild CCI

We next examined whether cortical injury stimulated a potential regenerative response in neuroblasts. In normal adult *Gli1-CreER^{T2};R26-YFP* mice, the majority of YFP cells generated from the SVZ were neuroblasts identified by DCX (41).

Figure 15. Shh-responsive cells are increased in the SVZ after CCI.
Immunohistochemistry on coronal sections in Gli1-CreERT2;R26-YFP mice to examine Gli1 fate labeled cells relative to markers for distinct SVZ cell populations after mild CCI. A-B: At 2 weeks post-CCI in the ventral SVZ of both CCI (A) and naïve (B) mice, YFP cells can be found double labeled with GFAP (arrows), a marker of SVZ neural stem cells. C: YFP cells were not typically double labeled for GFAP in the dorsolateral SVZ at 2 weeks post-CCI. D: In contrast, YFP cells often express EGFR (arrows), indicating fate labeling of transit amplifying cells through at least 6 weeks post-CCI. E: The density of YFP cells is increased in the SVZ (injury effect, $p = 0.0359$; $n = 4$ mice per condition). F: Further quantification using stereological methods shows an increase in YFP cells relative to total cells (DAPI nuclear marker) in the SVZ (injury effect, $p = 0.0051$; $n = 4$ mice per condition). LV= lateral ventricle. Scale bars A and B = 100 μm, C and D = 50 μm.

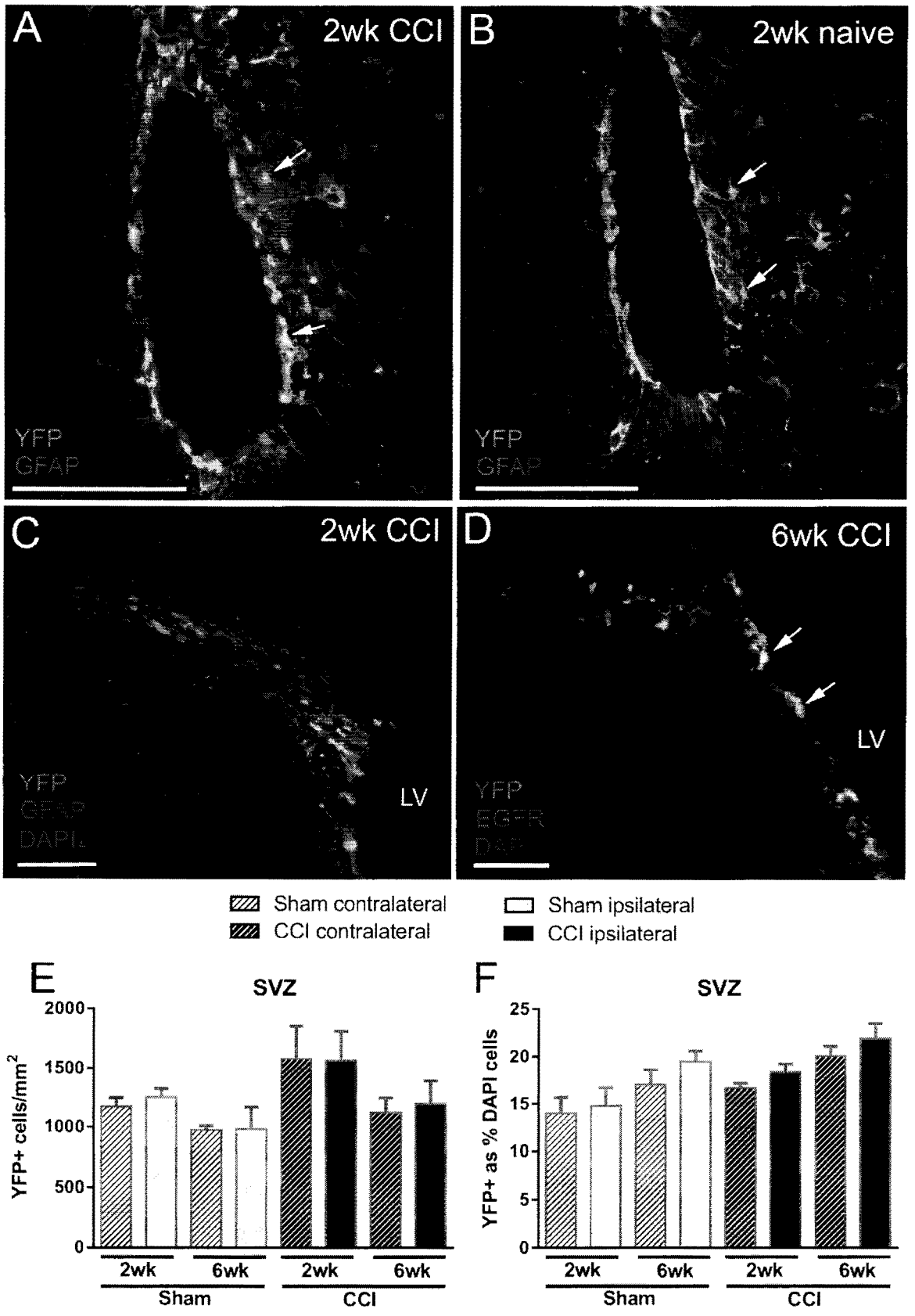
A
2wk CCI
YFP
GFAP
B
2wk naive
YFP
GFAP
C
2wk CCI
YFP
GFAP
DAPI
LV
D
6wk CCI
YFP
EGFR
DAPI
LV
Sham contralateral
CCI contralateral
Sham ipsilateral
CCI ipsilateral
E
SVZ
YFP+ cells/mm2
2000
1500
1000
500
0
2wk
6wk
2wk
6wk
Sham
CCI
F
SVZ
YFP+ as % DAPI cells
25
20
15
10
5
0
2wk
6wk
2wk
6wk
Sham
CCI

After both CCI and sham surgery, DCX neuroblasts were associated with the SVZ (Fig. 3A-D) and were not observed in the cerebral cortex, including the lesion and penumbra (data not shown). DCX cells within the SVZ exhibited double labeling with YFP and the density of double labeled cells was significantly increased after CCI (Fig. 3E). The injury effect in the SVZ also trended toward an increase of DCX cells, regardless of YFP status (Fig. 3F). An injury effect was also apparent among cells extending (> 400μm) from the dorsolateral SVZ. In this extension, overall DCX cells were significantly increased while the subset of DCX cells double labeled with YFP trended toward an increase but did not reach significance (Fig. 3G-H). Thus, cortical injury stimulated Shh-responsive cells within the SVZ, including neuroblasts.

Heritable labeling of Shh-responsive cells after corpus callosum TAI

To determine whether the SVZ response differs between cortical damage and white matter injury, we next examined the *Gli1-CreER*^{T2} mice using a model of axon damage in the corpus callosum adjacent to the SVZ. This TAI model does not stimulate proliferation within the overall population of SVZ cells, but does induce a reaction in NG2 oligodendrocyte progenitors in the SVZ and corpus callosum (90). Since *Gli1-CreER*^{T2} mice are on an outbred genetic background, in contrast to our prior study in C57BL/6 mice, we first confirmed that the skull impact generated sufficient TAI. βAPP immunohistochemistry detected impaired axonal transport in the corpus callosum of *Gli1-CreER*^{T2}*;R26-YFP* mice (Fig. 4). βAPP accumulations were significantly increased at 3 days after TAI. Therefore, we administered tamoxifen on days

Figure 16. *Shh pathway activation is increased in neuroblasts after CCI.* Immunohistochemistry of coronal sections from Gli1-CreERT2;R26-YFP mice to examine Gli1 fate labeled cells relative to the DCX marker for neuroblasts after CCI. A-D: Cells within the SVZ and extending out from the dorsolateral SVZ are labeled with YFP (green), DCX (red), and DAPI (blue). YFP labeled cells are often double labeled for DCX (C, inset arrowheads). E-H: Quantification of YFP and DCX immunolabeling in the SVZ (E-F) and in the extension from the dorsolateral SVZ (G-H, i.e. > 400 □m from the lateral ventricle edge; n = 4 mice per condition). YFP/DCX double labeled cells are increased in the SVZ following CCI (E, injury effect, $p = 0.0356$). The total number of DCX neuroblasts trends toward an increase at 6 weeks but does not reach significance (F, injury effect, $p = 0.1064$). Cells in the SVZ extension show a trend toward an increase in DCX cells double labeled for YFP after CCI (G, injury effect, $p = 0.0703$) and a significant increase in total DCX neuroblasts (H, injury effect, $p = 0.0250$). CC = corpus callosum, LV = lateral ventricle. Scale bar 100 μm.

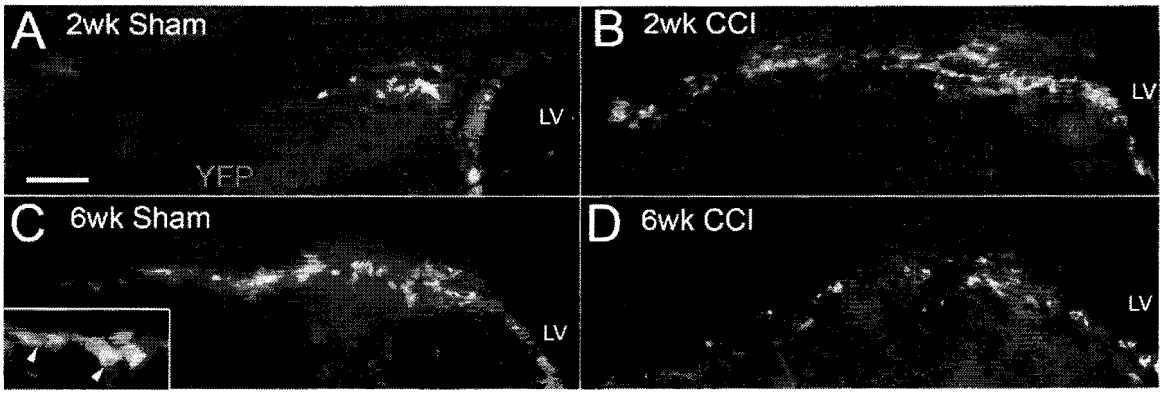
A 2wk Sham
LV
YFP/DCX
B 2wk CCI
LV
C 6wk Sham
LV
D 6wk CCI
LV

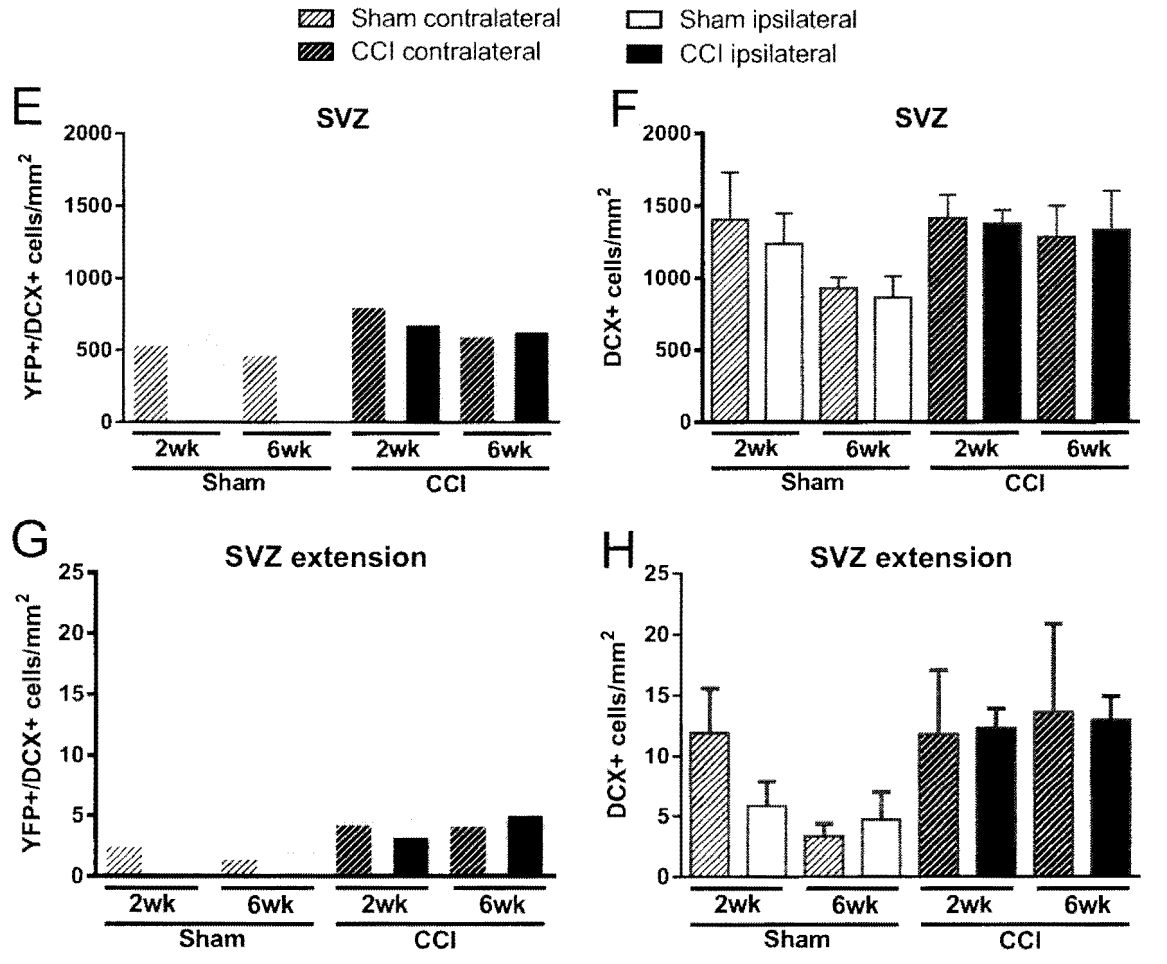
Sham contralateral
CCI contralateral
Sham ipsilateral
CCI ipsilateral
E
SVZ
YFP+/DCX+ cells/mm2
2000
1500
1000
500
0
2wk
6wk
2wk
6wk
Sham
CCI
F
SVZ
DCX+ cells/mm2
2000
1500
1000
500
0
2wk
6wk
2wk
6wk
Sham
CCI
G
SVZ extension
YFP+/DCX+ cells/mm2
25
20
15
10
5
0
2wk
6wk
2wk
6wk
Sham
CCI
H
SVZ extension
DCX+ cells/mm2
25
20
15
10
5
0
2wk
6wk
2wk
6wk
Sham
CCI

2 and 3 post-injury to capture the Shh response during ongoing axonal damage and to facilitate comparison of the same time points as used in the mild CCI study.

The *Gli1-CreER^{T2};R26-IAP* mice were used for an overall evaluation of Shh-responsive cells after TAI in the corpus callosum. AP labeling in sham mice was similar to that observed in TAI mice (Fig. 5). In contrast to the CCI model, after TAI the density of cortical AP labeled cells (Fig. 5B) was not significantly different from sham (Fig. 5A, D; 2 wk Sham = 55.34 ± 6.03; 2 wk TAI = 54.80 ± 6.17; $p = 0.9526$). Based on the localization of damage to the white matter, it was also of particular interest to examine the oligodendrocyte lineage and myelin repair. The membrane bound AP reporter accumulates in myelin sheaths and facilitates the detection of oligodendrocytes, which can be seen in the example of an oligodendrocyte cluster observed in the basal forebrain (Fig. 5C). However, AP labeled cells with an oligodendrocyte morphology were rarely detected, even in areas of TAI in the corpus callosum (Fig. 5D). In the SVZ, the overall distribution of *Gli1* fate labeled cells was not markedly different after TAI (Fig. 5E, F).

Shh-responsive cells in the SVZ after corpus callosum TAI

For more specific analysis of the SVZ response to TAI, NG2 progenitors were examined relative to the YFP labeled population in *Gli1-CreER^{T2};R26-YFP* mice (Fig. 6A-D). Surprisingly, YFP double labeling with NG2 was extremely rare in the SVZ, representing less than 2% of the YFP cells in naïve mice. TAI tended to further reduce the population of YFP and NG2 double labeled cells in the SVZ (injury effect, $p = 0.0544$). Therefore, quantitative analysis of the heritably labeled cells is essentially the YFP population that does not express NG2 (Fig. 6E-G). Contrary to observations after CCI, in the TAI model the YFP labeled cell density was decreased in the SVZ at 2 weeks

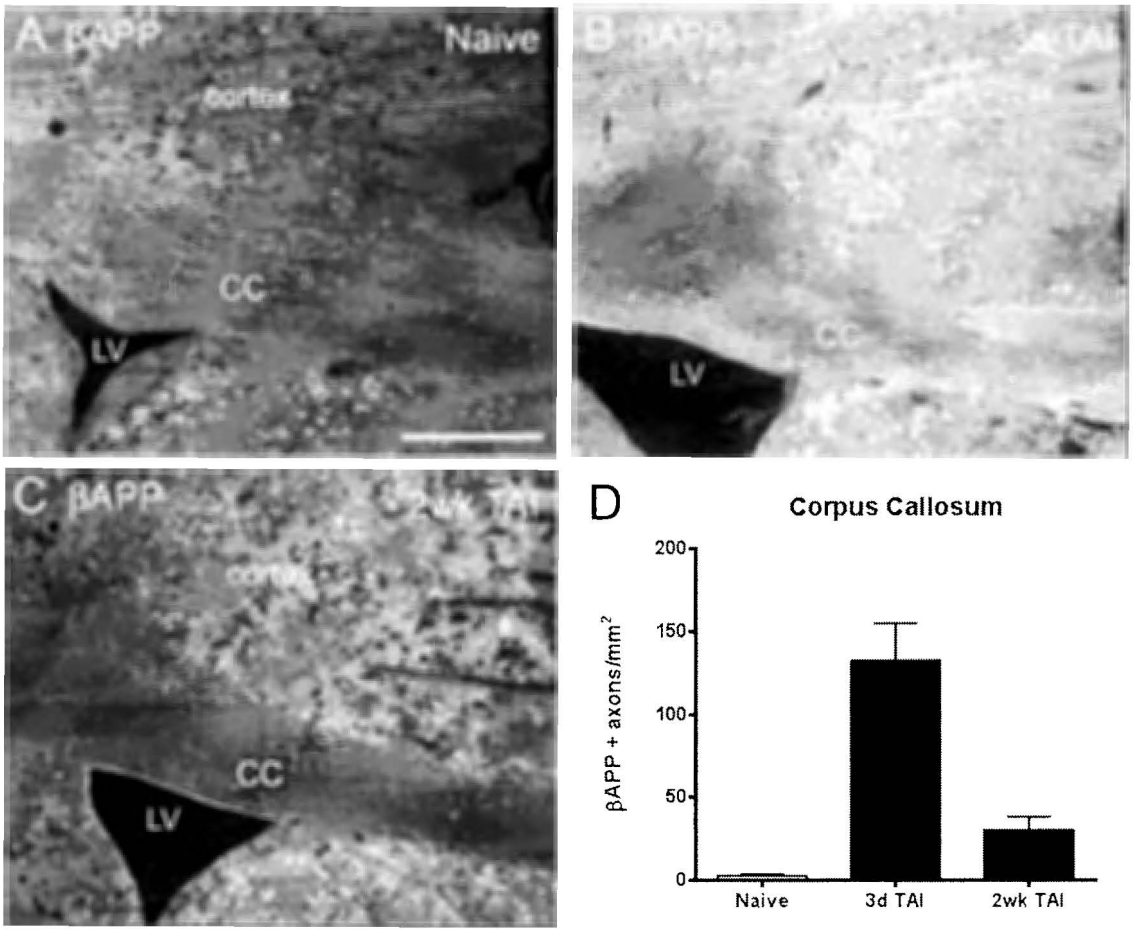

Figure 17. Closed skull impact produces TAI in the corpus callosum. **A-C:** Coronal sections through the corpus callosum of *Gli1-CreER^{T2};R26-YFP* mice immunostained for βAPP to detect impaired axonal transport, indicating TAI. βAPP is present in the cytoplasm of cortical neuron cell bodies (A-C) and is markedly increased in axons of the corpus callosum at 3 days post-TBI (B). **D:** βAPP axonal profiles are significantly increased at 3 days post-TAI with return to near baseline by 2 weeks post-TAI ($p = 0.0002$ across time points, with $p < 0.05$ for post-hoc comparison of 3 day TAI to naïve; n = 3 mice per condition). Scale bar A = 200 μm. CC = corpus callosum, LV = lateral ventricle.

Figure 5. ***Shh-responsive cells heritably labeled with the AP reporter after TAI.*** AP reaction in coronal sections from *Gli1-CreER^{T2};R26-IAP* mice administered tamoxifen on days 2 and 3 after surgery and analyzed at 2 weeks post-TAI or sham surgery. **A:** Sham mouse showing AP labeling of cells in the SVZ, cerebral cortex, and ventral forebrain. **B:** AP labeling in cortical cells from sham mouse with astrocytic morphology. **C:** *Gli1* heritably labeled cells were rarely present in white matter, although labeling of cells with the morphology of myelinating oligodendrocytes was easily detected due to the accumulation of membrane-associated AP in the myelin sheaths. **D:** TAI mouse showing a similar pattern of AP labeling in sham (A) and TAI (D) mice. **E-F:** Shh-responsive cells were abundant in the SVZ of sham (E) and TAI mice (F). AP = alkaline phosphatase, CC = corpus callosum, LV = lateral ventricle. Scale bars A = 1 mm, B = 100 μm, C = 100 μm, D = 1 mm, E = 200 μm, F = 250 μm.

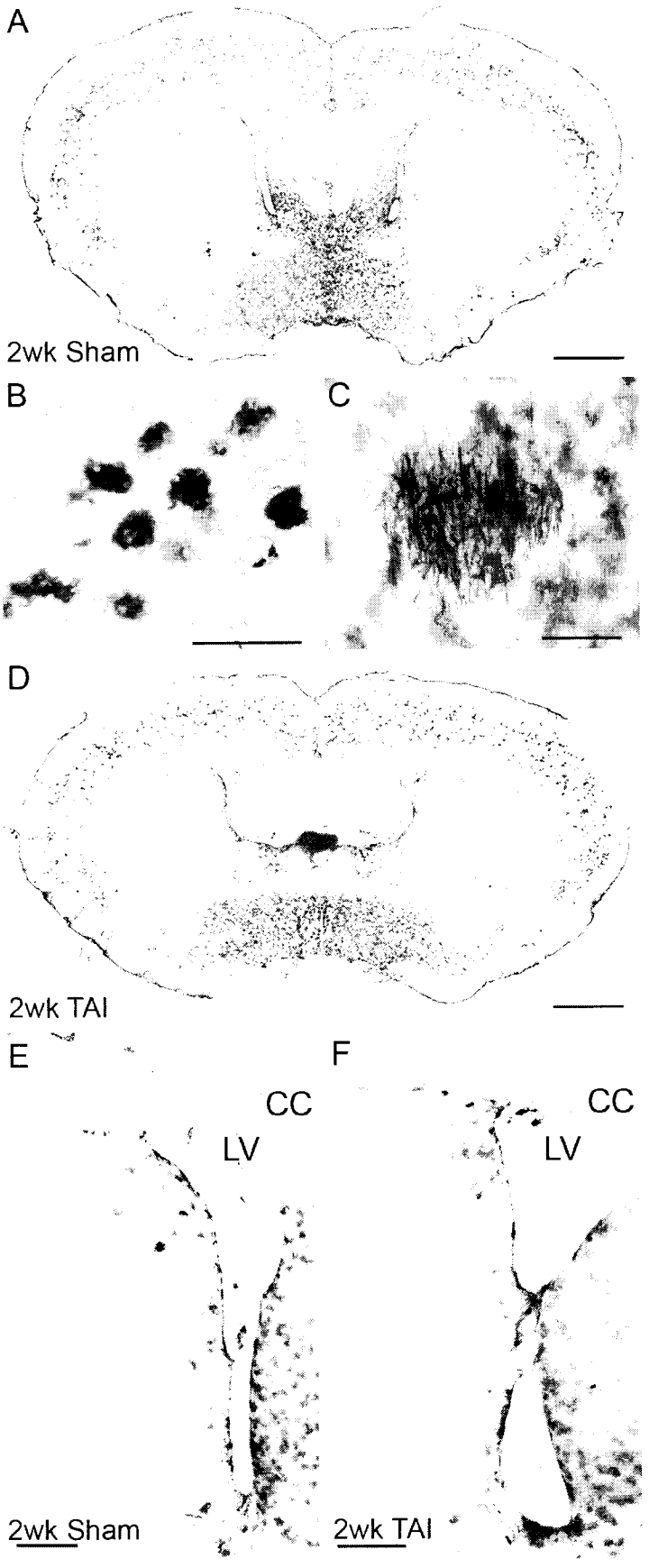
A
2wk Sham
B
C
D
2wk TAI
E
F
CC
LV
CC
LV
2wk Sham
2wk TAI

post-injury and normalized by 6 weeks post-injury (Fig. 6E). A similar decrease and subsequent normalization trend was observed with stereological quantification of YFP labeled cells relative to the overall cell population within the SVZ (Fig. 6F). A more marked increase of YFP cells occurred at 6 weeks in the region of the SVZ dorsolateral extension (Fig. 6G-I).

Oligodendrocyte progenitor response to corpus callosum TAI

Oligodendrocyte progenitors, immunolabeled with NG2, were not a significant component of populations heritably labeled in *Gli1-CreER^{T2};R26-YFP* mice (Fig. 6). NG2 cells were not YFP labeled even in the corpus callosum or cortical regions that could be affected after TAI (Fig. 6A-J). Immunolabeling with Olig2 as a broad marker of the oligodendrocyte lineage also only rarely identified cells double labeled with YFP (Fig. 6K). Oligodendrocyte lineage cells that were infrequently labeled for *Gli1* transcriptional activation could, in fact, differentiate into mature myelinating oligodendrocytes, as was evident in *Gli1-CreER^{T2}; R26-IAP* mice (Fig. 5C). TAI injury in the corpus callosum increased NG2 progenitors in multiple regions, but did not induce YFP labeling of NG2 progenitors (Fig. 6L-Q). After TAI, NG2 progenitors were significantly increased in the SVZ extension (Fig. 6L) and in the cortex (Fig. 6M). NG2 progenitors in the corpus callosum also trended toward an increase without reaching significance (Fig. 6N).

Response of SVZ and corpus callosum cells to SAG microinjection

Pharmacological activation of the Shh pathway with SAG microinjection was used for comparison with the opposing effects observed among YFP cells in the SVZ after CCI versus TAI. In addition, the lack of YFP cells in the corpus callosum was

Figure 18. TAI in the corpus callosum alters SVZ cells and oligodendrocyte progenitors.

A-D: Coronal sections from *Gli1-CreER^{T2};R26-YFP* mice, which were administered tamoxifen on days 2 and 3 after injury, followed by analysis at 2 and 6 weeks after injury. Immunohistochemistry for NG2 to identify oligodendrocyte progenitors and YFP as the reporter of the heritable *Gli1* labeling, with DAPI nuclear stain. Cortical Shh-responsive cells are only weakly labeled at 2 weeks (A, C), however, YFP labeling of cortical cells becomes more readily detected by 6 weeks in both naïve and TAI cohorts (B, D). **E:** YFP cell density is decreased in the SVZ at 2 weeks after TAI compared to naïve and is normalized by 6 weeks post injury, resulting in a significant effect of both time and injury (E, time effect, $p = 0.0272$; injury effect, $p = 0.0011$; for each time point, n = 3 naïve, n = 4 TAI). **F:** Stereological quantification of YFP labeled cells relative to the density of DAPI+ nuclei in the SVZ showed a similar trend ($p < 0.05$ 2 weeks post-TAI compared to 6 weeks post-TAI; n = 4 mice per condition). **G-I:** In the dorsolateral SVZ extension (H-I, enlarged view), YFP cells were significantly increased at 6 weeks post-TAI (interaction effect, $p = 0.0084$; $p < 0.05$ for 6 weeks post-TAI compared to either 2 weeks post-TAI or 6 week naïve; for each time point, n = 3 naïve, n = 4 injured). **J:** NG2 progenitors were only rarely heritably labeled with YFP, as shown in this enlarged view from the cortex. **K:** Olig2, a broad marker of the oligodendrocyte lineage, also only rarely double labeled YFP cells. **L-N:** Although not expressing YFP, NG2 progenitors did respond significantly to TAI (for each time point, n = 3 naïve, n = 4 injured). NG2 progenitors extending from the dorsolateral SVZ were increased at 2 and 6 weeks after TAI (L, injury effect, $p = 0.0283$). After TAI, NG2 progenitors were also significantly increased in the cortex (M; injury effect, $p = 0.0307$), with a similar trend in the corpus callosum that did not reach significance (N; injury effect, $p = 0.1243$). **O-Q:** These effects of TAI on NG2 cells in the cortex and corpus callosum are more easily viewed without YFP visible, given the lack of double labeling. CC = corpus callosum, LV = lateral ventricle. Scale bars C = 200 μm, H = 200 μm, J= 20 μm, K = 10 μm, Q = 200 μm.

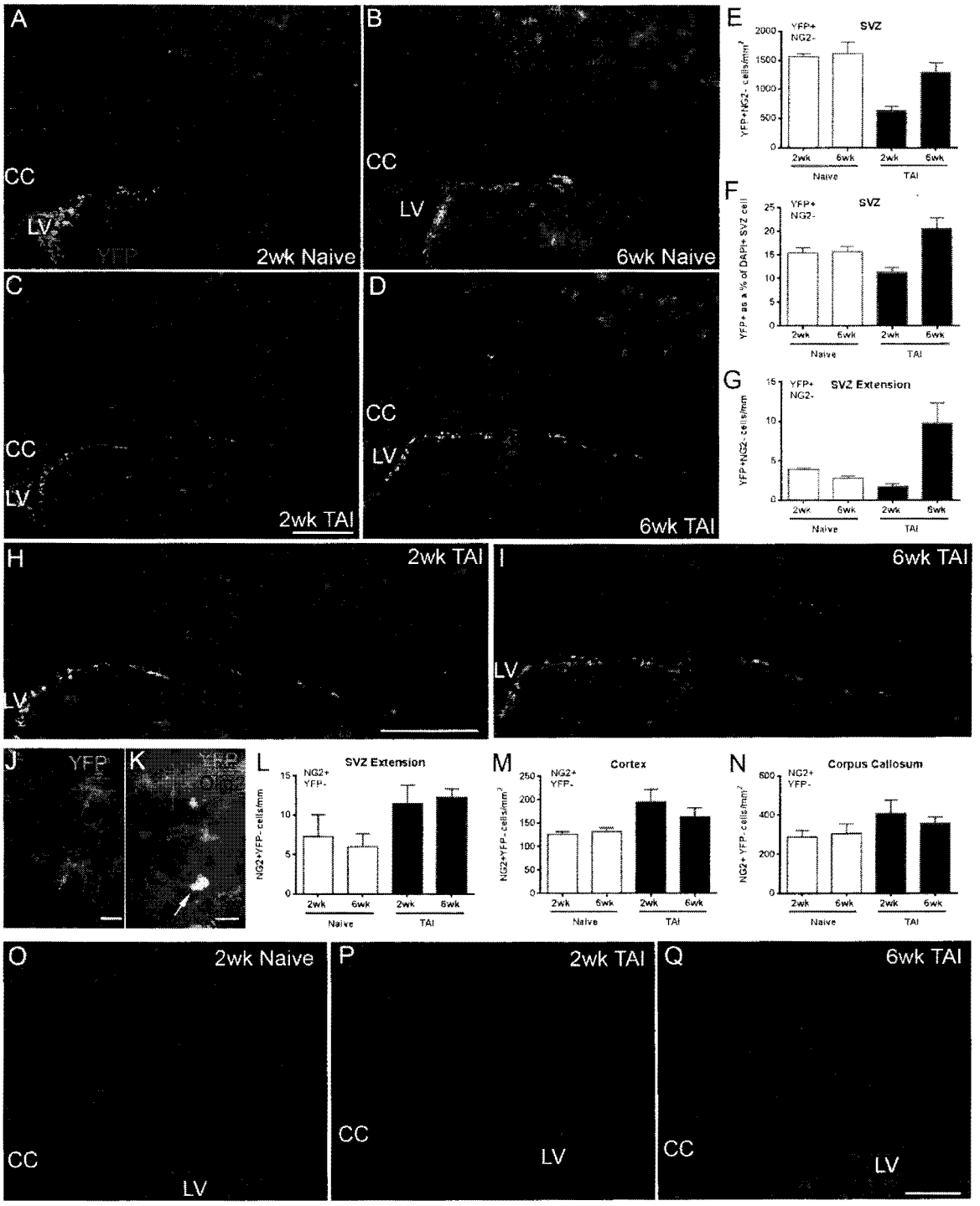
A
CC
LV
YFP
2wk Naive
B
CC
LV
6wk Naive
C
CC
LV
2wk TAI
D
CC
LV
6wk TAI
E
YFP+ NG2-
SVZ
YFP+NG2- cells/mm²
2000
1500
1000
500
0
2wk
6wk
2wk
6wk
Naive
TAI
F
YFP+ NG2-
SVZ
YFP+ as a % of DAPI+ SVZ cell
25
20
15
10
5
0
2wk
6wk
2wk
6wk
Naive
TAI
G
YFP+ NG2-
SVZ Extension
YFP+NG2- cells/mm
15
10
5
0
2wk
6wk
2wk
6wk
Naive
TAI
H
2wk TAI
LV
I
6wk TAI
LV
J
YFP
K
YFP
L
SVZ Extension
NG2+ YFP-
NG2+YFP- cells/mm
15
10
5
0
2wk
6wk
2wk
6wk
Naive
TAI
M
Cortex
NG2+ YFP-
NG2+YFP- cells/mm²
250
200
150
100
50
0
2wk
6wk
2wk
6wk
Naive
TAI
N
Corpus Callosum
NG2+ YFP-
NG2+YFP- cells/mm²
600
400
200
0
2wk
6wk
2wk
6wk
Naive
TAI
O
2wk Naive
CC
LV
P
2wk TAI
CC
LV
Q
6wk TAI
CC
LV

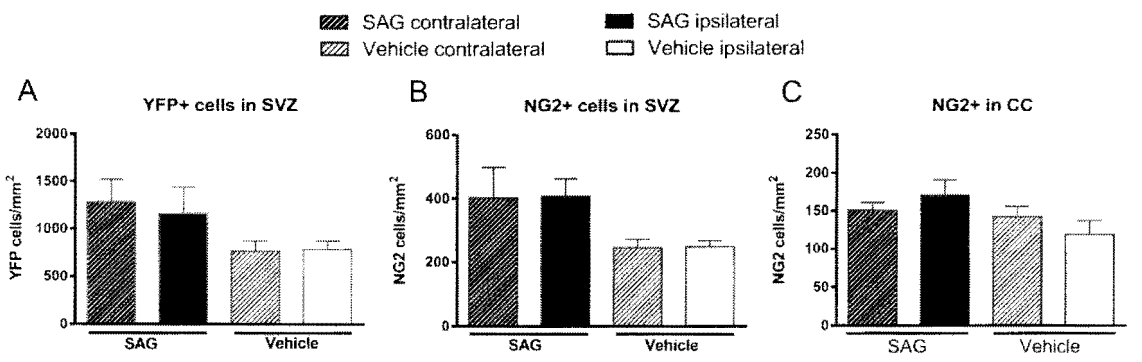

Figure 19. Pharmacological activation of Shh signaling.

Non-injured *Gli1-CreER^{T2};R26-YFP* mice were treated by microinjection of SAG, a Smo agonist, directly into the corpus callosum to examine the effect of pharmacological activation of the Shh pathway. Tamoxifen was administered on days 2 and 3 after SAG or vehicle injection. Mice were perfused for tissue analysis at 2 weeks after injection. **A:** SAG increased the number of YFP cells in both the ipsilateral and contralateral SVZ (treatment effect, $p = 0.0376$). **B**: NG2 cells in the SVZ are also increased with SAG administration (treatment effect, $p = 0.0181$). NG2 cells were still not double labeled with YFP in SAG injected mice (data not shown). **C:** NG2 cells trend toward an increase within the corpus callosum (CC) after SAG administration (treatment effect, $p = 0.0893$). N = 4 mice per condition.

striking, given that CCI causes cortical damage to callosal projection neurons and TAI damages axons within the corpus callosum itself. Therefore, this pharmacological activation was targeted to the corpus callosum to test for *Gli1* transcriptional activation and heritable labeling.

We injected SAG into the corpus callosum over the ventricle in non-injured adult *Gli1-CreER^{T2};R26-YFP* mice. Tamoxifen was administered on days 2 and 3 with tissue analysis at 2 weeks post-injection. SAG injection increased YFP labeling in cells of the SVZ, demonstrating effective activation of the Shh pathway through Smo and GLI1 (Fig. 7A). Similarly, after SAG injection, an increase of NG2 progenitors was observed in the SVZ (Fig. 7B) along with a trend toward an increase of NG2 cells within the corpus callosum (Fig. 7C). NG2 cell density in the cortex was not altered by injection of SAG or vehicle (SAG ipsi = 64.91 ± 11.96, contra = 64.22 ± 11.45; vehicle ipsi = 67.71 ± 15.00, contra = 66.70 ± 11.31 cells/mm^2; treatment effect, $p = 0.6807$; injection side effect, $p = 0.8942$). A lack of *Gli1* transcriptional activation and YFP labeling in NG2 cells was again observed, even in the SVZ where NG2 cells were increased after SAG injection. Furthermore, SAG injection did not result in YFP labeling of either NG2 or other cell types within the corpus callosum.

DISCUSSION

CNS damage mobilizes diverse populations of neural stem and progenitor cells. Immature neural cells that persist in the adult CNS often increase proliferation and take on developmental characteristics in lesion environments. The fate mapping approach used in the current study enabled YFP or AP heritable labeling of cells transcribing *Gli1* as an indicator of Shh pathway activation in the early post-TBI period. To our

knowledge, this is the first study to monitor the in vivo activation of a specific signaling pathway in the SVZ after TBI. This approach using *Gli1-CreER^{T2}* driver mice reveals opposite effects among Shh-responsive cells in the SVZ following CNS damage in the cerebral cortex versus corpus callosum. We show that within the SVZ, cortical damage from mild CCI increases the number of cells fate labeled with YFP. In contrast, corpus callosum damage from TAI produces an initial decrease of YFP labeled cells in the SVZ. These studies also demonstrate differential Shh pathway utilization between neuroblasts and oligodendrocyte progenitors in the normal adult that is maintained during the response to injury.

Prior studies in experimental TBI have examined the SVZ response based on proliferation and the frequency of immature cell types, such as DCX neuroblasts and NG2 oligodendrocyte progenitors. Studies with various severities of the CCI model have shown increased BrdU incorporation during the first few days post-injury (69; 70). A small proportion of these proliferating cells may be DCX neuroblasts that migrate from the SVZ or proliferate locally and are present in the lesion area of the cortex at 3 days post-injury (70; 92; 106). However, these BrdU labeled DCX neuroblasts are not maintained, which may indicate poor survival or loss of labeling due to proliferative dilution of detectable BrdU and reduction of DCX with differentiation (92; 106). For analysis of cortical injury in *Gli1-CreER^{T2};R26-YFP* mice the parameters used are classified as mild CCI (8; 98). DCX neuroblasts were not observed in cortical lesion areas at 2 or 6 weeks post-injury. This mild CCI may not have been sufficient to recruit DCX neuroblasts into cortical lesions via migration or local proliferation. We cannot distinguish whether DCX cells may have been present at earlier time points. However,

YFP heritable labeling was not observed in cortical cells with a neuronal morphology, which argues against differentiation and productive integration of Shh-responsive neuroblasts after CCI. Importantly, this mild CCI was sufficient to induce an injury response among DCX neuroblasts with and without YFP labeling in the SVZ and/or SVZ dorsolateral extension.

NG2 progenitors rapidly exhibit reactive changes to even mild levels of CNS damage (40; 46). In the CCI model, NG2 cells have previously been shown to exhibit a strong reaction in the lesion penumbra (21) and are the most highly proliferative of the cortical cell types (92). NG2 progenitors are also significantly increased in the cortex in the current TAI model, reflecting the high sensitivity of NG2 cells to changes in cortical homeostasis (40). Our prior study of TAI characterized the glial and myelin changes in C57BL/6 mice and showed that NG2 progenitors proliferate and are increased in the corpus callosum (90). In *Gli1-CreER^{T2};R26-YFP* mice, after TAI, the total NG2 progenitor population also increased in the corpus callosum but did not reach significance. The reduced NG2 response in the corpus callosum of *Gli1-CreER^{T2};R26-YFP* mice may reflect the longer time point examined here or a milder TAI severity since the extent of axon damage in the *Gli1-CreER^{T2};R26-YFP* mice was approximately half the level observed in C57BL/6 mice when compared at 3 days post-injury.

Interestingly, SAG injection into the corpus callosum demonstrated a potent effect of Shh signaling to increase YFP cells and NG2 progenitors in the SVZ of *Gli1-CreER^{T2};R26-YFP* mice. However, SAG did not result in YFP double labeling of NG2 cells. It is unlikely that the increase of NG2 cells in the SVZ, and less robustly in the corpus callosum, was due to injection artifact. The density of cortical NG2 cells was not

significantly different with SAG versus vehicle or in comparison between the ipsilateral and contralateral sides. Therefore, the microinjection technique did not cause a significant NG2 reaction from the pipette penetrating the cortex.

Shh signaling contributes to regenerative responses after damage to diverse regions in the CNS, including the cerebral cortex and corpus callosum, which are the target sites compared in this study. Cortical cryoinjury in *Gli1*-luciferase reporter mice showed maximal Shh pathway activation at 3 days after injury with normalization by 2 weeks (7). Shh in these cryolesions induced proliferation of astrocytes and Olig2 labeled oligodendrocyte lineage cells that was inhibited by cyclopamine (7). After cortical stab wound, Shh signaling produced in vitro conversion of cortical astrocytes to neural stem cells (82). Shh pathway activation by the SAG was sufficient to further promote in vivo proliferation of reactive astrocytes in the stab wound lesion (82). Our CCI data in *Gli1-CreER*^{T2} mice differs from these prior studies in that heritable labeling for Shh pathway activation was reduced in the cortical lesion area at 2 weeks post injury, and this was maintained through 6 weeks. Shh stimulated proliferation of astrocytes may require breakdown of the blood-brain barrier (82). Our mild CCI is expected to cause breakdown of the blood-brain barrier but should not compromise the dura. The mild injury and intact dura may contribute to the differences from the cryolesion and stab wound studies. Alternative mechanisms include differential involvement of the Shh pathway, either the timing or the specific signaling components, that is revealed by the fate labeling in *Gli1-CreER*^{T2} mice.

GLI1 expression is relatively low in the corpus callosum of non-injured adult mice (30; 66), which is consistent with the striking lack of *Gli1* heritable labeling using

Gli1-CreER^{T2} driver mice (34; current study). In contrast, experimental demyelination in the corpus callosum has been reported to induce broad reactivation of the Shh pathway that promotes oligodendrocyte survival as well as the proliferation and differentiation of oligodendrocyte progenitors (30). Smo expression was increased in the demyelinated lesions in microglia and oligodendrocyte lineage cells, with a subset of Olig2 cells also expressing GLI1 (30). Our TBI model targeting the corpus callosum induced axon damage but not *Gli1* fate labeling. Furthermore, SAG injection directly into the corpus callosum induced heritable *Gli1* labeling in the SVZ but not in the cells of the corpus callosum. These findings could indicate that SAG requires additional signaling partners to be effective within corpus callosum cells, akin to the requirement hypothesized for blood-brain barrier disruption for the Shh conversion of cortical astrocytes into neural stem cells (Sirko et al., 2013). Another possibility is that *Gli1* transcriptional activation may not be the predominant response to Shh signaling among the oligodendrocyte lineage cells and other cell types within the corpus callosum. Consistent with this possibility, NG2 cells were rarely double labeled with YFP. Furthermore, YFP cells were transiently reduced in the SVZ after TAI, which may divert slow cycling and/or transit amplifying populations of neural stem cells toward the oligodendrocyte lineage.

Canonical Shh signaling is dependent on the balance of activator and repressor effects among the *Gli* family members (18). *Gli1* expression serves as a read out for activation of the Shh signaling pathway. GLI2 acts as a transcriptional activator of *Gli1* in the presence of high levels of Shh. GLI2 is expressed in normal adult mouse corpus callosum (56; 66) while GLI3 is not detected (30; 56). Whether GLI2 levels modulate the oligodendrocyte lineage response to corpus callosum damage is not clear. Two studies of

experimental demyelination with lysolecithin injection into the corpus callosum do not corroborate one another readily. GLI2 mRNA transcripts were increased in lesion areas after 10 days (30). However, GLI2 protein was decreased at 3 days post lesion induction (56). In spinal cord, GLI1 expression was observed in NG2 cells of normal adult mice but down regulated in demyelinated lesions (96). Further studies will be important to delineate the potential role of GLI2 and modulation of GLI1 in the oligodendrocyte lineage in the normal adult CNS and in response to white matter damage. Based on the current findings and these prior studies, Shh signaling in the oligodendrocyte lineage may occur via modulation of repressive effects of GLI2 given the lack of *Gli1* transcriptional activation observed in *Gli1-CreER^{T2};R26-YFP* mice. However, more complex interactions may regulate the response of oligodendrocyte lineage cells to Shh. Smo is expressed at 4.7 fold higher levels in oligodendrocyte progenitors compared to myelinating oligodendrocytes(20). Conversely, expression of hedgehog interacting protein increases 17.2 fold with oligodendrocyte progenitor differentiation into myelinating oligodendrocytes (20). Interestingly, hedgehog interacting protein sequesters hedgehog ligand and limits diffusion (18), which could limit Shh signaling in the white matter as observed in our data. In the SVZ of non-injured adult mice, *Gli1* transcriptional activation is Smo dependent and strongest in ventral neural stem cells that then migrate into the dorsal SVZ (41; 66). GLI2 is expressed throughout the dorsal-ventral extent of the SVZ (66). However, GLI3 appears to have a predominant role in modulating the Shh pathway in the SVZ neural stem cells. In the absence of Shh, GLI3 acts as a repressor. Shh is required for negative regulation of this repressive GLI3 effect to allow for normal proliferation of the slow cycling neural stem cells in the adult SVZ (66). The heritable

labeling in our TBI studies using *Gli1-CreER*^{T2} driver mice was designed to fate label based on Shh pathway activation with tamoxifen on days 2 and 3 to capture the early response to injury. The mice survived through at least 2 weeks post-injury to allow time for migration and differentiation. Different approaches would be required to identify the specific cell stage at the time of fate labeling since the extent of recombination among different cell populations was not detected accurately at shorter time points using two different reporter constructs (34; data not shown).

Optimizing the repair capacity of the adult CNS will require modulating the complex interplay among Gli family members that impact the regenerative potential from the SVZ as well as from conversion of cortical astrocytes. The data presented highlight the need to more fully appreciate the specificity of the neural stem cell and progenitor response to distinct forms of cell and tissue damage. This analysis is particularly relevant to TBI in which the patients may have extremely different involvement of neuronal cell bodies in the cerebral cortex relative to traumatic axonal injury in white matter tracts.

Chapter 4
Discussion

It is import to understand the pathological mechanisms that result from TBI and the endogenous cell response that follows, in order to develop strategies to promote repair of damaged tissue. Characterization of a white matter injury model at the cornel level of the SVZ was required to compare the regenerative responses that occur following either white or gray matter injury. Shh responsive cells were heritably labeled in *Gli1-CreER^{T2};R26-YFP* mice in order to compare the involvement of Shh signaling in the regenerative response following gray or white matter injury These papers provide additional understanding of the regenerative response from neural stems of the SVZ following injury, and progress further discussion of questions that should be addressed in future studies. The following discussion will provide an overview of the significance, the limitations, and the ideas for future experiments that will complement this work in the field of regeneration following TBI.

The Significance of the TAI Model

Axon degeneration throughout white matter regions of the human brain, known as diffuse axonal injury (DAI), is not limited to acute and sub-acute periods after injury and is actually a progressive long-term process detected years after the initial injury (22). Currently, clinicians target therapy based on the phase of injury, and therapies are designed to attenuate numerous pathophysiological processes that occur after TBI (Algattas and Huang, 2014). Better understanding of the pathological mechanisms that occur after TBI may allow for the development of more specific therapies. Therefore, in the TAI injury model (Sullivan et al., 2013), which replicates the pathological

mechanisms of white matter damage focally in the corpus callosum, further analysis is needed to determine if the neuroinflammatory response and axon damage persist in the corpus callosum following the first week of injury. Developing a model in which relevant pathology persists will be useful to investigate the mechanisms that drive chronic pathology and perhaps expand the understanding of the pathological mechanisms that occur in TBI patients (42).

In these studies the TAI mouse model was developed to investigate the pathological and regenerative processes that occur following damage to white matter. The procedure developed to create white matter damage reproducibly produced consistent traumatic axonal injury within the corpus callosum of C57BL/6J mice, which was verified by MRI DTI analysis and βAPP immunohistochemistry. Importantly, elevated βAPP in the corpus callosum throughout the first week of injury parallels findings that detected βAPP in the corpus callosum of human TBI patients (36). Additionally, parameters such as apnea, skull fractures, bleeding after impact, and righting reflex are particularly useful because they allow for classification of cohorts, which reduces variability between cohorts. Skull fractures were observed in this model of closed skull TBI, which parallels findings that skull fractures occur in 30% of mild to moderate patients with TBI (103). The majority of skull fractures were either branched or linear but some depressed skull fractures were observed. In future studies, mice with depressed skull fractures could be analyzed as a separate cohort in order to study more complex pathology involving both white and gray matter damage simultaneously, which would be more representative of the pathology that occurs in ~3% of human mild TBIs (103).

The initial analysis of the TAI model focused on the pathological mechanisms occurring during the first week after injury. Further investigation of the mechanisms involved in this acute phase might illuminate potential targets for intervention. One week following injury, activated hypertrophic macrophages and microglia were observed in the corpus callosum following TAI. Microglia have diverse functions and can assume distinct activation states after injury, such as hypertrophic, bushy, or ameboid (44; 80). Microglia are classified as either pro-inflammatory or anti-inflammatory immuno-regulatory (Miron and Franklin, 2014). Further analysis could include investigation of the activation stage of microglia within the damaged white matter throughout the first week of injury and to study whether microglia could be modified to promote repair and reduce inflammation at later time points. Investigation into the timing of myelin clearance by microglia may also be interesting. If myelin debris is cleared early and efficiently after injury this would improve axon regeneration. However, if myelin debris persists, because of continued synthesis of myelin, continued axon degeneration, or inefficient clearance, it could potentially perpetuate the inflammatory response by inducing microglia to become activated (23; 58).

EM analysis showed the presence of redundant myelin figures at 1 week after TAI, which correlated with the number of damaged axons in the corpus callosum (90). Redundant myelin is an outfolding of myelin sheath that is too large for the enclosed axon(65). Future studies should investigate if excess myelin persists at chronic time point after injury because these redundant myelin figures may be recognized by microglia as debris and perpetuate the inflammatory response.

THE ROLE OF SHH IN THE REGENERATIVE RESPONSE FOLLOWING EITHER WHITE MATTER DAMAGE OR GRAY MATTER DAMAGE

Heterogeneous forms of TBI differentially affect cell populations within the adult CNS(55). The regenerative response from Gli1 heritably labeled cell populations were analyzed after white or gray matter damage(55). The following section provides an overview of the significance, the limitations, and the ideas for future experiments that will be important for understanding the role of Shh signaling in regeneration following TBI.

Gli1 heritably labeled cells in the cortex following TBI

Gli1 heritably labeled cells are affected differently in white matter versus gray matter TBI. The cell density of this population decreased in the cortex following CCI but remained close to control levels following TAI (Mierzwa et al., Submitted). Gli1 heritably labeled cells in the cortex are a unique subset of astrocytes that do not increase proliferation in response to injury (34). This is surprising because Shh has been shown to elicit a stem cell response from cortical astrocytes in vivo and in vitro (82). Also, YFP+ cortical cells were not DCX+ or NG2+ in naïve or injured mice. Therefore these cells are not contributing to neurogenesis or oligodendrogenesis in control or injured mice.

Gli1 heritably labeled cells in the SVZ following TBI

White matter and gray matter injury differentially affects neural stem progenitor cells in the SVZ based on the observation of the response from Gli1 heritably labeled cells in the SVZ(55). There are several potential reasons for why Gli1 heritably labeled (YFP) cells in the SVZ respond differently after gray matter versus white matter injury. The molecular signals present in the damaged area are possibly connected to the type of cell needed for generating repair. Also the signals connected to the cell replacement process may involve many other molecular signaling components in addition to Shh.

Differential Shh synthesis and secretion could occur following CCI or TAI. Low abundance of Shh in white matter damage and high abundance of Shh following gray matter damage may explain why YFP cell density in the SVZ increased in response to CCI and initially decreased after TAI. Further analysis of Shh synthesiswith western blot, immunohistochemistry, or insitu-hybridization would help to determine if the levels of Shh produced are significantly different following gray or white matter damage. These analyses would also demonstrate the peak time point of Shh signaling after gray and white matter injury.. Furthermore, factors that inhibit Shh signaling such as soluble or membrane bound Hhip, which is expressed in the corpus callosum of the adult CNS(5), could be highly expressed in the SVZ or corpus callosum following TAI, but not significantly altered, or even down regulated, following CCI. Overexpression of Hhip via injection of Ad-mHip into the lateral ventricle 2 days before LPC injection in the corpus callosum blocked oligodendrocyte proliferation and differentiation, which prevented tissue repair(30). Furthermore, expression of Hip increases with oligodendrocyte progenitor differentiation into myelinating oligodendrocytes (20). Therefore it might be possible that oligodendrocyte progenitors undergoing differentiation the corpus callosum may induce expression of Hhip, or release of Hhip, from cells in the corpus callosum and affect the adjacent cells in the SVZ by sequestering Shh following TAI. This theory could be tested with immunohistochemical analysis that shows colocalization of HhiP with PLP+ cells as well as increased labeling of these cells in the corpus callosum after injury.

TAI may induce cells in the SVZ to respond to Shh through a pathway independent of Gli1 transcriptional activation. Shh expression has been shown to be

increased in white and gray matter after injury (7; 30),and coincide with Olig2+ oligodendrocyte lineage cells and microglia (30). It is therefore possible that Shh is being produced in response to TAI, which also produces damaged axons, demyelinated axons, and neuroinflammation. In order to investigate whether NSCs or oligodendrocyte progenitors in the SVZ are responding to Shh independent of Gli1 transcription after TAI, nuclear localization of GLI2 in these cells would identify cells actively responding to Shh through the canonical pathway. Activation of noncanonical Shh signaling could also be determined with further investigation. A potential readout of noncanonical Shh signaling would be the intracellular localization of Ptch and the polarization of Smo to other regions outside the primary cilium(discussed in further detail below).

Involvement of Shh in migration following TBI

Modulation of the lesioned microenvironment may enhance neuroregeneration from *Gli1* heritably labeled cells in the SVZ. Others have shown SVZ DCX+ cells increase proliferation and migrate to the lesion area 3 days after mild CCI (70). Therefore, it was not surprising that DCX+YFP+ cell density increased in the SVZ following CCI. However, it was surprising that DCX+YFP+ cells were not detected in the lesion at 2 and 6 weeks after CCI and that YFP+ cells with neuronal morphology were not observed (55). Others have shown in more severe cortical injury models that BrdU labeled DCX+ cells are capable of migrating from the SVZ to the lesion area but are not maintained (92; 106). Therefore DCX+YFP+ cells may have migrated to the lesion but were unable to survive because the lesion microenvironment is inhospitable. Unfortunately, analysis at earlier time points would not allow for significant reporter

accumulation in order to effectively label Shh responsive cells in *Gli1-CreERT;R26-YFP* mice(55).

The mild CCI technique that was used in chapter 2 would allow for investigation into modulating the cortical lesion environment to promote cell survival whereas it may be too difficult to tease out the molecular mechanism that should be enhanced in other more severe CCI models that create an extreme cytotoxic microenvironment. Further investigation into creating a more permissive environment in the cortex may promote survival of the endogenous cells. It is also possible that factors that induce a migratory response after injury are dampened in this milder cortical injury model. In this case, recruitment of cells to damaged areas after mild injury would be important for regeneration. Therefore future experiments could also analyze the factors that stimulate and inhibit the migratory response. For example, Shh has been shown to elicit migration of neuroblasts from the SVZ to the olfactory bulb (9). Moreover, Smo is required for Shh to induce this chemotaxis but localization of Smo to the primary cilium is not (17). Future analyses could include localization of Smo with immunohistochemistry to determine if Shh is inducing YFP+ or YFP- cells to migrate after mild cortical injury.

Shh signaling independent of Gli1 transcriptional activation

Shh may play a role in regeneration after white matter damage that is not detectable with *Gli1* heritably labeled cells. During the time the experiments for the previous chapters were being performed several studies have been published that inform the interpretation of the results discussed in the previous chapter. In adult naïve conditions Smo and Ptch are not detectable in the corpus callosum and GLI1 expression is extremely low (30). In fact there is almost a complete absence of *Gli1* labeling in the

corpus callosum of adult *Gli1CreER*^{T2} driver mice (34). However, GLI2 is expressed in the corpus callosum and SVZ, which as mentioned before becomes active and travels to the nucleus after Shh signaling induces Smo activation. Therefore, immunohistochemistry to observe co-labeling of nuclear GLI2 with NG2 could be performed to verify Shh signaling is active in oligodendrocyte progenitors of the corpus callosum or SVZ in naïve and injured mice.

Additionally, administration of SAG, which activates the Shh signaling pathway through Smo, is not sufficient to recruit YFP+ cells to the corpus callosum or induce local cells to express YFP(90). This is contrary to evidence that Smo is increased in Olig2 lineage cells, and that Olig2 lineage cells express GLI1 following damage to the corpus callosum (30). However, oligodendrocyte lineage cells may require additional signaling from other factors present after blood brain barrier breakdown in order to become responsive to Shh (82). SAG administration into the corpus callosum did invoke a response from oligodendrocyte progenitors and YFP+ cells in the SVZ and oligodendrocyte progenitor cells trended towards a response in the corpus callosum(55). The increase in YFP cell density in the SVZ indicates that SAG is effectively activating Gli1 transcription through Smo. The oligodendrocyte progenitor population may also be responding directly to Smo activation, but independent of *Gli1* transcriptional activation. It is also possible that the oligodendrocyte progenitors are responding indirectly through signaling from other cells that are responsive to Smo activation.

The role of Shh in the oligodendrocyte progenitor response following TBI

Heritably labeled cells that became oligodendrocyte lineage cells were rare in the SVZ and extremely rare in the corpus callosum even after TAI(55). However, in *Gli1*-

CreER^{T2} driver mice it was not determined if cells from the SVZ migrate into the corpus callosum and contribute to the significant increase in oligodendrocyte progenitor population that was observed after injury, as the Shh canonical pathway does not have to result in *Gli1* transcriptional activation. YFP+ cell density in the SVZ was decreased after injury, which may be evidence these cells are migrating out of the SVZ to damaged areas. The absence of YFP+ cells in the corpus callosum suggests that these cells transition to the NG2 lineage prior to tamoxifen administration, which makes them less likely to be labeled through *Gli1* transcription activation.

OLIGODENDROCYTE LINEAGE RESPONSE FOLLOWING TBI

Oligodendrocyte progenitor cell density significantly increased along the SVZ extension following TAI (55). Additionally proliferation of oligodendrocyte progenitors in the SVZ was shown to be increased during the first week following injury.Oligodendrocyte progenitors are derived from the heterogeneous population of neural stem cells in the SVZ (Menn et al., 2006, Giachino et al., 2014), but the specific parent cell from which oligodendrocyte progenitors are derived is unknown . It has been shown that there are two types of type B cells as well as an early transit amplifying cell that are capable of directly giving rise to Olig2 + cells (Giachino et al., 2014) . Further investigation into the origin of the oligodendrocyte progenitors in the SVZ extension and whether these cells are migrating out from the SVZ is needed. Injection of a lenti virus with a fluorescent label, into the SVZ of *Ascl1-CreER*^{T2} driver mice after tamoxifen delivery could be followed by immunohistochemistry for NG2 in coronal sections. This would determine if early transit amplifying cells in the SVZ could give rise to NG2 cells, and whether the NG2 cells in the SVZ extension are derived from the SVZ. If these cells

do not co-label with the fluorescent reporter from the lentiviral injection, the Ascl1 driver, and NG2, than it would be possible to eliminate this cell population as a source for the NG2 population that is extending out of the SVZ (Giachino et al., 2014). Further analysis could determine if NG2 cells arise from further back in the NSC lineage by using either a EGFRCreERT2 driver to identify type 2 and 3 B cells or Hes5CreERT2 driver to identify type 1 B cells as the source of NG2 cells in the SVZ (Giachino et al., 2014). Furthermore, the proliferative response of *Gli1* heritably labeled cells in the SVZ to injury is unknown. Comparison of the proliferative response from *Gli1* heritably labeled cells to the proliferative response of cells with nuclear localization of GLI2 in the SVZ, may provide evidence Shh induces a proliferative response from cell population within the SVZ that response to Shh independently of *Gli1* transcriptional activation following injury.

SUMMARY

These studies investigate the complex pathological and molecular mechanisms that occur after heterogeneous forms of TBI in order to elucidate repair strategies targeted for either white matter or gray matter damage. The data presented in this thesis along with the work of others demonstrates that the Shh signaling pathway may be a potential target for modulation to promote regeneration of neuronal and oligodendrocyte lineages after injury in the adult CNS. Therefore further analysis of involvement of the Shh pathway in regeneration may be beneficial for those designing therapeutic strategies. Our work provides evidence that modulation of Shh signaling to produce either oligodendrocyte lineage cells or neuronal lineage cells from the Shh responsive type B cells in the SVZ may be feasible. The timing, location, and amount of Shh that

determines the fate of these cells, through complex regulation of the GLI transcription factors in the adult CNS, remain unknown and are relevant for designing therapeutic strategies to target regeneration in damaged white or gray matter. This data also highlights that further analysis is needed to determine other factors involved in recruiting induced lineage cells to the site of injury and promoting their survival. Comparison of the pathological mechanisms that occur following two distinct models of TBI may help to elucidate factors unique to the damaged microenvironment and factors that inhibit or recruit cells to the damaged area.

REFERENCES

[1. Numbered references, alphabetical order, apply the "reference" style once all references are inserted. Follow the formatting guidelines for Annual Reviews in Genetics]

[2. You can find example references in the Author Instruction Booklet for Genetics here: http://www.annualreviews.org/page/authors/author-instructions/preparing/handbooks]

1. Adams JH, Doyle D, Ford I, Gennarelli TA, Graham DI, McLellan DR. 1989. Diffuse axonal injury in head injury: definition, diagnosis and grading. *Histopathology* 15:49-59
2. Aguirre A, Gallo V. 2007. Reduced EGFR signaling in progenitor cells of the adult subventricular zone attenuates oligodendrogenesis after demyelination. *Neuron glia biology* 3:209-20
3. Ahn S, Joyner AL. 2004. Dynamic changes in the response of cells to positive hedgehog signaling during mouse limb patterning. *Cell* 118:505-16
4. Ahn S, Joyner AL. 2005. In vivo analysis of quiescent adult neural stem cells responding to Sonic hedgehog. *Nature* 437:894-7
5. Allen Institute for Brain Science ABA. ©2014.
6. Alvarez JI, Dodelet-Devillers A, Kebir H, Ifergan I, Fabre PJ, et al. 2011. The Hedgehog pathway promotes blood-brain barrier integrity and CNS immune quiescence. *Science* 334:1727-31
7. Amankulor NM, Hambardzumyan D, Pyonteck SM, Becher OJ, Joyce JA, Holland EC. 2009. Sonic hedgehog pathway activation is induced by acute brain injury and regulated by injury-related inflammation. *The Journal of neuroscience : the official journal of the Society for Neuroscience* 29:10299-308
8. Andrews EM, Richards RJ, Yin FQ, Viapiano MS, Jakeman LB. 2012. Alterations in chondroitin sulfate proteoglycan expression occur both at and far from the site of spinal contusion injury. *Experimental neurology* 235:174-87
9. Angot E, Loulier K, Nguyen-Ba-Charvet KT, Gadeau AP, Ruat M, Traiffort E. 2008. Chemoattractive activity of sonic hedgehog in the adult subventricular zone modulates the number of neural precursors reaching the olfactory bulb. *Stem cells* 26:2311-20
10. Armstrong RC, Le TQ, Flint NC, Vana AC, Zhou YX. 2006. Endogenous cell repair of chronic demyelination. *Journal of neuropathology and experimental neurology* 65:245-56
11. Armstrong RC, Le TQ, Frost EE, Borke RC, Vana AC. 2002. Absence of fibroblast growth factor 2 promotes oligodendroglial repopulation of demyelinated white matter. *The Journal of neuroscience : the official journal of the Society for Neuroscience* 22:8574-85

12. Badea TC, Hua ZL, Smallwood PM, Williams J, Rotolo T, et al. 2009. New mouse lines for the analysis of neuronal morphology using CreER(T)/loxP-directed sparse labeling. *PloS one* 4:e7859
13. Balordi F, Fishell G. 2007. Hedgehog signaling in the subventricular zone is required for both the maintenance of stem cells and the migration of newborn neurons. *The Journal of neuroscience : the official journal of the Society for Neuroscience* 27:5936-47
14. Bennett RE, Mac Donald CL, Brody DL. Diffusion tensor imaging detects axonal injury in a mouse model of repetitive closed-skull traumatic brain injury. *Neuroscience letters* 513:160-5
15. Bigler ED. 2012. Mild traumatic brain injury: the elusive timing of "recovery". *Neuroscience letters* 509:1-4
16. Bigler ED, Maxwell WL. 2012. Neuropathology of mild traumatic brain injury: relationship to neuroimaging findings. *Brain imaging and behavior* 6:108-36
17. Bijlsma MF, Damhofer H, Roelink H. 2012. Hedgehog-stimulated chemotaxis is mediated by smoothened located outside the primary cilium. *Science signaling* 5:ra60
18. Briscoe J, Therond PP. 2013. The mechanisms of Hedgehog signalling and its roles in development and disease. *Nature reviews. Molecular cell biology* 14:416-29
19. Buffo A, Rite I, Tripathi P, Lepier A, Colak D, et al. 2008. Origin and progeny of reactive gliosis: A source of multipotent cells in the injured brain. *Proceedings of the National Academy of Sciences of the United States of America* 105:3581-6
20. Cahoy JD, Emery B, Kaushal A, Foo LC, Zamanian JL, et al. 2008. A transcriptome database for astrocytes, neurons, and oligodendrocytes: a new resource for understanding brain development and function. *The Journal of neuroscience : the official journal of the Society for Neuroscience* 28:264-78
21. Chen XH, Iwata A, Nonaka M, Browne KD, Smith DH. 2003. Neurogenesis and glial proliferation persist for at least one year in the subventricular zone following brain trauma in rats. *Journal of neurotrauma* 20:623-31
22. Chen XH, Johnson VE, Uryu K, Trojanowski JQ, Smith DH. 2009. A lack of amyloid beta plaques despite persistent accumulation of amyloid beta in axons of long-term survivors of traumatic brain injury. *Brain pathology* 19:214-23
23. Clarner T, Diederichs F, Berger K, Denecke B, Gan L, et al. 2012. Myelin debris regulates inflammatory responses in an experimental demyelination animal model and multiple sclerosis lesions. *Glia* 60:1468-80
24. Creed JA, DiLeonardi AM, Fox DP, Tessler AR, Raghupathi R. 2011. Concussive brain trauma in the mouse results in acute cognitive deficits and sustained impairment of axonal function. *Journal of neurotrauma* 28:547-63
25. DiLeonardi AM, Huh JW, Raghupathi R. 2009. Impaired axonal transport and neurofilament compaction occur in separate populations of injured axons following diffuse brain injury in the immature rat. *Brain Res* 1263:174-82
26. Dileonardi AM, Huh JW, Raghupathi R. 2012. Differential effects of FK506 on structural and functional axonal deficits after diffuse brain injury in the immature rat. *Journal of neuropathology and experimental neurology* 71:959-72

27. Doerflinger NH, Macklin WB, Popko B. 2003. Inducible site-specific recombination in myelinating cells. *Genesis* 35:63-72
28. Doetsch F, Garcia-Verdugo JM, Alvarez-Buylla A. 1997. Cellular composition and three-dimensional organization of the subventricular germinal zone in the adult mammalian brain. *The Journal of neuroscience : the official journal of the Society for Neuroscience* 17:5046-61
29. Farzan SF, Singh S, Schilling NS, Robbins DJ. 2008. The adventures of sonic hedgehog in development and repair. III. Hedgehog processing and biological activity. *American journal of physiology. Gastrointestinal and liver physiology* 294:G844-9
30. Ferent J, Zimmer C, Durbec P, Ruat M, Traiffort E. 2013. Sonic Hedgehog signaling is a positive oligodendrocyte regulator during demyelination. *The Journal of neuroscience : the official journal of the Society for Neuroscience* 33:1759-72
31. Flygt J, Djupsjo A, Lenne F, Marklund N. 2013. Myelin loss and oligodendrocyte pathology in white matter tracts following traumatic brain injury in the rat. *The European journal of neuroscience*
32. Fuccillo M, Joyner AL, Fishell G. 2006. Morphogen to mitogen: the multiple roles of hedgehog signalling in vertebrate neural development. *Nature reviews. Neuroscience* 7:772-83
33. Gallo V, Armstrong RC. 2008. Myelin repair strategies: a cellular view. *Current opinion in neurology* 21:278-83
34. Garcia AD, Petrova R, Eng L, Joyner AL. 2010. Sonic hedgehog regulates discrete populations of astrocytes in the adult mouse forebrain. *The Journal of neuroscience : the official journal of the Society for Neuroscience* 30:13597-608
35. Gensert JM, Goldman JE. 1997. Endogenous progenitors remyelinate demyelinated axons in the adult CNS. *Neuron* 19:197-203
36. Gentleman SM, Roberts GW, Gennarelli TA, Maxwell WL, Adams JH, et al. 1995. Axonal injury: a universal consequence of fatal closed head injury? *Acta neuropathologica* 89:537-43
37. Giachino C, Basak O, Lugert S, Knuckles P, Obernier K, et al. 2014. Molecular diversity subdivides the adult forebrain neural stem cell population. *Stem cells* 32:70-84
38. Hannay HJ, Feldman Z, Phan P, Keyani A, Panwar N, et al. 1999. Validation of a controlled cortical impact model of head injury in mice. *Journal of neurotrauma* 16:1103-14
39. Hellyer PJ, Leech R, Ham TE, Bonnelle V, Sharp DJ. 2013. Individual prediction of white matter injury following traumatic brain injury. *Annals of neurology* 73:489-99
40. Hughes EG, Kang SH, Fukaya M, Bergles DE. 2013. Oligodendrocyte progenitors balance growth with self-repulsion to achieve homeostasis in the adult brain. *Nature neuroscience* 16:668-76
41. Ihrie RA, Shah JK, Harwell CC, Levine JH, Guinto CD, et al. 2011. Persistent sonic hedgehog signaling in adult brain determines neural stem cell positional identity. *Neuron* 71:250-62

42. Johnson VE, Stewart JE, Begbie FD, Trojanowski JQ, Smith DH, Stewart W. 2013. Inflammation and white matter degeneration persist for years after a single traumatic brain injury. *Brain* 136:28-42
43. Kim JJ, Gean AD. 2011. Imaging for the diagnosis and management of traumatic brain injury. *Neurotherapeutics* 8:39-53
44. Kumar A, Stoica BA, Sabirzhanov B, Burns MP, Faden AI, Loane DJ. 2013. Traumatic brain injury in aged animals increases lesion size and chronically alters microglial/macrophage classical and alternative activation states. *Neurobiol Aging* 34:1397-411
45. Kuo LW, Chen JH, Wedeen VJ, Tseng WY. 2008. Optimization of diffusion spectrum imaging and q-ball imaging on clinical MRI system. *NeuroImage* 41:7-18
46. Levine JM. 1994. Increased expression of the NG2 chondroitin-sulfate proteoglycan after brain injury. *The Journal of neuroscience : the official journal of the Society for Neuroscience* 14:4716-30
47. Lindner M, Heine S, Haastert K, Garde N, Fokuhl J, et al. 2008. Sequential myelin protein expression during remyelination reveals fast and efficient repair after central nervous system demyelination. *Neuropathol Appl Neurobiol* 34:105-14
48. Lotocki G, de Rivero Vaccari J, Alonso O, Molano JS, Nixon R, et al. Oligodendrocyte Vulnerability Following Traumatic Brain Injury in Rats: Effect of Moderate Hypothermia. *Ther Hypothermia Temp Manag* 1:43-51
49. Mason JL, Langaman C, Morell P, Suzuki K, Matsushima GK. 2001. Episodic demyelination and subsequent remyelination within the murine central nervous system: changes in axonal calibre. *Neuropathol Appl Neurobiol* 27:50-8
50. McAllister TW, Ford JC, Ji S, Beckwith JG, Flashman LA, et al. 2012. Maximum principal strain and strain rate associated with concussion diagnosis correlates with changes in corpus callosum white matter indices. *Annals of biomedical engineering* 40:127-40
51. McKee AC, Cantu RC, Nowinski CJ, Hedley-Whyte ET, Gavett BE, et al. 2009. Chronic traumatic encephalopathy in athletes: progressive tauopathy after repetitive head injury. *Journal of neuropathology and experimental neurology* 68:709-35
52. McMahon P, Hricik A, Yue JK, Puccio AM, Inoue T, et al. 2014. Symptomatology and functional outcome in mild traumatic brain injury: results from the prospective TRACK-TBI study. *Journal of neurotrauma* 31:26-33
53. Menn B, Garcia-Verdugo JM, Yaschine C, Gonzalez-Perez O, Rowitch D, Alvarez-Buylla A. 2006. Origin of oligodendrocytes in the subventricular zone of the adult brain. *The Journal of neuroscience : the official journal of the Society for Neuroscience* 26:7907-18
54. Metting Z, Cerliani L, Rodiger LA, van der Naalt J. 2013. Pathophysiological concepts in mild traumatic brain injury: diffusion tensor imaging related to acute perfusion CT imaging. *PloS one* 8:e64461
55. Mierzwa A, Sullivan G, Beer L, Ahn S, Armstrong RC. Submitted. Heterogeneous Traumatic Brain Injury Models Reveal Differential Effects in the

Subventricular Zone and Divergent Sonic Hedgehog Signaling Pathways in Neuroblasts and Oligodendroglial Progenitors. *ASN neuro*

56. Ming X, Chew LJ, Gallo V. 2013. Transgenic overexpression of Sox17 promotes oligodendrocyte development and attenuates demyelination. *The Journal of neuroscience : the official journal of the Society for Neuroscience* 33:12528-42
57. Miron VE, Boyd A, Zhao JW, Yuen TJ, Ruckh JM, et al. 2013. M2 microglia and macrophages drive oligodendrocyte differentiation during CNS remyelination. *Nature neuroscience* 16:1211-8
58. Miron VE, Franklin RJ. 2014. Macrophages and CNS remyelination. *Journal of neurochemistry*
59. Mokarram N, Bellamkonda RV. 2011. Overcoming endogenous constraints on neuronal regeneration. *IEEE transactions on bio-medical engineering* 58:1900-6
60. Mouzon B, Chaytow H, Crynen G, Bachmeier C, Stewart J, et al. 2012. Repetitive mild traumatic brain injury in a mouse model produces learning and memory deficits accompanied by histological changes. *Journal of neurotrauma* 29:2761-73
61. Murtie JC, Zhou YX, Le TQ, Vana AC, Armstrong RC. 2005. PDGF and FGF2 pathways regulate distinct oligodendrocyte lineage responses in experimental demyelination with spontaneous remyelination. *Neurobiology of disease* 19:171-82
62. Nait-Oumesmar B, Picard-Riera N, Kerninon C, Decker L, Seilhean D, et al. 2007. Activation of the subventricular zone in multiple sclerosis: evidence for early glial progenitors. *Proceedings of the National Academy of Sciences of the United States of America* 104:4694-9
63. Niogi SN, Mukherjee P. Diffusion tensor imaging of mild traumatic brain injury. *J Head Trauma Rehabil* 25:241-55
64. Palma V, Lim DA, Dahmane N, Sanchez P, Brionne TC, et al. 2005. Sonic hedgehog controls stem cell behavior in the postnatal and adult brain. *Development* 132:335-44
65. Peters A. 2002. The effects of normal aging on myelin and nerve fibers: a review. *J Neurocytol* 31:581-93
66. Petrova R, Garcia AD, Joyner AL. 2013. Titration of GLI3 repressor activity by sonic hedgehog signaling is critical for maintaining multiple adult neural stem cell and astrocyte functions. *The Journal of neuroscience : the official journal of the Society for Neuroscience* 33:17490-505
67. Pierpaoli C. 2010. Quantitative brain MRI. *Top Magn Reson Imaging* 21:63
68. Powers BE, Sellers DL, Lovelett EA, Cheung W, Aalami SP, et al. 2013. Remyelination reporter reveals prolonged refinement of spontaneously regenerated myelin. *Proceedings of the National Academy of Sciences of the United States of America* 110:4075-80
69. Radomski KL, Zhou Q, Yi KJ, Doughty ML. 2013. Cortical contusion injury disrupts olfactory bulb neurogenesis in adult mice. *BMC neuroscience* 14:142
70. Ramaswamy S, Goings GE, Soderstrom KE, Szele FG, Kozlowski DA. 2005. Cellular proliferation and migration following a controlled cortical impact in the mouse. *Brain Res* 1053:38-53

71. Rasmussen S, Imitola J, Ayuso-Sacido A, Wang Y, Starossom SC, et al. 2011. Reversible neural stem cell niche dysfunction in a model of multiple sclerosis. *Annals of neurology* 69:878-91
72. Reeves TM, Phillips LL, Povlishock JT. 2005. Myelinated and unmyelinated axons of the corpus callosum differ in vulnerability and functional recovery following traumatic brain injury. *Experimental neurology* 196:126-37
73. Rohatgi R, Milenkovic L, Scott MP. 2007. Patched1 regulates hedgehog signaling at the primary cilium. *Science* 317:372-6
74. Roozenbeek B, Maas AI, Menon DK. 2013. Changing patterns in the epidemiology of traumatic brain injury. *Nat Rev Neurol* 9:231-6
75. Rosenbluth J. 1966. Redundant myelin sheaths and other ultrastructural features of the toad cerebellum. *J Cell Biol* 28:73-93
76. Ruat M, Roudaut H, Ferent J, Traiffort E. 2012. Hedgehog trafficking, cilia and brain functions. *Differentiation; research in biological diversity* 83:S97-104
77. Ruiz i Altaba A, Sanchez P, Dahmane N. 2002. Gli and hedgehog in cancer: tumours, embryos and stem cells. *Nature reviews. Cancer* 2:361-72
78. Shaw K, MacKinnon MA, Raghupathi R, Saatman KE, McLntosh TK, Graham DI. 2001. TUNEL-positive staining in white and grey matter after fatal head injury in man. *Clin Neuropathol* 20:106-12
79. Shigemoto-Mogami Y, Hoshikawa K, Goldman JE, Sekino Y, Sato K. 2014. Microglia enhance neurogenesis and oligodendrogenesis in the early postnatal subventricular zone. *The Journal of neuroscience : the official journal of the Society for Neuroscience* 34:2231-43
80. Shitaka Y, Tran HT, Bennett RE, Sanchez L, Levy MA, et al. 2011. Repetitive closed-skull traumatic brain injury in mice causes persistent multifocal axonal injury and microglial reactivity. *Journal of neuropathology and experimental neurology* 70:551-67
81. Simons M, Snaidero N, Aggarwal S. 2012. Cell polarity in myelinating glia: from membrane flow to diffusion barriers. *Biochim Biophys Acta* 1821:1146-53
82. Sirko S, Behrendt G, Johansson PA, Tripathi P, Costa M, et al. 2013. Reactive glia in the injured brain acquire stem cell properties in response to sonic hedgehog. [corrected]. *Cell stem cell* 12:426-39
83. Smith DH, Hicks R, Povlishock JT. 2013. Therapy development for diffuse axonal injury. *Journal of neurotrauma* 30:307-23
84. Smith JA, Das A, Ray SK, Banik NL. 2012. Role of pro-inflammatory cytokines released from microglia in neurodegenerative diseases. *Brain Res Bull* 87:10-20
85. Sofroniew MV, Vinters HV. 2010. Astrocytes: biology and pathology. *Acta neuropathologica* 119:7-35
86. Song SK, Yoshino J, Le TQ, Lin SJ, Sun SW, et al. 2005. Demyelination increases radial diffusivity in corpus callosum of mouse brain. *NeuroImage* 26:132-40
87. Srinivas S, Watanabe T, Lin CS, William CM, Tanabe Y, et al. 2001. Cre reporter strains produced by targeted insertion of EYFP and ECFP into the ROSA26 locus. *BMC developmental biology* 1:4

88. Stone JR, Singleton RH, Povlishock JT. 2000. Antibodies to the C-terminus of the beta-amyloid precursor protein (APP): a site specific marker for the detection of traumatic axonal injury. *Brain Res* 871:288-302
89. Sturrock RR. 1980. Myelination of the mouse corpus callosum. *Neuropathol Appl Neurobiol* 6:415-20
90. Sullivan GM, Mierzwa AJ, Kijpaisalratana N, Tang H, Wang Y, et al. 2013. Oligodendrocyte lineage and subventricular zone response to traumatic axonal injury in the corpus callosum. *Journal of neuropathology and experimental neurology* 72:1106-25
91. Sun SW, Liang HF, Trinkaus K, Cross AH, Armstrong RC, Song SK. 2006. Noninvasive detection of cuprizone induced axonal damage and demyelination in the mouse corpus callosum. *Magnetic resonance in medicine : official journal of the Society of Magnetic Resonance in Medicine / Society of Magnetic Resonance in Medicine* 55:302-8
92. Susarla BT, Villapol S, Yi JH, Geller HM, Symes AJ. 2014. Temporal patterns of cortical proliferation of glial cell populations after traumatic brain injury in mice. *ASN neuro*
93. Tang-Schomer MD, Johnson VE, Baas PW, Stewart W, Smith DH. 2012. Partial interruption of axonal transport due to microtubule breakage accounts for the formation of periodic varicosities after traumatic axonal injury. *Experimental neurology* 233:364-72
94. Tobin JE, Xie M, Le TQ, Song SK, Armstrong RC. 2011. Reduced axonopathy and enhanced remyelination after chronic demyelination in fibroblast growth factor 2 (Fgf2)-null mice: differential detection with diffusion tensor imaging. *Journal of neuropathology and experimental neurology* 70:157-65
95. Wang H, Ge G, Uchida Y, Luu B, Ahn S. 2011. Gli3 is required for maintenance and fate specification of cortical progenitors. *The Journal of neuroscience : the official journal of the Society for Neuroscience* 31:6440-8
96. Wang Y, Imitola J, Rasmussen S, O'Connor KC, Khoury SJ. 2008. Paradoxical dysregulation of the neural stem cell pathway sonic hedgehog-Gli1 in autoimmune encephalomyelitis and multiple sclerosis. *Annals of neurology* 64:417-27
97. Wang Y, Li W, Li Q, Yang W, Zhu J, Wang W. 2011. White matter impairment in heroin addicts undergoing methadone maintenance treatment and prolonged abstinence: a preliminary DTI study. *Neuroscience letters* 494:49-53
98. Washington PM, Forcelli PA, Wilkins T, Zapple DN, Parsadanian M, Burns MP. 2012. The effect of injury severity on behavior: a phenotypic study of cognitive and emotional deficits after mild, moderate, and severe controlled cortical impact injury in mice. *Journal of neurotrauma* 29:2283-96
99. Wedeen VJ, Hagmann P, Tseng WY, Reese TG, Weisskoff RM. 2005. Mapping complex tissue architecture with diffusion spectrum magnetic resonance imaging. *Magnetic resonance in medicine : official journal of the Society of Magnetic Resonance in Medicine / Society of Magnetic Resonance in Medicine* 54:1377-86
100. White RE, Rao M, Gensel JC, McTigue DM, Kaspar BK, Jakeman LB. 2011. Transforming growth factor alpha transforms astrocytes to a growth-supportive

phenotype after spinal cord injury. *The Journal of neuroscience : the official journal of the Society for Neuroscience* 31:15173-87

101. Wilson S, Raghupathi R, Saatman KE, MacKinnon MA, McIntosh TK, Graham DI. 2004. Continued in situ DNA fragmentation of microglia/macrophages in white matter weeks and months after traumatic brain injury. *Journal of neurotrauma* 21:239-50
102. Wong SY, Reiter JF. 2008. The primary cilium at the crossroads of mammalian hedgehog signaling. *Current topics in developmental biology* 85:225-60
103. Wu C, Orringer DA, Lau D, Fletcher JJ. 2012. Cumulative incidence and predictors of neurosurgical interventions following nonsevere traumatic brain injury with mildly abnormal head imaging findings. *J Trauma Acute Care Surg* 73:1247-53
104. Xie M, Tobin JE, Budde MD, Chen CI, Trinkaus K, et al. 2010. Rostrocaudal analysis of corpus callosum demyelination and axon damage across disease stages refines diffusion tensor imaging correlations with pathological features. *Journal of neuropathology and experimental neurology* 69:704-16
105. Xiong Y, Mahmood A, Chopp M. 2013. Animal models of traumatic brain injury. *Nature reviews. Neuroscience* 14:128-42
106. Yi X, Jin G, Zhang X, Mao W, Li H, et al. 2013. Cortical endogenic neural regeneration of adult rat after traumatic brain injury. *PloS one* 8:e70306
107. Zakaria N, Kallakuri S, Bandaru S, Cavanaugh JM. 2012. Temporal assessment of traumatic axonal injury in the rat corpus callosum and optic chiasm. *Brain Res* 1467:81-90
108. Zhao Z, Loane DJ, Murray MG, 2nd, Stoica BA, Faden AI. 2012. Comparing the predictive value of multiple cognitive, affective, and motor tasks after rodent traumatic brain injury. *Journal of neurotrauma* 29:2475-89
109. Zhou YX, Pannu R, Le TQ, Armstrong RC. 2012. Fibroblast growth factor 1 (FGFR1) modulation regulates repair capacity of oligodendrocyte progenitor cells following chronic demyelination. *Neurobiology of disease* 45:196-205
110. Zhu H, Lo HW. 2010. The Human Glioma-Associated Oncogene Homolog 1 (GLI1) Family of Transcription Factors in Gene Regulation and Diseases. *Current genomics* 11:238-45